Studying the Impact of Solar Photovoltaic on Transient Stability of Power Systems using Direct Methods

Chetan Mishra

Dissertation submitted to the faculty of the **Virginia Polytechnic Institute and State University** in partial fulfillment of the requirements for the degree of

Doctor of Philosophy in

Electrical Engineering

Virgilio A. Centeno, Chair

James S. Thorp

Jaime De La Reelopez

William T. Baumann

Yang Cao

October 24th, 2017

Blacksburg, VA

Keywords: Transient stability, Sum of squares, Low voltage ride through, Photovoltaic

Copyright 2017

Studying the Impact of Solar Photovoltaic on Transient Stability of Power Systems using Direct Methods

Chetan Mishra

(ABSTRACT)

The increasing penetration of inverter based renewable generation in the form of solar photo-voltaic (PV) or wind has introduced numerous operational challenges and uncertainties. Among these challenges, one of the major ones is the impact on the transient stability of the grid. On the other hand, the direct methods for transient stability assessment of power systems have also fairly evolved over the past 30 years. These set of techniques inspired from the Lyapunov's direct method provide a clear insight into the system stability changes with a changing grid. The most attractive feature of these types of techniques is the heavy reduction in the computational burden by cutting down on the simulation time. These advancements were still aimed at analyzing the stability of a non-linear autonomous dynamical system and the existing power system perfectly fits that definition. Due to the changing renewable portfolio standards, the power system is undergoing serious structural and performance alterations. The whole idea of power system stability is changing and there is a major lack of work in the field of direct methods in keeping up with these changes. This dissertation aims at employing the pre-existing direct methods as well as developing new techniques to visualize and analyze the stability of a power system with an added subset of complexities introduced by PV generation.

Studying the Impact of Solar Photovoltaic on Transient Stability of Power Systems using Direct Methods

Chetan Mishra

(General Audience Abstract)

The increasing penetration of inverter based renewable generation in the form of solar photo-voltaic (PV) or wind has introduced numerous operational challenges and uncertainties. Among these challenges, one of the major ones is the impact on the transient stability of the grid. A set of techniques called the direct methods significantly cut down the simulation time required for transient stability studies. However, these techniques did not keep up with the changing power system dynamics due to renewable generation and thus there is a need to develop new methods to study this changing system which is the aim of this thesis.

Acknowledgements

I would like to extend by sincerest gratitude to my advisor Dr. Virgilio Centeno for encouraging me to pursue a Ph.D. He has been the biggest support in my graduate school journey making it a very smooth and memorable experience. He gave me tremendous confidence in my own abilities whenever I fell into self-doubt. More than being a good researcher, he taught me how to be a good person and I have all the respect in the world for him.

A year into my Ph.D. program, due to the inclination towards solving more practical problems, I joined Dominion Energy as an engineer. Few months into the job, I had lost all the motivation to continue Ph.D. My advisor brought me back on track by asking me to seek Dr. James Thorp's guidance in deciding a research direction which proved to be the best advice I had ever received. Dr. Thorp introduced me to the world of non-linear dynamics and several complex phenomena observed in power systems which I instantly fell in love with. These made every other thing I had worked on or was working on seem less appealing. Subsequently, I had the honor of working with him and Dr. Centeno on transient stability for my thesis. His ingenious insights into the problems we tackled inspired me to work harder and strive to be like him. I am extremely grateful to him for his perfect guidance in my research and showing a great deal of patience when addressing my abstract emails. I hope to continue to learn from him.

I am also thankful to Dr. Jaime De La Ree for his support and creating a perfect learning environment. His strong intuition when it comes to understanding the various power system phenomena is very impressive. I hope to learn more from him which will be really helpful when dealing with various issues we encounter in our grid as a part of my job. I would also like to thank Dr. William Baumann for his course on Linear Systems Theory which is by far the best course I have ever taken. The various discussions I've had with him in his class helped build a foundation making it possible to pursue my research in stability. Dr. Yang Cao's course on Numerical Analysis strengthened my background in Linear Algebra which I needed often in my work.

I owe a great deal to the numerous technical discussions I had with my friends and lab mates Tong, Elliot, Jacques, Srivats, Ahmad, Marcos, Anamitra, and Andreas at Virginia Tech which helped shape my work. I will forever cherish the various collaborative efforts we had when working on papers and courses and hope to continue those.

Lastly, I would like thank my colleagues at Dominion Energy starting with Kevin Jones for being the perfect mentor during my summer internships and always being there as a friend, Matthew Gardner for having the confidence in me by hiring me in his research team, Kyle Thomas, my supervisor at Dominion, for supporting my Ph.D. pursuit and my teammates Rui, Hung-Ming, Tania, Chris, and Terry.

In memory of my mother Mrs. Abha Mishra. Also dedicated to my father Mr. Subodh Mishra, my girlfriend Juzi Zhou and my brother Chinmaya Mishra for their unconditional love and support.

Contents

Chapter 1 Introduction 1

1.1 Industry Experiences 2

1.1.1 Germany's 50.2 Hz Problem 2

1.1.2 California's Duck Curve 3

1.2 Transient Stability of Power Systems 5

1.2.1 Swing Equation 6

1.2.2 Power-Angle Relationship and Stability Phenomenon 8

1.2.3 Multi-machine System Network Reduced Model 10

1.2.4 Transient Stability During Power System Faults (Concept of Critical Clearing Time) .. 12

1.3 Multi-Machine Test System 16

1.4 Thesis Overview and Contribution 17

Chapter 2 Review of Direct Methods for Transient Stability Assessment 20

2.1 Boundary of Stability Region Based Controlling Unstable Equilibrium (BCU) Method and its Development 22

2.1.1 Characterization of Stability Boundary for Non Linear Dynamical System 26

2.1.2 Energy Function 28

2.1.3 Energy Function for Power Systems Network Reduced Model 28

2.1.4 Controlling Unstable Equilibrium (CUEP) 31

2.1.5 BCU Method 33

2.2 Lyapunov Functions Approach to Transient Stability Assessment using Sum of Squares Programming 42

2.2.1 SOS Problem 42

2.2.2 Positivstellensatz (P-Satz) Theorem 45

2.2.3 Estimating Region of Attraction (Expanding Interior Algorithm) 46

2.2.4 Expanding Interior Algorithm 47

2.2.5 Application to Transient Stability Assessment of Power Systems Classical Model 52

2.2.6 Estimating the Relevant Portion of Stability Region for Power Systems Classical Model 63

Chapter 3 Impact of Inertia Displacement and Generator Redispatch 70

3.1 Inertia Reduction Issues 70

3.1.1 Literature Review 71

3.1.2 Inertia Case Study 72

3.2 Impact of Generation Dispatch 81

3.2.1 Generation Dispatch Case Study 81

Chapter 4 Studying the Impact of Low Voltage Ride Through (Inverter Protection) using Direct Methods 85

4.1 Constrained System Approach 87

4.1.1 Challenges in Analytical Energy Function Based Methods for TSA of Systems with Inequality Constraints 89

4.1.2 Modeling 97

4.1.3 Using Max LVRT Curve 99

4.1.4 Using Augmented State to Envelop LVRT Curve 104

4.1.5 Using Lyapunov Level Set + Barrier Functions 115

4.2 Switched System Approach 121

4.2.1 Network Reduced Classical Model for Switched Systems 123

4.2.2 Multistep BCU 124

4.2.3 Stability Under Cascading Tripping of PVs 129

4.2.4 Multiple CSR Approach 139

Chapter 5 Conclusions and Future Work 152

References 156

List of Figures

Figure 1.1 Germany Installed PV Capacity 3
Figure 1.2 Solar Profile (top), California Duck Curve (bottom) [7] 4
Figure 1.3 Two Machine System 8
Figure 1.4 Single Machine Infinite Bus System 13
Figure 1.5 Power Angle Curve for Different Network Topologies 14
Figure 1.6 CCT 15
Figure 1.7 3-Machine System 17
Figure 2.1 Rolling Ball Analogy 21
Figure 2.2 Tangent space (grey) of a manifold (sphere) at point (0,0,1) 23
Figure 2.3 Transverse (left) vs Non Transverse (right) Intersection of Manifolds (sphere and plane) 23
Figure 2.4 Type 1 UEP 24
Figure 2.5 Some Non-Hyperbolic EPs. . Left Plot: Both Imaginary Eigen Values. Right Plot: Both Real Eigen Values - One Negative One 0. 25
Figure 2.6 Attracting Limit Cycle (green) 26
Figure 2.7 Closest UEP Stability Region Estimate by Min Energy UEP $\boldsymbol{\delta 1}$ 32
Figure 2.8 Controlling UEP Stability Region estimates for faults approaching the left boundary (left) and the right boundary (left) 33
Figure 2.9 Example 2.1 Test System 38
Figure 2.10 Example 2.1 Fault On Trajectory in Post Fault UE Surface 39
Figure 2.11 Example 2.1 Exit Metric and Potential Energy along Fault Trajectory 39
Figure 2.12 Example 2.1 MGP Tracing 40
Figure 2.13 Example 2.1 Boundary Test 40
Figure 2.14 Example 2.1 Energy Function Value Along Fault Trajectory 41
Figure 2.15 Example 2.1 $\boldsymbol{x - xsep}$ 41
Figure 2.16 Expanding D vs Expanding Interior Algorithm SR Estimates 48
Figure 2.17 Example 2.1 Expanding SR Estimate 57

Figure 2.18 Example 2.1 Value of Lyapunov Function along Fault Trajectory 58
Figure 2.19 Generator Angle vs Loading Curve 59
Figure 2.20 Example 2.1 Continuation Traces for Locating All EPs 62
Figure 2.21 BCU vs SOS SR Estimate 63
Figure 2.22 Comparing SR Estimates for a Fault Trajectory 63
Figure 2.23 p(z) contours using $\boldsymbol{\lambda i}$ (lower) vs $\boldsymbol{\lambda i}^{1/2}$ (upper) 66
Figure 2.24 Example 2.2 Test Case 67
Figure 2.25 Example 2.2 SR Estimate for Fault on Bus 2 67
Figure 2.26 Example 2.2 Lyapunov Value Along Fault Trajectory for Fault on Bus 2 68
Figure 2.27 Example 2.2 SR Estimate for Fault on Bus 1 68
Figure 2.28 Example 2.2 Lyapunov Value Along Fault Trajectory for Fault on Bus 1 69
Figure 3.1 Inertia Studies - Fault Bus 1, Trip Line 1-2 CCT changes vs Local PV Penetration 75
Figure 3.2 Inertia Studies - Fault Bus 2, Trip Line 1-2 CCT changes vs Local PV Penetration 75
Figure 3.3 Inertia Studies - Fault Bus 3, Trip Line 1-3 CCT changes vs Local PV Penetration 76
Figure 3.4 Inertia Study – FB = 1, PB = 1, L = 1-2 Estimated Relevant Stability Boundary Projection vs Local PV Penetration 77
Figure 3.5 Inertia Study – FB = 2, PB = 2, L = 1-2 Estimated Relevant Stability Boundary Projection vs Local PV Penetration 78
Figure 3.6 Inertia Study – FB = 2, PB = 1, L = 1-2 Estimated Relevant Stability Boundary Projection vs Local PV Penetration 79
Figure 3.7 Inertia Study - FB = 1, PB = 2, L = 1-2 Estimated Relevant Stability Boundary Projection vs Local PV Penetration..... 79
Figure 3.8 Inertia Study - FB = 3, PB = 2, L = 1-3 Estimated Relevant Stability Boundary Projection vs Local PV Penetration..... 80
Figure 3.9 Inertia Study - FB = 3, PB = 1, L = 1-3 Estimated Relevant Stability Boundary Projection vs Local PV Penetration..... 80
Figure 3.10 PEBS Changes with Increasing PV Accommodated by Generator 1 83
Figure 3.11 PEBS Changes with Increasing PV Accommodated by Generator 2 84
Figure 4.1 LVRT Standards 86

Figure 4.2 Constrained Stability Region (Grey) 88
Figure 4.3 Dynamics Around Pseudo EPs 91
Figure 4.4 Field Lines Around Saddle Pseudo EP 91
Figure 4.5 Stable Trajectories Around Feasibility Boundary $\boldsymbol{h1}(\boldsymbol{x}) = \boldsymbol{0}$ 95
Figure 4.6 Stable Trajectories Around Feasibility Boundary $\boldsymbol{h2}(\boldsymbol{x}) = \boldsymbol{0}$ 95
Figure 4.7 Example 4.1 Test System 100
Figure 4.8 Example 4.1 LVRT Curve 101
Figure 4.9 Example 4.1 Max LVRT Approach Trajectories on Angle Plane Starting from Estimated SR Boundary 102
Figure 4.10 Example 4.1 Max LVRT Approach PV Bus Voltage Trajectories Starting from Estimated SR Boundary 103
Figure 4.11 Example 4.1 Max LVRT Approach Unconstrained vs Constrained Stability Region 103
Figure 4.12 Example 4.1 Max LVRT Approach Estimated vs Actual Constrained Stability Region 104
Figure 4.13 Sigmoid Response for Different Values of K 106
Figure 4.14 Sigmoid Response for Different Values of $\boldsymbol{csep}$ 106
Figure 4.15 IEEE 1547 LVRT Curve Sigmoid Fit 108
Figure 4.16 FERC LVRT Curve Sigmoid Fit Negative Error Penalty (0 (above) vs 100 (below))... 108
Figure 4.17 Example 4.1 Augmented State Approach vs Max LVRT Approach SR 113
Figure 4.18 Example 4.1 Augmented State Approach Lyapunov Level Set vs Starting Point on LVRT 114
Figure 4.19 Example 4.1 Augmented State Approach True Constrained Stability Region 114
Figure 4.20 Expanding Interior Using Barrier Functions 116
Figure 4.21 Example 4.1 Comparison of Constrained SR Estimates using Different Approaches 120
Figure 4.22 Example 4.1 Barrier Function Approach Lyapunov Level Set vs Starting Point on LVRT 120
Figure 4.23 Impact of PV Trip at Accelerating Generator vs PV Size 121
Figure 4.24 Switched System 122

Figure 4.25 Absence of CCT for Switched Systems 123
Figure 4.26 Example 4.2 Multistep BCU Test Case 126
Figure 4.27 Example 4.2 Actual System Trajectory in Angle Domain 128
Figure 4.28 Example 4.2 $\mathbf{Vpv}$ vs LVRT Curve 128
Figure 4.29 Example 4.2 Energy Plot of Unstable Trajectory 129
Figure 4.30 Stability Under Fixed Switching using Nested SRs 133
Figure 4.31 Example 4.4 Test System 135
Figure 4.32 Example 4.4 SR Estimate for all Cascading Sequences 137
Figure 4.33 Example 4.4 Risk of Instability Region 138
Figure 4.34 Example 4.4 Risk of Instability Under Trip Blocking 138
Figure 4.35 Multiple CSR Approach 141
Figure 4.36 Example 4.5 Test System 143
Figure 4.37 Example 4.5 Fault Voltages 144
Figure 4.38 Example 4.5 Constrained SR Estimates 145
Figure 4.39 Example 4.5 Active Lyapunov Function Value Along Fault Trajectory 145
Figure 4.40 Example 4.6 Test System 146
Figure 4.41 Example 4.6 CSR Estimate 147
Figure 4.42 Example 4.7 Test System 147
Figure 4.43 Example 4.7 Unconstrained SR Estimates 148
Figure 4.44 Example 4.7 Fault Voltage 149
Figure 4.45 Example 4.7 CSR Estimates 150
Figure 4.46 Example 4.7 Relaxed CSR Estimates 151

List of Tables

Table 2.1 Variable Transformation for Power System Model 54
Table 2.2 Example 2.1 Variable Transformation for Polynomial System 55
Table 2.3 Example 2.1 SOS Degrees..... 56
Table 2.4 Example 2.1 Type 1 UEP on Stability Boundary 62
Table 3.1 PV Generator Model Parameters as Pseudosynchronous Machine for Inertia Studies73
Table 3.2 Inertia Case Studies BCU Results for Single PV 73
Table 4.1 Example 4.1 Max LVRT Approach Variable Transformation 101
Table 4.2 Example 4.1 Max LVRT Approach SOS Multiplier Degrees 101
Table 4.3 Example 4.1 SOS Multiplier Degrees..... 112
Table 4.4 Example 4.1 Lyapunov Level Set + Barrier Functions Approach SOS Multiplier Degrees 119
Table 4.5 Example 4.2 Post fault SEP for All Statuses..... 126
Table 4.6 Example 4.2 Multistep BCU Results 126
Table 4.7 Example 4.2 Encountered Status Stability Table 126
Table 4.8 Example 4.4 SEPs for All Switching States..... 135
Table 4.9 Example 4.4 Cascading Sequences..... 136
Table 4.10 Example 4.5 143
Table 4.11 Example 4.5 SEP 144
Table 4.12 Example 4.5 Stability Results 146
Table 4.13 Example 4.7 Stability Results 147
Table 4.14 Example 4.7 SEPs..... 148
Table 4.15 Example 4.7 Constraints..... 149
Table 4.16 Example 4.7 Stability Results 150
Table 4.17 Example 4.7 Relaxed Constraints..... 150
Table 4.18 Example 4.7 Stability Results Relaxed Constraints 151

Chapter 1 Introduction

With the continuous increase in electric load, power generation must increase at a similar rate to keep up with the demand. In the last few decades, the sources of power generation were mainly coal, nuclear, and natural gas. In recent years, however, it has become mandatory to include a percentage of clean electric power generation. The Department of Energy has set requirements by 2030 to use renewable resources that do not produce harmful by-products, like CO2, coal ash and nuclear waste [1]. While other sources of renewable energy resources can be more efficient, solar energy can be optimum to use in certain locations when the amount of sun radiation is high and the price of land is relatively inexpensive [2]. One of the ways to convert solar radiation into electricity is using Photovoltaic (PV) cells. PV cells can convert solar radiation into DC electricity, which then is converted to AC through inverters before integrating it to the grid [3]. Owing to the EPA regulations [4], utilities are driven to heavily reduce their carbon footprints. In the case of Dominion VA Power, this drive is further fueled by a 30% tax credit for solar developers. Thus, a lot of distribution and transmission interconnected PV is expected. To get the maximum economic benefits, it seems attractive to displace the more expensive conventional peaking units. While being an economically as well as environmentally justifiable option, this has led to serious unprecedented reliability concerns due to uncertainty in solar output coupled with the nature of this type of generation. Currently PV is not thought of as a support for the grid owing to its output uncertainties. While being an inverter based generation provides tremendous flexibility in controlling, it comes at an added cost. Some of the popular case studies highlighting the reliability issues due to renewable generation in utilities around the world are discussed below.

1.1 Industry Experiences

1.1.1 Germany's 50.2 Hz Problem

This is a very popular case study of the German system showing the implications of having inverter protection standards not keeping up with the changing grid. The detailed analysis of the issue was done in [5] which is summarized here. Around 2005/2006, protection requirements were introduced in Germany for generating plants connected to low voltage network (majorly renewable) to trip offline immediately if the frequency exceeded 50.2 Hz (50 Hz is nominal there as opposed to 60 Hz in North America). This was justifiable since this type of generation was never considered for grid support and also the installed capacity was really low. However the following years saw a great increase in renewable energy in Germany due to the promotion of Renewable Energy Sources Act. Around 2010 for example, around 14 GW of solar was installed at low kV level. Based on the locations of these connected PV's, in the worst case scenario, the system would see a loss of around 9000 MW generation from PV if the frequency reaches above 50.2 Hz. Now this frequency value is highly unlikely in normal operations. However, since PV and other renewables are intermittent sources of generation and the energy market (where power generation is bid to match load) has a longer forecast horizon (how much time before the bidding is done) which is not suitable for a resource which fluctuates rapidly a lot, seeing higher frequency deviations might not have been out of question. Large scale unexpected disturbances could lead to insufficient transmission to supply the generated power thus posing over frequency risk in regions due to over generation. For example in the European grid failure in 2006, Germany was a major exporter to rest of the European grid and the frequencies reached 50.2 Hz during the event. Now, the European grid can deal with a sudden loss of only 3000 MW of generation so having such disturbances on a peak PV day would be very dangerous. The installed PV capacity is still growing and has long surpassed the 3000 MW value as shown in figure below.

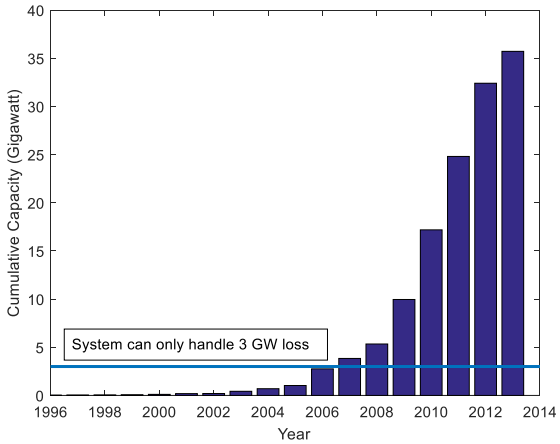

Figure 1.1 Germany Installed PV Capacity

Due to this issue, Germany had to retrofit a significant portion of the installed PV to reduce the impact on network stability and operations during high frequency levels along with modifications to PV system transition rules and generation interconnection standards.

1.1.2 California's Duck Curve

This case study [6] helped foresee the challenges faced when trying to reliably operate a grid with high penetration of PV. In California, the electric grid is seeing significant changes due to energy and environmental policy initiatives. These entail having 50% of electricity from renewable power by 2030 and major reductions in greenhouse gas emissions to the 1990 levels to name a few. California ISO performed detailed generation planning studies for cases up to the year 2020 and realized that there would be some major challenges in operating the grid with so much renewable–

1. Limited generation ramping.
2. Risk of over-generation (leading to increasing frequency).
3. Reduction in frequency response due to displaced conventional generation (having inertia and governor controls) with renewable.

Some of the major requirements need from the grid that stemmed from the concerns above for operating a green grid were –

1. Quicker generation ramping rates so more peaking units rather than base load units.
2. Stored energy for better balancing short term generation-load imbalances.
3. Reduced startup costs for generating plants.
4. More accurate forecasts for better system operations planning.

These requirements are important because renewable generation is not controllable and highly variable. Thus, when fluctuations happen, ISO has to use other controllable conventional generators to match an generation-load imbalances emerging from load and now generation uncertainties (renewable). This can also be seen through the projected net load curves (net load = load – renewable generation vs time of the day) popularly known as the duck curve which is what the ISO generation is expected to match in successive years (increasing PV).

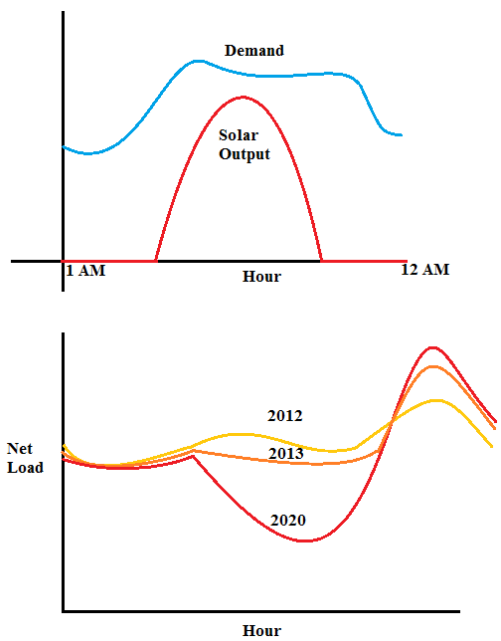

Figure 1.2 Solar Profile (top), California Duck Curve (bottom) [7]

Around 4 AM, there is a pickup in load while at this time solar is not there to this would be met totally by conventional generation. Now from 7 AM onwards, a lot of load rapidly transfers to solar generation from the conventional generation which will mostly be switched off. Now during these periods the grid has a significant reduction in inertia and frequency control. This is because the conventional generators have speed governors which sense deviations and accordingly change the fuel inputs to the generation thus speeding or slowing them down

which is coupled to frequency. Displacing these generators by PV which are not required to have these capabilities would result in a grid which cannot heal itself well against bigger generation-load imbalances during system disturbances/major events like loss of line, etc leading frequency excursions. Moving on with the duck curve, the most important portion is around 4 PM when solar starts declining to 0 and now generators are needed to quickly ramp up and pick up all that load which shows a major requirement for faster peaking units (expensive). Immediately following this generation ramp up with solar not in picture anymore, load demand decreases seen by the downward ramp so a lot of generation has to be reduced or shut down. The situation seems to get worse marked by steeper generator ramping required with increasing PV penetration.

Summarizing the above two case studies, some of the key challenges faced by a grid with considerable PV are the uncertain nature of generation which requires fast acting conventional generators to balance cycle, reduction in the overall system inertia leading to worsening of frequency response and inverter protection standards not keeping up with the evolving grid. These issues have serious consequences when it comes to power system stability which we plan on exploring in our work. But first, let us understand what exactly means by transient stability and the necessary tools required to study it.

1.2 Transient Stability of Power Systems

Transient stability is defined as the ability of a system to return to the equilibrium following a severe disturbance such as faults, loss of generation, etc. The phenomenon is marked by large excursions in generator rotor angles, voltages, etc requiring non-linear models to simulate and study. This type of instability is usually evident within few seconds of the disturbance. Before diving further into the idea of transient stability, we would first give the reader a general background on the electromechanical dynamics (swing equation) that go on inside a synchronous machine during these disturbances. This will be followed by an insight into the phenomenon of how a multi machine system typically loses stability. This section is derived from [8] .

1.2.1 Swing Equation

A synchronous machine (conventional generators) is comprised of a cylindrical rotor covered by coils carrying DC current, rotating to create a magnetic field rotating in space with the same speed in space. These rotating magnetic field lines cut the spatially distributed windings on the fixed component of the generator (called the stator) to induce an electrical potential in them (through Faraday's law). This potential is AC type with an angular frequency (ω_e) related to the frequency of rotor's mechanical speed (ω_m) having P magnetic poles on the rotor as –

$$\omega_m = \frac{2}{P} \times \omega_e \tag{1.1}$$

This denotes the relationship between electrical and mechanical quantities in a synchronous machine. The current resulting from this induced potential creates a rotating magnetic field of its own (due to AC nature) rotating at same speed as that of rotor creating a counter torque on it [9]. There are also damper windings embedded in the rotor which are not energized by any external source and thus under ideal situation do not carry any current. However when the rotor and stator fields rotate at different speeds, these windings see a flux rotating at an angular velocity equal to the relative angular velocity between rotor and stator fields which cuts them inducing a current. This current creates a counter torque T_d which resists this flux cutting by trying to bring this relative speed to 0. Thus the net torque on rotor is $T_m(mechanical) - T_e(electrical) - T_d$ which leads us to the equation of motion [8] –

$$J\alpha_m = J\dot{\omega_m} = J\ddot{\theta_m} = T_m - T_e - T_d, \qquad N - m \tag{1.2}$$

Where J is the generator rotor + turbine inertia and α is its mechanical angular acceleration ($mec - rad/s^2$). Multiplying both sides by rotor speed ω_m and dividing by base values to get per unit representation,

$$\frac{J\omega_m\dot{\omega_m}}{VA_{base}} = \frac{P_m - P_e - P_d}{VA_{base}}, pu \tag{1.3}$$

VA_{base} is power base/rated power and ω_{0m} is rated mechanical angular velocity. Define H (per unit inertia constant) as –

$$H = \frac{\frac{1}{2} J \omega_{0m}^2}{VA_{base}} \tag{1.4}$$

Equation becomes –

$$\frac{2H}{\omega_{0m}^2} \omega_m \dot{\omega_m} = \overline{P_m} - \overline{P_e} - \overline{P_d}\,, pu \tag{1.5}$$

In the left hand side expression, $\frac{\omega_m}{\omega_{0m}}$ is the per unit mechanical speed ($\overline{\omega_m}$) and is equal to per unit angular frequency on electrical side $\frac{\omega_r}{\omega_0}$ ($\overline{\omega_r}$). Here $^{-}$ sign denotes per unit. Rewriting,

$$\frac{2H}{\omega_0^2} \omega_r \dot{\omega_r} = \overline{P_m} - \overline{P_e} - \overline{P_d}\,, pu \tag{1.6}$$

Now, we define $\delta(t)$ as the relative angular difference in electrical radians wrt a reference frame rotating at nominal angular frequency ω_0 at time t –

$$\delta(t) = \omega_r t - \omega_0 t + \delta(t = 0) = \Delta\omega_r t + \delta(t = 0) \tag{1.7}$$

Now, we define $\delta(t)$ as the relative angular difference in electrical radians wrt a reference frame rotating at nominal angular frequency ω_0 at time t –

$$\delta(t) = \omega_r t - \omega_0 t + \delta(t = 0) = \Delta\omega_r t + \delta(t = 0) \tag{1.8}$$

$$\dot{\delta} = \Delta\omega_r = \omega_0 \overline{\Delta\omega_r} \tag{1.9}$$

$$\ddot{\delta} = \dot{\omega_r} = \Delta\dot{\omega_r} = \omega_0 \overline{\Delta\dot{\omega_r}} \tag{1.10}$$

Rewriting the equation of motion in terms of δ and its derivatives after simplifications,

$$\frac{2H}{\omega_0^2} \omega_r \ddot{\delta} = \overline{P_m} - \overline{P_e} - \overline{P_d}\,, pu \tag{1.11}$$

Define $M(\omega_r) = \frac{2H}{\omega_0^2} \omega_r$,

$$M(\omega_r) \ddot{\delta} = \overline{P_m} - \overline{P_e} - \overline{P_d}\,, pu \tag{1.12}$$

Assuming under normal conditions $\omega_r \sim \omega_0$, substitute $M = \frac{2H}{\omega_0}$ which is a constant to get the final swing equation,

$$M\ddot{\delta} = \overline{P_m} - \overline{P_e} - \overline{P_d}\,, pu \tag{1.13}$$

As defined before, the damping torque is proportional to relative speed between stator and rotor's rotating fields –

$$M\ddot{\delta} = \bar{P}_m - \bar{P}_e - K_D\,\overline{\Delta\omega_r} = \bar{P}_m - \bar{P}_e - K_D\frac{\dot{\delta}}{\omega_0} = \bar{P}_m - \bar{P}_e - D\dot{\delta} \tag{1.14}$$

Multiplying both sides by angular speed ω_r and assuming $\omega_r \sim \omega_0$ under normal conditions, we convert RHS to power,

$$M\ddot{\delta} = \bar{P}_m - \bar{P}_e - D\dot{\delta}\,, pu \tag{1.15}$$

This is often written as two single order equations –

$$\dot{\delta} = \omega \tag{1.16}$$

$$M\dot{\omega} = \bar{P}_m - \bar{P}_e - D\omega \tag{1.17}$$

Here, $\omega = \Delta\omega_r$ (relative angular speed in electrical radians/s wrt synchronously rotating frame).

1.2.2 Power-Angle Relationship and Stability Phenomenon

In this section we discuss the relationship between the interchange power and angular position of the rotor of synchronous machines which is an important characteristic governing power system stability [8]. The power exchange in a two machine system given below with machine 1 (generator) feeding machine 2 (motor) is of the form -

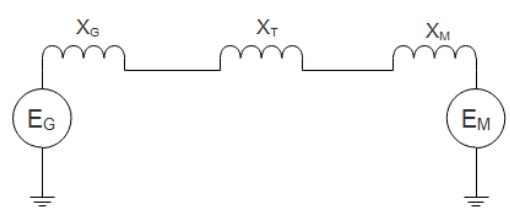

Figure 1.3 Two Machine System

$$P = \frac{E_G E_M \sin(\delta)}{X_G + X_L + X_M} = P_{max}\sin(\delta) \tag{1.18}$$

In a synchronous machine, the rotor creates a rotating field which induces potential in the stator. This induced potential creates a rotating field of its own (Lenz's law). Angle δ is the

overall phase difference between the rotating field of generator and motor and is comprised of the following angles : δ_G (angle with which the generator rotor field leads the stator field called the generator rotor angle), δ_L (the angular difference between generator and rotor stator voltages) and δ_M (angle with which the rotor's rotating electrical field lags that of stator). This power angle relationship is for a simplified classical generator model which is not the same in case of more complex generator models. However the structure would be similar. E_G is the generator internal voltage while E_M is that of the motor. It can be seen that the power transferred is proportional to the sine of δ (maximum at $\delta = \frac{\pi}{2}$). This can be further increased by increasing internal voltages (through increased excitation/current in rotor) and decreasing impedance X coupling the machines. However in a multi machine system things get more complex in terms of transfer limits. Regardless, at steady state, δ is expected to be constant leading to constant power exchanges. This can only happen if the speed with which each machine's rotor magnetic field is rotating is the same leading (called synchronism) to a fixed angle difference maintained.

When a multi machine system is at steady state, the two opposing forces acting on each generator (mechanical input and electrical output) are equal (as seen in swing equation). Any disturbance that creates imbalance results in the machine accelerating/decelerating. When a machine runs faster than the others temporarily, its angle deviation from other machines increases thus increasing the net electrical power output from that machine (as formulated before) up to a certain extent. What this means is that a part of the electrical load is transferred from the other machines to the accelerating machine. This increase in output at that machine helps slow it down. However beyond a certain value of angle difference as seen in the sinusoidal nature of power, the output power starts decreasing thus further accelerating the machine making it impossible to run again at the same speed as others (referred to as losing synchronism). This is detected by out of step protection at the machine which trips it offline. The loss of synchronism phenomenon can be more complex in some systems where a group of machines lose synchronism with rest of the grid while remaining synchronized with each other.

1.2.3 Multi-machine System Network Reduced Model

The overall power system model consists of buses (nodes) inter-connected through transmission lines. These buses have devices attached to them (say for simplicity generators with its controls and loads). Loads can range from simple static ones like constant power consumption to complex dynamic ones like induction motors. The generator and its controls (AVR,governor,PSS) can have very sophisticated complex models [10].

In power systems transient stability analysis, a popular simplified representation of the electromechanical dynamics is by modeling generators using the so called classical model [11] which makes it much more easier to handle multi machine systems. This model represents generators as constant voltage sources leading/lagging in phase wrt the synchronously rotating frame. This was found to be adequate by power engineers for transient stability analysis mainly for capturing the instability phenomenon observed within the first second. As for the loads, we use a simplified representation modeling them as constant impedances. This makes it possible to include them into the network admittance matrix itself thus leaving us with only generator buses interconnected through impedances. The network reduction process for creating such model for any network configuration (pre fault, fault or post fault) for a particular transient stability study is summarized below –

Algorithm 1.1 Creating a network reduced model

1. Run load flow [12] for the pre-fault system to get steady state voltage magnitudes and angles at each network bus. For i^{th} bus, use the pre-fault load flow voltage magnitude V_i to convert the complex load $P_{di} + jQ_{di}$ into an admittance $Y_{di} = \frac{P_{di} - jQ_{di}}{(V_i)^2}$. This is added to the ith diagonal element of admittance matrix for the given system configuration. For details on creating the initial network admittance matrix for any network, please refer to [12]. Do this for all buses to obtain the new admittance matrix Y_{bus}^{new}.

2. Create an internal bus for each generator. This is connected to the corresponding

transmission system bus by the generator's internal impedance x_d. Append these buses to create a new extended admittance matrix Y_{ext}. This matrix includes generator internal buses with current injections besides the original network buses with no injection (loads converted to passive impedances). Here $Y_{12} = Y_{21}$ contain elements of connection between internal generator buses and original network buses while Y_{22} contains only elements of interaction between internal generator buses.

$$Y_{ext} = \begin{bmatrix} Y_{bus}^{new} & Y_{12} \\ Y_{21} & Y_{22} \end{bmatrix} \tag{1.19}$$

3. Now, writing the current balance equations in matrix form (Kirchoffs eqn) for this extended network,

$$\begin{bmatrix} 0 \\ I_g \end{bmatrix} = \begin{bmatrix} Y_{bus}^{new} & Y_{12} \\ Y_{21} & Y_{22} \end{bmatrix} \begin{bmatrix} V \\ E \end{bmatrix} \tag{1.20}$$

Simplifying, we get,

$$I_g = [Y_{22} - Y_{21}[Y_{bus}^{new}]^{-1} Y_{12}][E] \tag{1.21}$$

The reduced network's admittance matrix is given in the first bracket on the right.

Finally, the state equations for n_g machine system for the network reduced classical model,

$$\begin{gathered} \dot{\delta}_i = \omega_i \\ M_i \dot{\omega}_i = P_{mi} - D_i \omega_i - E_i \sum_{j=1}^{n_g} E_j (G_{ij} \cos(\delta_i - \delta_j) + B_{ij} \sin(\delta_i - \delta_i)) \\ \forall\, i \in [1, n_g] \end{gathered} \tag{1.22}$$

It can be seen that there are $2n_g$ first order differential equations. It is also evident that at equilibrium $\omega_i = 0\ \forall i$. Since the equations are in the form of angle differences, if $\delta_{ep} \in R^{n_g}$ represents the angles at an equilibrium, so does $\delta_{ep} + a$, where a is any constant. Thus the actual number of states are $< 2n_g$. To overcome this problem, relative angles rather than absolute angles are assessed [11]. Two most widely used reference frames are center of angle (COA) and single machine reference. Here, we will only deriving the formulation for center of angle which is more popular in stability studies due to it being related to system frequency up

to a certain extent. One machine reference frame will be discussed later in our work as a part of polynomial formulation of the state equations.

Assuming uniform damping in generators ($\frac{D_i}{M_i} = \lambda$), the dynamics in terms of COA reference frame (δ_0, ω_0) can be easily written as –

$$\dot{\delta_i}^{coa} = \omega_i^{coa}$$

$$M_i \dot{\omega_i}^{coa} = P_{m_i} - P_{e_i} - \left(\frac{M_i}{M_{total}}\right) \times P_{coa} - D_i \omega_i^{coa}$$

$$P_{e_i} = E_i \sum_j E_j \times (G_{ij} \cos\left(\delta_i^{coa} - \delta_j^{coa}\right) + B_{ij} \sin\left(\delta_i^{coa} - \delta_j^{coa}\right)) \tag{1.23}$$

$$\delta_i^{coa} = \delta_i - \delta_0$$

$$\delta_0 = \frac{\sum_i M_i \, \delta_i}{M_{total} = \sum_i M_i}, \omega_0 = \frac{\sum_i M_i \, \omega_i}{M_{total} = \sum_i M_i}$$

$$P_{coa} = \sum_i (P_{m_i} - P_{e_i})$$

In the system above, $\sum_i M_i \delta_i^{coa} = 0$, and so we can represent n_g^{th} generator's angle and speed in COA reference frame as a linear combination of those of other generators. So, the state equations for only first $(n_g - 1)$ machines are required in the COA reference frame giving us $2 \times (n_g - 1)$ state equations. The state vector $x = \left[\delta_1^{coa}, \delta_2^{coa}, \dots, \delta_{n_g-1}^{coa}, \omega_1^{coa}, \omega_2^{coa}, \dots, \omega_{n_g-1}^{coa}\right]^T$.

1.2.4 Transient Stability During Power System Faults (Concept of Critical Clearing Time)

The most severe types of disturbances when it comes to maintaining transient stability are transmission network faults. These refer to situations when one more phases of a transmission line get unintentionally connected to each other or to the ground or both. This type of an event is usually marked by dangerously low voltages and high currents in the system. The system usually does not have a satisfactory equilibrium as long as the fault sustains. So, these need to

be cleared which is usually done by relays which isolate the faulted region (line, generator, etc) of the system.

Let us analyze a system with a single machine with internal impedance x_d providing power to an infinite bus through 2 parallel lines with X_1 and X_2 reactances respectively as shown in figure below.

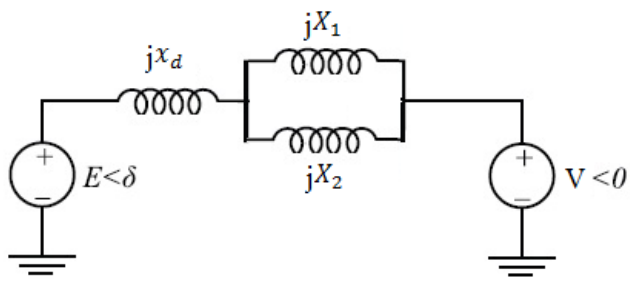

Figure 1.4 Single Machine Infinite Bus System

An infinite bus is a node with constant voltage and angle/phase (say 0). It can be thought of as a hypothetical generator with infinite inertia and very small internal impedance with constant voltage source behind that impedance. Let δ be the rotor angle difference between the study machine and infinite bus. Then, we can write the governing dynamics /swing equation for this system –

$$\begin{aligned} \dot{\delta} &= \omega \\ M\dot{\omega} &= P_m - P_{max}\sin(\delta) \\ P_{max} &= \frac{EV}{X}\sin(\delta) \\ X_{prefault} &= x_d + \frac{X_1 X_2}{X_1 + X_2} \end{aligned} \tag{1.24}$$

Suppose the machine is at steady state supplying P_{m0} power = mechanical input power (constant). Thus, we can estimate the system states (δ, ω) at equilibrium by substituting $P_m = P_{m0}$ and $(\dot{\delta}, \dot{\omega})$ = 0 and solving for states to get, $\omega_0 = 0, \delta_0 = \text{asin}(\frac{P_{m0}}{\frac{EV}{X_{prefault}}})$

Now suppose a 3 phase line to ground fault happens at the infinite bus followed by tripping of line 2 (X_2). During a ground fault in power systems, the voltage at the point of fault is driven to

0 ie. $V = 0$ resulting in $P_{max} = 0$. Thus the power angle curve for faulted system is x axis ($P = 0$). The net impedance for post fault system between the machine and infinite bus is $X_{postfault} = x_d + X_1 > X_{prefault}$ thus changing the power angle curve once the fault is clear. The equilibrium point (EP) for post fault system can be computed as, $\omega_1 = 0, \delta_1 = \text{asin}(\frac{P_{m0}}{\frac{EV}{X_{postfault}}})$. The power angle curves for all 3 conditions are shown.

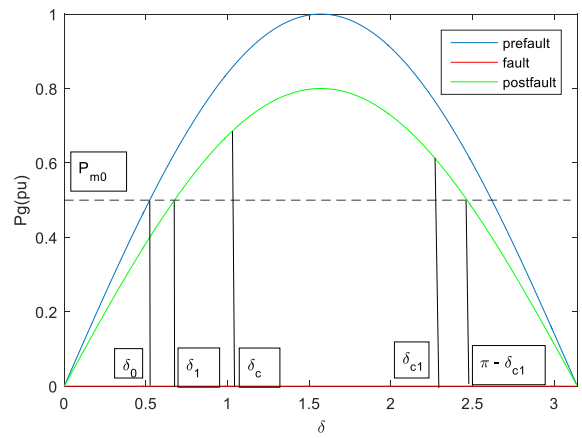

Figure 1.5 Power Angle Curve for Different Network Topologies

Now when a fault happens, $P_{m0} - P_{max}(= 0)\sin(\delta) > 0$ so ω, δ start increasing and the system starts moving right on the fault on power angle curve. Suppose the fault is cleared at $t = t_c$ when state values are δ_c, ω_c. When the fault is cleared, δ, ω don't change instantaneously. At this moment the system starts operating on the post fault power angle curve with generator output power given by $\frac{EV}{X_{postfault}}\sin(\delta_c)$. Since this value > P_{m0}, there is a negative power acting on the generator and it starts decelerating and the ω becomes 0 followed by negative. Now δ starts decreasing till it crosses δ_1 after which $P_{m0} >$ electrical output. Thus the system keeps oscillating about the equilibrium and we can assume the system has a chance at being stable. Now suppose the fault was cleared at a later time say $t = t_{c1}$ where , $\omega = \delta_{c1} > \frac{\pi}{2} > \delta_c, \omega_{c1} > \omega_c$. The generator starts decelerating but assume δ, ω continue to increase due to inertia and cross $\pi - \delta_1$. Here it is easy to see that $(\pi - \delta_1, 0)$ is another EP. At this moment, output power becomes < P_{m0} thus the generator again begins accelerating and is not able to come back the post fault equilibrium $\delta_1, 0$ thus becoming

unstable. This means that the threat of instability increases with increasing fault time which gives a maximum fault clearing time at which the system can safely return to its equilibrium, referred to as the critical clearing time (CCT/t_{cr}). Here it should be noted that this correlation between the degree of instability and the fault clearing time is valid only in the systems with no discrete changes in the post fault system which we will see in later sections. Clearing the fault after the CCT of the given post fault system results in an unstable trajectory if the given post fault system sustains. Situations where a few generators further trip after clearing the fault and stabilize the system though w.r.t. a new EP. The system responses for clearing of a fault at $t < t_{cr}$ and $t > t_{cr}$ are shown below.

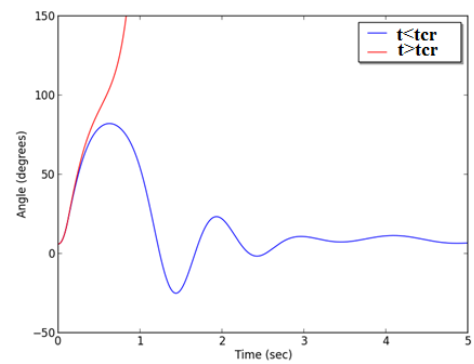

Figure 1.6 CCT

Based on our discussion, some of the factors that evidently impact transient stability are –

1. Generator parameters (M&D). Lower the value of these parameters, more is the speed gained during disturbance.
2. Base loading on the generator (P_{m0}). Higher the P_{m0}, more is the acceleration (for the same amount of power mismatch), more is the speed gained and more changes of δ reaches unstable value.
3. Terminal voltage E. Lower the E, lesser the impact of P_e for same increase in δ after the fault is cleared. We can see that when δ increases, P_e increases and becomes more than P_m which is the only force that opposes the generator which has gained speed during fault.

4. Post fault system impedances. Lower the impedance value, higher is the power angle curve and thus lower is the angle for same amount of output power.

Now the question comes, does having high penetration of PV generation have any impact on the transient stability? Some peculiar characteristics of this type of generation which seems to directly influence the parameters listed above are –

1. **Inverter based generation is 0 inertia:** While the conventional generation has rotating mass i.e. kinetic energy to provide inertia to certain system disturbances, inverter based generation does not [13]. Thus, displacing generation with inertia with a non-inertia one will effectively reduce the system inertia.
2. **Inverter protection standards:** As discussed in previous sections, renewable generation is made to trip offline during system abnormalities as these are not fully considered for grid support. This translates to losing generation even in events that may require excess generation.
3. **Location dependence:** The best solar resources may be at sites which are not grid optimal. Since the transmission systems are built around existing generation, this could mean requiring new transmission infrastructure. As the PV penetration increases, this could mean major changes in the network flows which means shifting the normal operating point of the system.

1.3 Multi-Machine Test System

We would be using Athay's 3 machine test system [14] for all our studies with modifications pertaining to each study. For simplicity uniform damping is assumed for all machines. Generator 3's states will be eliminated when taking a reference frame and thus won't be analyzed.

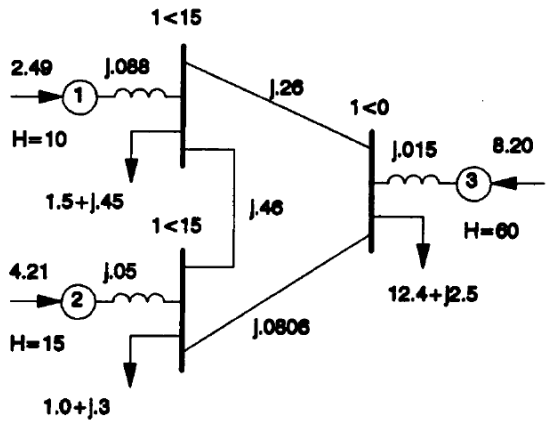

Figure 1.7 3-Machine System

Also, a network reduced model as discussed before would be used for modeling dynamics. While we restrict ourselves to a small system, our current focus is addressing the complexities associated with transient stability assessment that PV generation brings to the system. It makes it easy to visualize the problem. Here, it is also important to mention that while in theory it is possible to extend these techniques to large scale practical systems, it requires a great deal of computational resources as well as several rigorous simplifications to the model which in itself is a major challenge faced by the power systems community and is therefore is not within the scope of our current work.

1.4 Thesis Overview and Contribution

The thesis outline is as follows –

Chapter 2 gives the required background on the direct methods for transient stability assessment of power systems which make online assessment possible. The first part of the chapter provides a brief overview of the developments in the characterization of SRs for non-linear systems. This is followed by the energy function theory and the concept of controlling unstable equilibrium point (CUEP) for estimating the relevant portion of the stability region. Also discussed is the BCU method which is by far the most successful computationally feasible technique for finding the CUEP. The associated algorithms for implementing it are presented and their use is illustrated through a classical multi-machine system example. The second part of this chapter gives an overview of the application of sum of squares (SOS) programming to the

estimation of SRs of generalized non-linear systems. Starting with a background in polynomial algebra, relevant concepts in SOS programming are discussed. Finally, a systematic methodology using those concepts referred to as the expanding interior algorithm is revisited with its applications in transient stability assessment of power systems explored. Comparisons are drawn between the two methods. In order to reduce the inherent conservativeness in CCT estimate for a given disturbance when using Lyapunov's direct method, a technique is proposed which takes into account the disturbance trajectory to estimate the more relevant portion of the SR inspired by the idea of CUEP.

Chapter 3 deals with studying the impact of locational inertia displacement due to asynchronous generators (PV). Modeling the PV as a zero inertia machine, for a multi-machine power system, various scenarios are studied differing in the amount of generator displacement by PV and fault location. The impact on CCT for network faults is studied using the BCU method. Also, a visualization of the problem using a projection of relevant portion of stability region through constant energy surface is proposed. Next, studies are done to understand the changes in stability due to various redispatching strategies when accommodating PV. The percentages of PV accommodated by each generator are varied in a multi-machine system and the changes to the Potential Energy Boundary Surface (PEBS) are studied to draw conclusions on the stability.

Chapter 4 addresses the challenges associated with using the traditional direct methods for transient stability assessment of power systems having PV generation prone to tripping under disturbances. Two approaches differing in their treatment of the PV tripping phenomenon are proposed. Within each category, multiple techniques for stability assessment are developed using Lyapunov functions constructed through SOS programming. The first category treats the tripping of PV as an instability phenomenon since it puts the system under the risk of cascading outages. The aim here is the estimation of a SR with an added constraint of not allowing any PV to trip. To make the problem more tractable, multiple time independent formulations of the PV ride through constraints are developed. Finally, the constrained stability region (CSR) estimates are compared in terms of size to identify the best approach. The second category of techniques treats the power system as a switched system with the switching representing the tripping of

PVs. This treatment of the phenomenon is shown to be much less conservative. The non-monotonic relationship of the fault clearing time vs stability margin in such systems is demonstrated through an example which shows the need for revision of the widely accepted idea of CCT. The typical characteristics of switching due to cascaded PV tripping events are discussed. Starting with a demonstration of the limitation of the BCU method to the stability assessment of such systems, a technique is proposed which uses multiple CSRs with its effectiveness as well as the reliability demonstrated through a few examples. Another methodology is developed to study the repercussions of cascading tripping of PVs in a network. A metric called risk of instability is proposed that combines stability with probability of cascading scenarios. The benefit of blocking mutual tripping of some PVs in reducing the overall risk is demonstrated through an example. While still in the conceptual phase, this could have potential applications in strategizing the ride through curves to better deal with cascading events.

Chapter 2 Review of Direct Methods for Transient Stability Assessment

In a fault scenario, the power system broadly goes through three different configurations viz. pre fault system (usually at steady state), fault system (sustained disturbance) and post fault system (fault is removed along with changes in system topology usually tripping of line(s)). The stability is studied for the post fault system since it's the final configuration in the timeline of events. A trivial way of studying it would be to simulate the whole system trajectory [15] starting with pre fault system leading up to the post fault system and continue simulating till the system becomes stable/unstable [16]. While this is an attractive option, it is extremely slow. The eastern grid in US comprises of around 70,000 nodes which means a system of minimum 140,000 state equations to integrate. Normally on an 8 CPU, 3GHZ system it takes close to 60 minutes to simulate a single 30 second trajectory. Now imagine a utility wants to know the CCT in order to check if the response of the protection system meets the reliability requirements. For that, they will have to simulate the whole trajectory multiple times with different fault durations. On top of that if they want to analyze 1000 such faults, it might take months to do so. Thus, there was a need for techniques that bypassed the requirement to simulate the whole trajectory or particularly the post fault trajectory which is a major portion (> 95%) of the overall simulation. So, a lot of techniques were developed [14] [17] [18] which were derived from the idea of Lyapunov's second method thus having a theoretical justification and these fall under the category of direct methods for transient stability assessment. *If there is a neighborhood D of 0 and a continuously differentiable positive definite function V s.t. along all trajectories $\dot{V} < 0\ \forall x \in D$ then 0 is an asymptotically stable solution* [19]. Thus, the idea is to formulate a scalar function of system states which decreases in the neighborhood of the equilibrium (say the origin) along all the trajectories starting within it. One or multiple thresholds on its value are used as the stability limit. If the value for this function calculated at the time of fault clearing violates that limit, it means there are higher chances of the emerging post fault trajectory being unstable. The idea can be understood by using an analogy of a ball inside a

bowl [8] where the position at the bottom of the bowl is a stable equilibrium point (SEP) for this system and the inside of the bowl is the corresponding SR with the bowl itself representing the potential energy surface. The ball has a kinetic energy (determined by its velocity) and potential energy (determined by its position on the bowl). Now, when a disturbance is introduced say a push to the ball, it gains kinetic energy and it starts travelling up the walls of the bowl. As its climbing, a part of the kinetic energy gets converted to potential energy and the ball slows down. As long as the total energy does not make the ball cross the rim of the bowl and get out, it will eventually return to the SEP (granted there's loss of energy in some form else it oscillate forever). In direct methods, the search is for a function that characterizes the energy in this bowl and as well as the rim (boundary). As long as the energy injected is lower than that required reaching the rim, system will remain inside the bowl and thus stable.

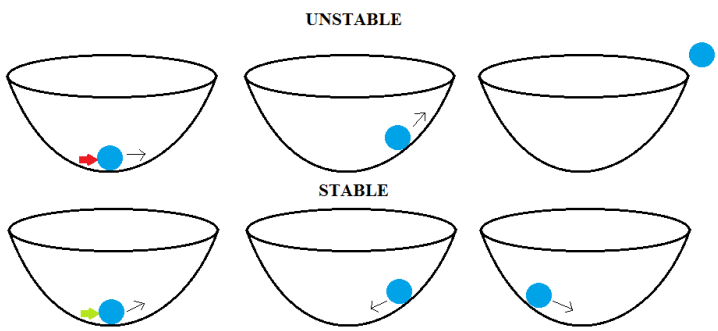

Figure 2.1 Rolling Ball Analogy

These techniques became really popular and the application of the most successful one out of those called the BCU method [17] has been demonstrated on a practical system of the east coast utilities [20]. Due to its success as well as a strong theoretical justification, we will be using BCU in our work to analyze the impact of inertia displacement and generator dispatch due to PV on stability. However, BCU as well as the rest of the energy function theory is built to deal with unconstrained autonomous non-linear systems. The inverter protection adds complexity to the system making the applications of BCU limited. Therefore, for studying the impact of inverter protection on transient stability, we taking a classical Lyapunov's direct method approach. A systematic way of constructing Lyapunov functions would also be discussed using sum of squares (SOS) programming.

With the growth of synchrophasors [21][22][23] in the last decade which provide time synchronized high frequency voltage and current phasor measurements as well as advancements in power system linear state estimation [24][25], data driven techniques have emerged aimed at solving a lot of problems such as system parameter validation [26], stability assessment [27][28] , control [29][30][31], islanding detection [32] etc. For stability assessment, these mainly operate by interpolating/ extrapolating the results from offline assessments made. One of the prohibitive requirements of these techniques is the creation of offline data base which is done through time domain simulations. Also, these techniques require a considerable portion of the post fault trajectory to be simulated online in order to make a decision and are also plagued by major reliability concerns as with changing system the offline data base may not be able to capture all types of instabilities.

2.1 Boundary of Stability Region Based Controlling Unstable Equilibrium (BCU) Method and its Development

The BCU method is based on the idea of approximating the portion of stability boundary relevant to the disturbance under study. Before proceeding with the details of the technique, it is important to give the reader a general background in non-linear dynamics.

Definition 2.1 (Manifold): It is a topological space that locally resembles a Euclidean space near each point. An n dimensional manifold has a neighborhood that is homeomorphic (continuous invertible function mapping) to Euclidean space of dimension n.

Definition 2.2 (Tangent Space of a Manifold): The tangent space $T_p(M)$ [33] of a manifold M at point p is a collection of all possible directions (vectors) from that point along the manifold. In the figure below, the tangent space of the point on sphere is shown.

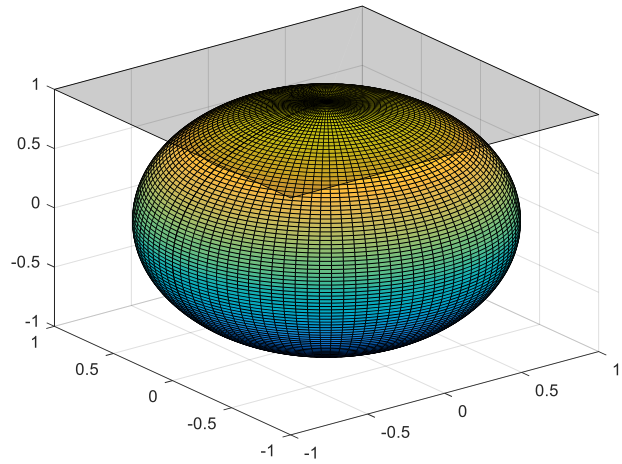

Figure 2.2 Tangent space (grey) of a manifold (sphere) at point (0,0,1)

Definition 2.3 (Transverse Intersection of Manifolds): Two manifolds A and B injectively immersed in a manifold M intersect transversally when –

1. $T(A) + T(B) = T(M)$ at all points of intersection.

   Or

2. They don't intersect at all.

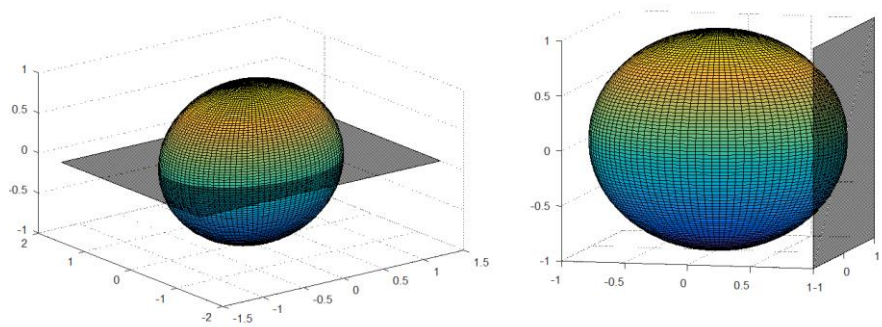

Figure 2.3 Transverse (left) vs Non Transverse (right) Intersection of Manifolds (sphere and plane)

Definition 2.4 (Equilibrium Point (EP)): Given an autonomous time invariant system defined by,

$$\dot{x} = f(x) \tag{2.1}$$

An EP x_{ep} is a stationary point s.t. $f(x_{ep}) = 0$. The various types of EPs are –

1. Hyperbolic:
    a. Stable: Attracts all the trajectories near it to itself. Characterized by all eigen values of $\frac{\partial f}{\partial x}$ having negative real part. This can be visualized as bottom of a bowl where any ball (trajectory) starting inside it settles to it as shown in Figure 2.1.
    b. Type k Unstable: Can be visualized as repelling trajectories on a k dimensional manifold. Characterized by k eigen values of $\frac{\partial f}{\partial x}$ having positive real part.

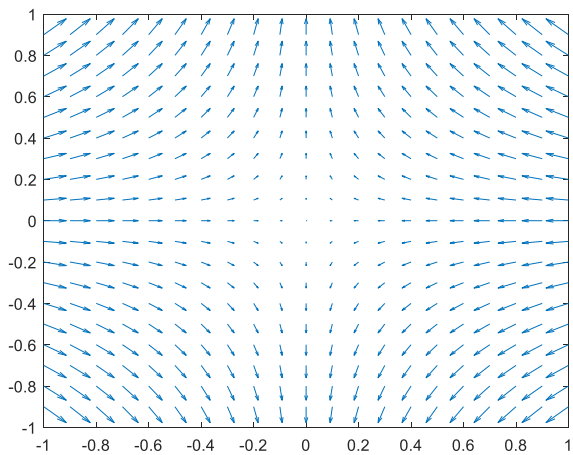

Figure 2.4 Type 1 UEP

For example, Figure 2.4 shows the dynamics around a type 1 UEP (at origin). It attracts trajectories approaching it along x axis while repels along y axis.

2. Non Hyperbolic: EPs with one or more eigen values having 0 real part. Example of dynamics around such points are shown in the following figures.

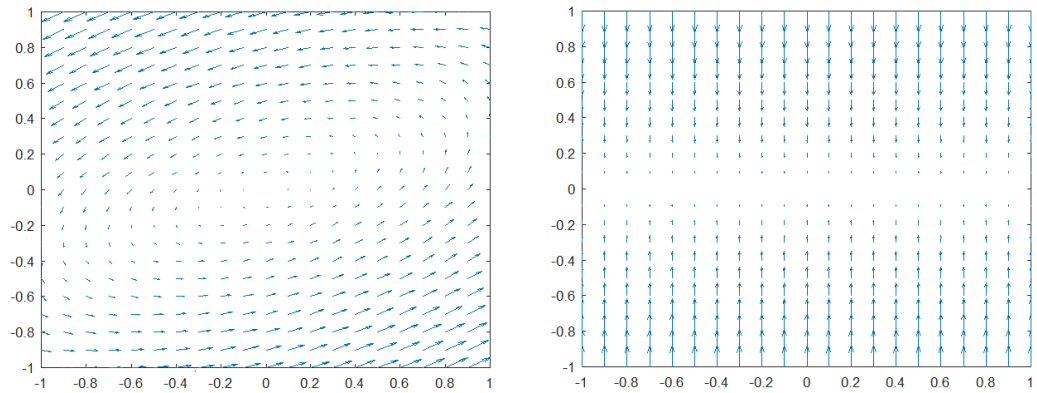

Figure 2.5 Some Non-Hyperbolic EPs. . Left Plot: Both Imaginary Eigen Values. Right Plot: Both Real Eigen Values - One Negative One 0.

Definition 2.5 (Stable/Unstable Manifold): For a given EP x_{ep}, these are defined as –

1. Stable Manifold: Manifold on which all trajectories eventually converge to x_{ep}. The dimension of stable manifold is equal to the number of Eigen values having negative real parts [33].

$$W^s(f, x_{ep}) = \{x_i \; st. \; x(0) = x_i \Rightarrow \lim_{t \to \infty} x(t) = x_{ep}\} \quad (2.2)$$

2. Unstable Manifold: Manifold on which all reversed (negative time) trajectories converge to x_{ep}. The dimension of stable manifold is equal to the number of Eigen values having negative real parts.

$$W^u(f, x_{ep}) = \left\{x_i \; st. \; x(0) = x_i \Rightarrow \lim_{t \to -\infty} x(t) = x_{ep}\right\} \quad (2.3)$$

It also means that that there could be points in the immediate neighborhood of an EP that don't belong to either of the manifolds. Thus, it would be incorrect to assume that all the trajectories repelled by equilibrium belong to its unstable manifold.

Definition 2.6 (Invariant Set): A set of points in state space st. all the trajectories starting inside it remain in it.

Definition 2.7 (Stability Region & Stability Boundary): A set of all the points lying on the stable manifold of a SEP x_{ep} make up its SR. It is an open and invariant set and denoted by the symbol

$A(x_{ep})$. The stability boundary $\partial A(x_{ep})$ (also called the separatrix) is defined as a set of limiting points in the immediate neighborhood of SR and is not a part of SR itself. In a system with two or more EPs, the dimension of the stability boundary is $n-1$ while that of the SR is n where n is the dimension of the state space (x).

Definition 2.8 (Limit Cycle): It is an isolated close trajectory. Shown below is an example of a stable(attracts nearby trajectories) limit cycle (green).

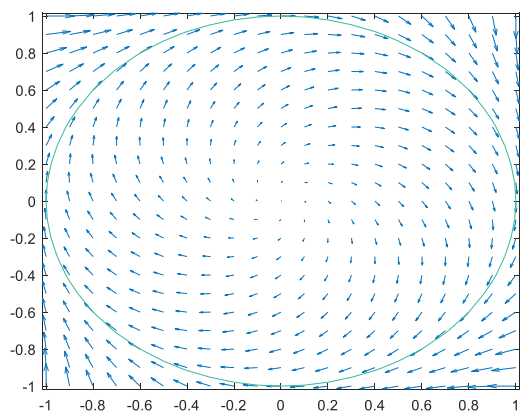

Figure 2.6 Attracting Limit Cycle (green)

Now we move on to characterizing the number and types of EPs lying on the stability boundary based some concepts from Morse Theory followed by the idea of Energy functions and BCU method.

2.1.1 Characterization of Stability Boundary for Non Linear Dynamical System

In many emerging research areas, estimating SRs continues to play an important role. In this section, derivations of dynamical and topological properties of stability boundary are presented. This section is a derived from [34]. We begin by assuming that all the EPs of the system under study are hyperbolic. Now a few theorems are discussed that characterize the equilibrium or limit cycles on the stability boundary. The derivations for these are omitted.

Theorem 2.1 Consider a general nonlinear continuous dynamical system $\dot{x} = f(x)$. Let $A(x_s)$ be the SR of an asymptotically stable equilibrium x_s. Let $\hat{x}$ be a hyperbolic EP. Then:

(a) If $\{W^u(\hat{x}) - \hat{x}\} \cap \overline{A(x_s)} \neq \emptyset$ then $\hat{x} \in \partial A(x_s)$; conversely if $\hat{x} \in \partial A(x_s)$ then $\{W^u(\hat{x}) - \hat{x}\} \cap \overline{A(x_s)} \neq \emptyset$.

(b) Suppose $\hat{x}$ is not a source then $\hat{x} \in \partial A(x_s)$ iff $\{W^s(\hat{x}) - \hat{x}\} \cap \partial A(x_s) \neq \emptyset$

A similar thing can be said about closed orbits.

Theorem 2.2 (Further characterization of EP on stability boundary) Assuming the following about the stability boundary –

(A1) All the EPs on $\partial A(x_s)$ are hyperbolic

(A2) The stable and unstable manifolds of EPs on $\partial A(x_s)$ intersect transversally

(A3) Every trajectory on $\partial A(x_s)$ approaches one of the EPs as $t \to \infty$

Then

(1) $\hat{x} \in \partial A(x_s)$ iff $\{W^u(\hat{x}) - \hat{x}\} \cap A(x_s) \neq \emptyset$

(2) $\hat{x} \in \partial A(x_s)$ iff $W^s(\hat{x}) \subseteq \partial A(x_s)$

Here it is easy to show that due to assumption (A3), $W^s(\hat{x}) \subseteq \partial A(x_s)$ implies $\partial A(x_s) = \cup_i W^s(\hat{x}_i)$ .This result can be extended to other hyperbolic critical element (closed orbit).

Lemma 2.3 If hyperbolic critical elements x_i and x_j satisfy the following condition regarding intersection of manifolds – $\{W^u(x_i) - x_i\} \cap \{W^s(x_j) - x_j\} \neq \emptyset$ then $\dim(W^u(x_i)) \geq \dim(W^u(x_j))$

Theorem 2.4 (Structure of EPs on stability boundary) For nonlinear autonomous dynamical system containing two or more SEPs, if assumptions (A1) and (A3) are satisfied then the stability boundary contains atleast one type-1 UEP. If furthermore the SR is bounded then the boundary must contain a source as well.

2.1.2 Energy Function

Consider a general nonlinear autonomous dynamical system –

$$\dot{x} = f(x) \tag{2.4}$$

We say a C^r function $V: \mathbb{R}^n \to \mathbb{R}$ is an energy function for this system if the following conditions are satisfied –

(E1) Derivative of V along any system trajectory is non positive i.e.

$$\dot{V}(x) = \frac{\partial V}{\partial x} f(x) \leq 0 \tag{2.5}$$

(E2) If $x(t)$ is not an equilibrium then,

$$\dot{V}(x) < 0 \tag{2.6}$$

(E3) Bounded value of V for trajectory $x(t)$ implies $x(t)$ is bounded.

While properties (A1) and (A2) are generic, it is easy to show that systems admitting energy functions satisfy property (A3) as well (using the properties (E1) and (E2) of energy functions).

2.1.3 Energy Function for Power Systems Network Reduced Model

Revisiting the power system network reduced model in COA frame as discussed in 1.2.3–

$$\begin{gathered}
\dot{\delta_i}^{coa} = \omega_i^{coa} \\
M_i \dot{\omega_i}^{coa} = P_{m_i} - P_{e_i} - \left(\frac{M_i}{M_{total}}\right) \times P_{coa} - D_i \omega_i^{coa} \\
P_{e_i} = E_i \sum_j E_j \times \left(G_{ij} \cos\left(\delta_i^{coa} - \delta_j^{coa}\right) + B_{ij} \sin\left(\delta_i^{coa} - \delta_j^{coa}\right)\right) \\
\delta_i^{coa} = \delta_i - \delta_0 \\
\delta_0 = \frac{\sum_i M_i \, \delta_i}{M_{total} = \sum_i M_i}, \omega_0 = \frac{\sum_i M_i \, \omega_i}{M_{total} = \sum_i M_i} \\
P_{coa} = \sum_i (P_{m_i} - P_{e_i})
\end{gathered} \tag{2.7}$$

To find the energy function of the above system, we write $\dot{\omega_i^{coa}} = \omega_i^{coa} \times \left(\frac{d\omega_i^{coa}}{d\delta_i^{coa}}\right)$ to get –

$$M_i \int \omega_i^{coa} d\omega_i^{coa} = \int \left(P_{m_i} - P_{e_i} - \left(\frac{M_i}{M_{total}} \right) \times P_{coa} - D_i \omega_i^{coa} \right) d\delta_i^{coa} \tag{2.8}$$

For the time being assume states of n_g^{th} generator not replaced by those of others. Now adding the equation $\forall i = 1{:}\, n_g$, rearranging and the substituting the expression for P_{ei} as before,

$$\sum_{i=1}^{n_g} \int M_i \omega_i^{coa} d\omega_i^{coa} - \sum_{i=1}^{n_g} \int \left(P_{m_i} - G_{ii} E_i^2 \right) d\delta_i^{coa} + \sum_{i=1}^{n_g - 1} \sum_{j=i+1}^{n_g} \int B_{ij} \sin\left(\delta_i^{coa} - \delta_j^{coa} \right) d\left(\delta_i^{coa} - \delta_j^{coa} \right) + \sum_{i=1}^{n_g - 1} \sum_{j=i+1}^{n_g} \int G_{ij} \cos\left(\delta_i^{coa} - \delta_j^{coa} \right) d\left(\delta_i^{coa} + \delta_j^{coa} \right) = - \sum_{i=1:n_g} \int D_i \omega_i^{coa} d\delta_i^{coa} - \frac{P_{coa}}{M_{total}} \sum_{i=1:n_g} \int M_i d\delta_i^{coa} \tag{2.9}$$

The last term on the RHS (containing P_{coa}) becomes 0 since $\sum_{i=1:n_g} M_i d\delta_i^{coa} = 0$. The left hand side can be used as an energy function W. To check the first 2 properties of energy functions, differentiate wrt time. The right hand side gives –

$$\dot{W} = - \sum_{i=1:n_g} D_i \omega_i^{coa} \left(\frac{d\delta_i^{coa}}{dt} \right) = - \sum_{i=1:n_g} D_i (\omega_i^{coa})^2 \leq 0 \tag{2.10}$$

$\dot{W}$ is 0 only when $\omega_i^{coa} = 0 \; \forall i$ which is only at EPs. The boundedness of trajectories for bounded value of energy function can also be proven [34].

Further simplifying the terms for energy function by integrating them from state vector x_{sep} to x and writing them separately –

$$\begin{aligned} Kinetic\ Energy &= \sum_{i=1}^{n_g} \int M_i \omega_i^{coa} d\omega_i^{coa} = \sum_{i=1}^{n_g} \frac{1}{2} M_i (\omega_i^{coa})^2 \\ UE_1 &= - \sum_{i=1}^{n_g} (P_{m_i} - G_{ii} E_i^2) \times (\delta_i^{coa} - \delta_i^{coa}{}_{sep}) \\ UE_2 &= \sum_{i=1}^{n_g - 1} \sum_{j=i+1}^{n_g} \int B_{ij} \sin\left(\delta_i^{coa} - \delta_j^{coa} \right) d\left(\delta_i^{coa} - \delta_j^{coa} \right) \\ &= - \sum_{i=1}^{n_g - 1} \sum_{j=i+1}^{n_g} \int B_{ij} \left(\cos\left(\delta_i^{coa} - \delta_j^{coa} \right) - \cos\left(\delta_i^{coa}{}_{sep} - \delta_j^{coa}{}_{sep} \right) \right) \end{aligned} \tag{2.11}$$

$$UE_{path} = \sum_{i=1}^{n_g-1} \sum_{j=i+1}^{n_g} \int G_{ij} \cos\left(\delta_i^{coa} - \delta_j^{coa}\right) d\left(\delta_i^{coa} + \delta_j^{coa}\right)$$

The last term (containing conductances G) is a path dependent term and does not have a closed form expression. This term is usually evaluated analytically using one of the following two schemes [35] –

1. Ray Approximation – Writing δ_j^{coa} as a linear combination of $\delta_i^{coa}, \delta_i^{coa}{}_{sep}, \delta_j^{coa}{}_{sep}$ by assuming a linear trajectory and integrating in one variable. No mathematical justification.
2. Trapezoidal Rule – Standard multi step trapezoidal rule. Known to be more accurate than Ray approximation. As an example of using single step trapezoidal rule for integration of one of the path dependent terms say $\int G_{ij} \cos\left(\delta_i^{coa} - \delta_j^{coa}\right) d\left(\delta_i^{coa} + \delta_j^{coa}\right)$ from time t_1 to t_2, we compute it as –

   $\int G_{ij} \cos\left(\delta_i^{coa} - \delta_j^{coa}\right) d\left(\delta_i^{coa} + \delta_j^{coa}\right) = G_{ij}(cos\left(\delta_i^{coa}(t_1) - \delta_j^{coa}(t_1)\right) +$
   $cos\left(\delta_i^{coa}(t_2) - \delta_j^{coa}(t_2)\right)) \times \frac{(\delta_i^{coa}(t_2)+\delta_j^{coa}(t_2))-(\delta_i^{coa}(t_1)+\delta_j^{coa}(t_1))}{2}$

A generic network reduced model for power systems is of the form

$$\begin{aligned} T\dot{x} &= -\frac{\partial UE}{\partial x}(x,y) + g_1(x,y) \\ \dot{y} &= z \\ M\dot{z} &= -Dz - \frac{\partial UE}{\partial y}(x,y) + g_2(x,y) \\ Energy\ Function &= \frac{1}{2} z^T M z + U(x,y) + U_{path}(x,y) \end{aligned} \tag{2.12}$$

Where x, y & z are state variables, U denotes the potential energy term corresponding to the gradient part of the field (path independent) while U_{path} is the path depended term resulting from the non-gradient portion of vector field (g_1, g_2). It has been seen that for power systems with high lossy terms (marked by large values of G(not too common)), energy functions are not possible due to a possibility of having non equilibrium critical elements (like limit cycles). In case

of a limit cycle, having an ever decreasing energy function would mean it will go to negative infinity ie unbounded but the trajectory in a limit cycle is bounded as we know which leads to a contradiction of energy function property (E3). To deal with this, the concept of generalized energy functions was proposed in [36]. These are no longer forced to decrease along all trajectories. In the present work, we will not be exploring this idea further.

2.1.4 Controlling Unstable Equilibrium (CUEP)

For systems admitting energy functions, the task is to estimate the SR for a given SEP. Here, we will present a few theorems that will help characterize the SR using level sets of energy function.

Theorem 2.5 (Constant Energy Surface and Stability Region) Let x_s be a SEP of system $\dot{x} = f(x)$ then the set $S(r) = \{x \in \mathbb{R}^n | V(x) \leq r\}$ contains only one connected component having a non empty intersection of with SR $A(x_s)$ iff $r > V(x_s)$ where V is the energy function.

Based on the above theorem, one way of to estimate SR would be to choose the biggest level set of V contained inside the SR. As we know based on Theorem 2.2 that the stability boundary is the union of stable manifolds of some UEP and V decreases along all trajectories (point on the stable manifold of an EP with minimum energy is the EP itself), the point on the stability boundary with minimum energy should be a UEP and is referred to as the closest UEP [18] and thus the connected component of level set $\{V \leq V(closest\ UEP)\}$ intersecting with the SR is the one contained inside it. For the example given below a system having two UEP's (δ_1, δ_2) on the stability boundary of SEP δ_s with the true SR as $\forall \delta \in \delta_1, \delta_3)$. The estimate of SR by this method is using the minimum energy UEP δ_1's energy function value is $\forall \delta \in \delta_1, \delta_4 < \delta_3)$.

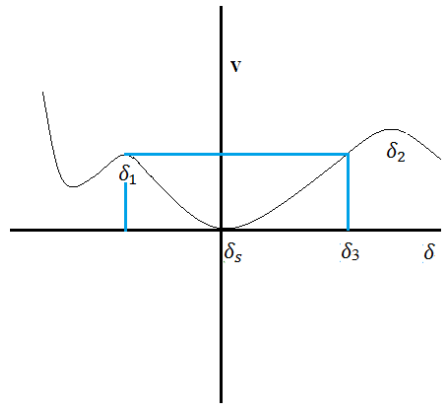

Figure 2.7 Closest UEP Stability Region Estimate by Min Energy UEP δ_1

This is however seen to give a conservative estimate since a significant portion of the SR given by $\forall\delta \in \delta_4, \delta_3)$ has higher energy. Thus, the direction in which stability boundary is to be estimated should be taken into account which leads us to the idea of controlling unstable equilibrium (CUEP) method proposed in the 80's [37]. This method utilizes the fault on trajectory to estimate the part of stability boundary relevant to the particular fault. By Theorem 2.2, under given assumptions, the stability boundary is the union of stable manifolds. Thus, the point at which the fault trajectory intersects the stability boundary (exit point) should lie on stable manifold of some equilibrium on the stability boundary referred to as the CUEP. It is safe to say that the energy of the exit point should be greater than the CUEP. Thus, the constant energy surface passing through CUEP can be used to accurately approximate the relevant part of the stability boundary which the fault on trajectory is approaching. Thus if the energy function value at the time of fault clearing is less than $V(x_{cuep})$, the post fault trajectory starting at that point would remain stable. It should be kept in mind that the CUEP for each fault on trajectory depends on the direction it takes the system in state space. This implies that there could be multiple faults which share the same CUEP. Continuing the previous example, the SR estimated for disturbances in positive and negative x direction respectively from the SEP are as shown below. We can see that this technique covers a larger portion of SR.

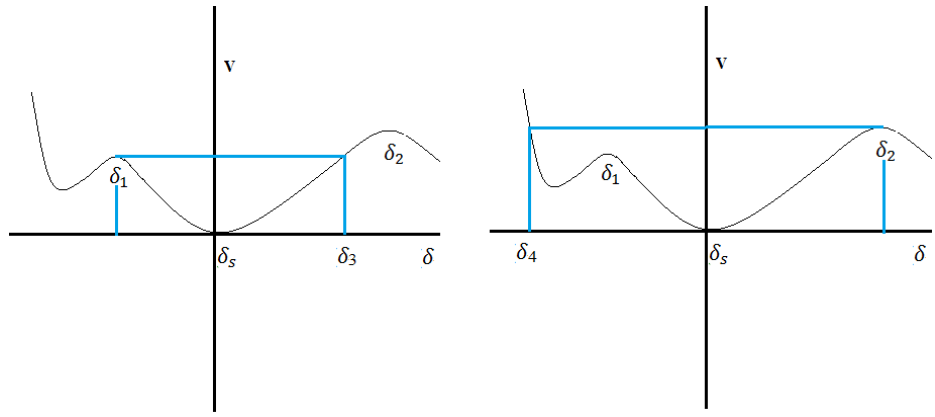

Figure 2.8 Controlling UEP Stability Region estimates for faults approaching the left boundary (left) and the right boundary (left)

2.1.5 BCU Method

Based on the previous discussion, computing the CUEP is vital for direct stability analysis. The Boundary of SR-based Controlling Unstable Equilibrium Point (BCU) method [17] is a method that uses the special structure of the power systems stability model to find the CUEP. This makes it computationally efficient for large scale power systems. First, an artificial reduced state model is defined that captures all the EPs on the stability boundary of the original model. This is followed by computing the CUEP of this reduced model which is much easier to compute.

The expressions for generic network reduced power systems model as introduced before along with a reduced state model chosen for the BCU are shown below.

Original System Model	Reduced State Model
$T\dot{x} = -\frac{\partial UE}{\partial x}(x,y) + g_1(x,y)$ $\dot{y} = z$ $M\dot{z} = -Dz - \frac{\partial UE}{\partial y}(x,y) + g_2(x,y)$	$T\dot{x} = -\frac{\partial UE}{\partial x}(x,y) + g_1(x,y)$ $\dot{y} = -\frac{\partial UE}{\partial y}(x,y) + g_2(x,y)$

Here, it can be noticed that the reduced state system's energy function is the same as the numerical potential energy function (including loss terms) of the original system. This system is also called the gradient system and the terms would be used interchangeably through rest of

the work. The required properties for the chosen reduced state model to be valid and favorable for BCU are as follows –

Static Properties

(S1) The location of reduced state model's EPs should correspond to that of the original system. For example in the above model,$(\hat{x}, \hat{y})$ is an equilibrium of reduced model iff $(\hat{x}, \hat{y}, 0)$ is that of the original model.

(S2) The corresponding EPs of both systems are of the same type. i.e. if $(\hat{x}, \hat{y}, 0)$ is a type -1 UEP for original system, $(\hat{x}, \hat{y})$ is a type-1 for reduced state system.

Dynamic Properties

(D1) Reduced state model should admit an energy function.

(D2) An EP $(\hat{x}, \hat{y})$ is on stability boundary $\partial A(x_s, y_s)$ of reduced state system iff $(\hat{x}, \hat{y}, 0)$ is on $\partial A(x_s, y_s, 0)$ of the original system.

(D3) It is computationally feasible to detect when the fault on trajectory intersects the stability boundary of the reduced state model.

The properties (S1), (S2), (D1) and (D2) for comparing static and dynamic relationships between original model and reduced state model are tested incrementally by comparing a list of intermediate systems [35].

The two necessary conditions to prove the properties (S2) and (D2) for the chosen reduced state system are –

1. Loss terms sufficiently low (almost always true for transmission networks).
2. Transverse intersection of stable and unstable manifolds of UEP's on the stability boundary of the original system (majorly impacts (D2)).

The condition number 2 (transverse intersection) is almost impossible to test for practical systems. However it has been shown [38] [39] that failure of this property does not always

mean failure of BCU in computing the correct CUEP. A weaker version of this property (D2') is sufficient for BCU to still give accurate estimates.

(D2') The reduced state controlling UEP lies on the stability boundary of the reduced state system iff the corresponding UEP lies on the stability boundary of the original system.

The reduced state system exit point along a given fault on trajectory is the first local maxima of potential energy. Thus, it can be easily computed without resorting to post fault system's time domain simulation also proving property (D3).

We will now obtain expressions for the familiar n_g machine power system network reduced model in COA reference frame while formulating the numerical tricks for implementing BCU for this type of system. We start by writing the reduced-state system–

$$\dot{\delta_i}^{coa} = P_{m_i} - P_{e_i} - \left(\frac{M_i}{M_{total}}\right) \times P_{coa}$$

$$P_{ei} = E_i \sum_j E_j \times (G_{ij} \cos\left(\delta_i^{coa} - \delta_j^{coa}\right) + B_{ij} \sin\left(\delta_i^{coa} - \delta_j^{coa}\right)) \tag{2.13}$$

$$P_{coa} = \sum_{i=1}^{n_g} (P_{mi} - P_{ei})$$

The lie derivative of numerical potential energy function along the fault on trajectory $(\delta_{fault}^{coa}, \omega_{fault}^{coa})$ can be formulated as –

$$-\sum_{i=1}^{n_g} \left(P_{mi} - P_{ei}(\delta_{fault}^{coa}) - \frac{M_i}{M_{total}} \times P_{coa}(\delta_{fault}^{coa})\right) \times \omega_{i_{fault}}^{coa} = -\sum_{i=1}^{n_g} \left(P_{mi} - P_{ei}(\delta_{fault}^{coa})\right) \times \omega_{i_{fault}}^{coa} \tag{2.14}$$

Now the second term on the right hand side is 0 because $\sum_{i=1}^{n_g} M_i \omega_i^{coa} = 0$ (explained previously). Thus, whenever the above metric changes sign from positive to negative means a local numerical UE maxima has occurred and the given point is the exit point of reduced state system as discussed before. Under ideal conditions, the BCU algorithm would be as shown below.

Algorithm 2.1 Conceptual BCU Method

1. Obtain SEP of post fault system $(\delta_{sep}, 0)$.
2. Integrate the fault on trajectory $(\delta_{fault}, \omega_{fault})$ till the exit point δ_{exit}^{red} of reduced state system is detected i.e. the point at which the projected fault trajectory exits the SR of reduced system.
3. Using δ_{exit}^{red} as initial condition, integrate the post fault reduced-state system till the controlling UEP δ_{cuep}^{red} is reached for the reduced state system.
4. The controlling UEP for original system is then assumed to be $(\delta_{cuep}^{red}, 0)$. Use the energy at $(\delta_{cuep}^{red}, 0)$ as the threshold for losing stability.

There are however multiple issues when it comes to implementation. While step 2 can be implemented as discussed before, step 3 is difficult to get correct. Even a slight error in the reduced state system exit point could result in a trajectory either converging to the SEP or going out of it. Thus, a stability boundary following procedure presented in [35] inspired by the idea proposed in [40] was used. The idea is based on the topology of reduced state system's stability boundary which has maximum potential energy transversal to it [41] and is comprised of stable manifolds of UEPS on it as discussed before.

Algorithm 2.2 Stability Boundary Following (From Exit point to Controlling UEP)

1. i = 1, $\delta_0 = \delta_{exit}$ (Starting the trajectory with exit point of reduced state system)
2. Integrate post fault reduced state system trajectory starting from δ_0 for ~ 0.3 s to get δ_1.
3. If $\sum_{i=1:n_g-1} |P_{m_i} - P_{e_i} - \left(\frac{M_i}{M_{total}}\right) \times P_{coa}|$ reaches a local minima at point δ_{mgp}, GOTO Step 5.
4. Find local maxima (δ_2) of numerical UE along the ray $\delta_1 \rightarrow \delta_{sep}$ starting from δ_1. Set $\delta_0 = \delta_2$. i = i + 1. GOTO Step 2.
5. Stop. δ_{mgp} is called the Minimum Gradient Point (MGP)

As for steps 1 (finding SEP of post fault system) and 4 (finding CUEP for post fault system) for BCU, we know that power system equations admit fractals when using Newton Raphson Algorithm [42] [43] for solution. Thus, it is a necessity for the starting point of Newton Raphson

to be sufficiently close to the equilibrium of interest. A good initial condition for SEP of post fault system is the SEP of pre fault system (usually the steady state solution where we begin the BCU). However, in rare cases when the technique fails, a method proposed in [44] can be used. As for the CUEP, the MGP obtained from stability boundary following procedure as presented above serves as a good initial condition. If the equilibrium found by the found MGP is the SEP itself, continue the algorithm from step 2.

Algorithm 2.3 Computing SEP and CUEP for Post-Fault System (Newton-Raphson)

The EPs of the gradient system (consequently those of original system) are solutions to the equations (according to the definition of equilibrium) –

$$f(\delta) = \left[P_{m_i} - P_{e_i} - \left(\frac{M_i}{M_{total}}\right) \times P_{coa} = 0 \; \forall i \in [1, n_g - 1]\right]$$

Where $\delta \in R^{n_g - 1}$

Here care must be taken that the n_g^{th} generator angle is not modeled as an independent state (correspondingly n_g equations being solved) else the system of equations is overdetermined as discussed before.

1. k = 0. $\delta^k = \delta_{mgp}(for\ CUEP)\ OR\ \delta_{sep_{prefault}}(for\ SEP)$
2. $\delta^{k+1} = \delta^k - \left[\frac{\partial f}{\partial \delta}(\delta^k)\right]_{(n_g-1)\times(n_g-1)} \times [f(\delta^k)]_{(n_g-1)\times 1}$
3. If $\left\|[f(\delta^{k+1})]_{(n_g-1)\times 1}\right\| > 10^{-6}$, k = k + 1. GOTO Step 2.
4. $\delta_{ep} = \delta^k$

Since BCU relies on some big assumptions in order to find the CUEP through the reduced state system, there have been numerous counter examples that showed where BCU failed. One key example can be seen in [45] where the failure is shown for under-damped system and high impedance fault. In order to deal these situation, a BCU-Exit Point method is used [35] which is basically checking if the CUEP found by BCU is actually on the stability boundary or not. This is called the boundary check and is done through simulating a single post fault trajectory. If this test fails then it means that the BCU results are wrong for the fault under study and the transient stability assessment is done through the traditional time domain simulation.

Algorithm 2.4 Boundary Check

1. Select a point in state space (x_{test}) in the immediate neighborhood of the found CUEP (x_{cuep}), likely to be inside the SR of the SEP (x_{sep}).

$$x_{test} = 0.99x_{cuep} + 0.01x_{sep}$$

2. Integrate the original system's trajectory starting from this point.
3. If it converges to x_{sep}, the found CUEP is on the stability boundary else not.

Let us now try to go over the whole BCU process through the following example to help the reader better understand it.

Example 2.1 Given the following 3-machine system. We want to estimate the CCT for the fault at bus 1 cleared by tripping the line connecting between bus 1 and 2.

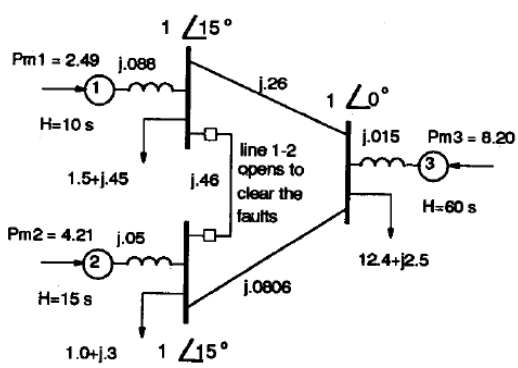

Figure 2.9 Example 2.1 Test System

Damping coefficient assumed is $\frac{D}{M} = \frac{D}{\frac{2H}{\omega_s}} = 4$. The fault impedance is $j5e^{-6}$. First step is creating the network reduced model (only internal generator nodes). Following the Algorithm 1.1, the resulting reduced system Y matrices for pre, fault and post fault configurations are

$$Y_{pre} = \begin{bmatrix} 0.6512 - 4.0176i & 0.1651 + 1.0533i & 0.5951 + 2.3641i \\ 0.1651 + 1.0533i & 0.4916 - 7.7883i & 1.1559 + 6.0228i \\ 0.5951 + 2.3641i & 1.1559 + 6.0228i & 8.6026 - 12.3444i \end{bmatrix}$$

$$Y_{fault} = \begin{bmatrix} 0.0000 - 11.3630i & 0.0000 + 0.0001i & 0.0000 + 0.0002i \\ 0.0000 + 0.0001i & 0.4575 - 7.9386i & 1.0472 + 5.6876i \\ 0.0000 + 0.0002i & 1.0472 + 5.6876i & 8.2852 - 13.0850i \end{bmatrix}$$

$$Y_{post} = \begin{bmatrix} 0.8153 - 3.1027i & 0.0729 + 0.2504i & 0.5729 + 2.2203i \\ 0.0729 + 0.2504i & 0.5277 - 7.0866i & 1.1673 + 6.1488i \\ 0.5729 + 2.2203i & 1.1673 + 6.1488i & 8.6055 - 12.3218i \end{bmatrix}$$

The pre fault equilibrium $(\delta_1, \delta_2, \omega_1, \omega_2)$ in COA reference frame is $(0.2473, 0.2430, 0, 0)$. Here it should be noted that the unit for δ is radians. The post fault SEP (x_s) found using Algorithm 2.3 is $(0.2468, 0.2431, 0, 0)$ which can be seen as quite close to pre fault one due to high impedance of line tripped so no major changes in Y matrix. Next, the fault on trajectory is simulated till the gradient system exit point (x_{exit}^{grad}) is found at $(2.1081, 0.0699, 0, 0)$ using the change in sign of exit metric value (lie derivative of UE along fault trajectory) as defined before.

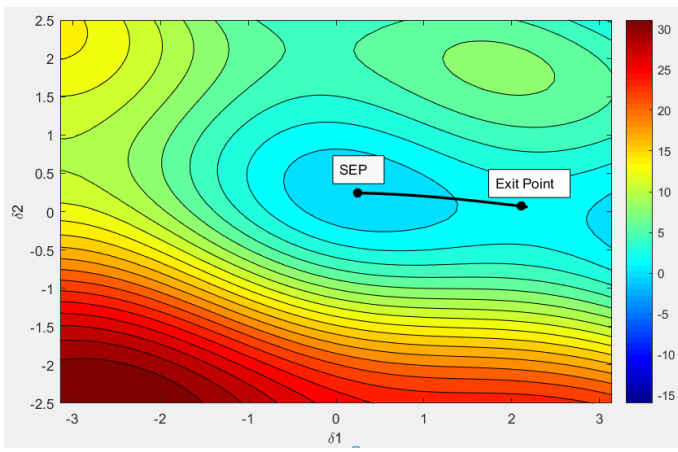

Figure 2.10 Example 2.1 Fault On Trajectory in Post Fault UE Surface

The trajectory in angle domain is shown above on the UE surface.

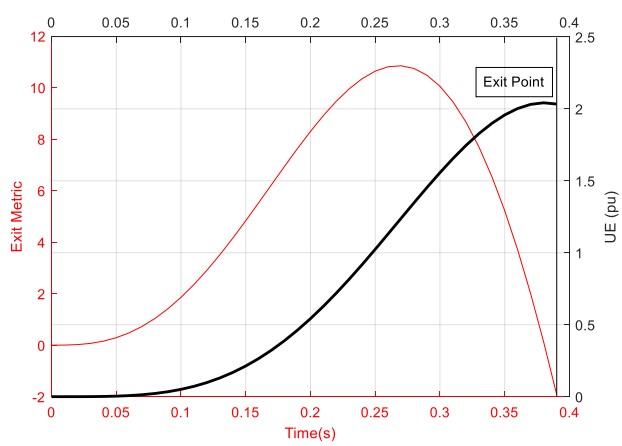

Figure 2.11 Example 2.1 Exit Metric and Potential Energy along Fault Trajectory

The value of exit metric is also plotted along the trajectory in Figure 2.11 where it is evident that max of UE occurs at the same time when exit metric changes from positive to negative. Now, the MGP is found using Algorithm 2.2 where the gradient system stability boundary is traced. Now using MGP as starting for Algorithm 2.3, CUEP is found at $(2.1175, -0.0156, 0, 0)$. Both the points are shown on the UE surface.

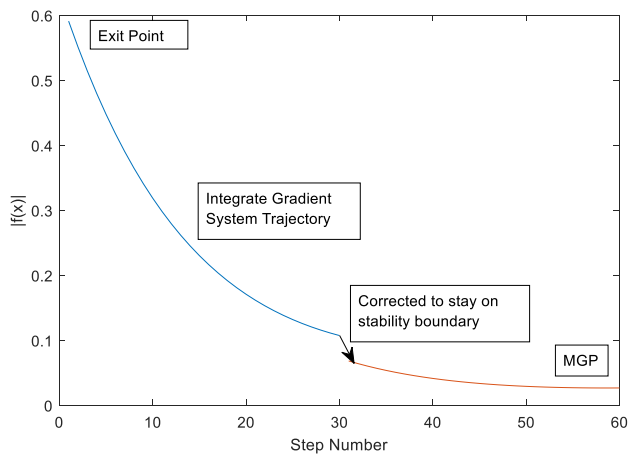

Figure 2.12 Example 2.1 MGP Tracing

Now we do a test to see if the found CUEP is on the stability boundary using Algorithm 2.4. We can see that the original system trajectory starting from the neighborhood of found CUEP reaches SEP thus the boundary check is passed.

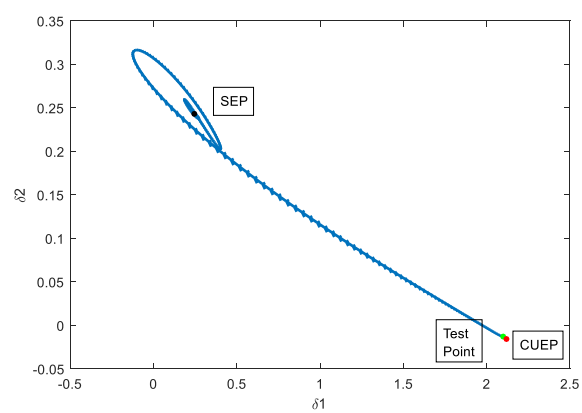

Figure 2.13 Example 2.1 Boundary Test

Finally calculating the energy at CUEP $\boldsymbol{W_{cuep}} = \mathbf{2.0062}$ to get **CCT = 0.2355 s**. This is seen from the plot of energy function value along fault trajectory as shown below where the energy crosses W_{cuep} at 0.2355 s.

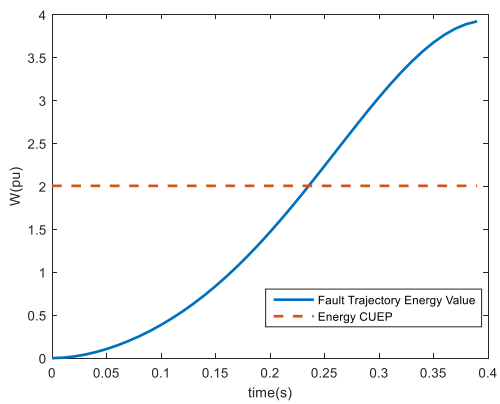

Figure 2.14 Example 2.1 Energy Function Value Along Fault Trajectory

We also obtain the CCT from time domain simulation by simply doing a binary search over different clearing times and found the value to be $t = 0.2750\ s$ which can also be seen from the system states vs time plot below.

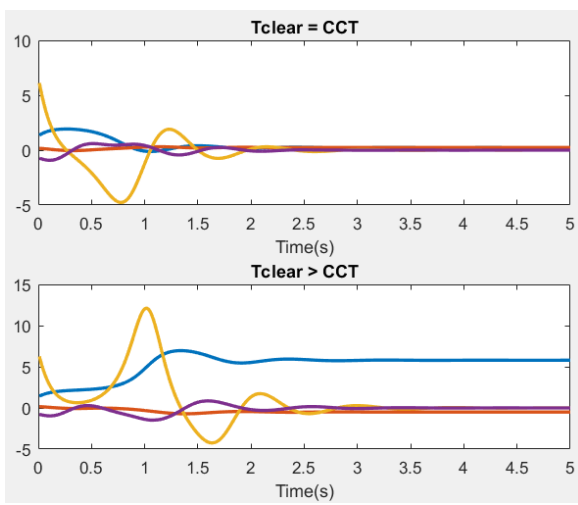

Figure 2.15 Example 2.1 $x - x_{sep}$

2.2 Lyapunov Functions Approach to Transient Stability Assessment using Sum of Squares Programming

In this section, we will present a systematic way of constructing a Lyapunov function for a generalized non-linear system. This technique estimates the SR through an algorithm that solves a convex optimization problem. We will start by giving the required background in polynomial algebra. This would be followed by a special category of polynomials called the 'Sum of Squares (SOS)' and LMI conditions for a polynomial to be one. Using those ideas, an algorithm for estimation of SR will be presented with its application to power systems transient stability problem. In the end, comparisons to the BCU method would be drawn through an example. Let us start by presenting some important definitions to give a background to the reader.

Definition 2.9 (Positive Semidefinite Polynomials) A polynomial $p(x)$ is called positive semidefinite (PSD) if $p(x) \geq 0 \; \forall \; x \in \mathbb{R}^n$

Definition 2.10 (Sum-of-Squares Polynomials) A polynomial $p(x)$ is classified as a Sum-of-Squares(SOS) polynomial denoted by Σ if there exist polynomials $h_i(x)$, $i = 1 \ldots r$ such that $p(x) = \sum_{i=1}^{r} h_i^2(x)$. For e.g. $p(x) = 2x^2 + 1 - 2x = (x-1)^2 + x^2 \in \Sigma$

SOS polynomials are PSD but the converse is not always true [46]. Also note that SOS polynomials are always even degree.

2.2.1 SOS Problem

Checking if a polynomial is SOS can be done through efficient semidefinite programming test which will be discussed here. Gram matrix approach can be used to obtain a full parameterization of all even degree $(2d)$ polynomials in n variables. Let $z_{n,d}$ be a vector of all monomials of degree $\leq d$ in the same n variables. Then a polynomial p of degree $2d$ in the same variables can be written as –

$$p(x) = z_{n,d}^T(x) Q z_{n,d}(x) \tag{2.15}$$

Where Q is called a Gram matrix. Thus iff a Q can be found such that $Q \geq 0$ and symmetric, $p(x)$ is an SOS [47]. One thing to note here is that there are many symmetric matrices Gram matrices that may not be positive semi definite. For e.g. [47] for $p(x) = x_1^4 + x_1^2 x_2^2 + x_2^4$ two options for Gram matrix are –

$$Q_1 = \begin{bmatrix} 0 & 0 & 0 & 0 & 0 & 0 \\ 0 & 0 & 0 & 0 & 0 & 0 \\ 0 & 0 & 0 & 0 & 0 & 0 \\ 0 & 0 & 0 & 1 & 0 & 0 \\ 0 & 0 & 0 & 0 & 1 & 0 \\ 0 & 0 & 0 & 0 & 0 & 1 \end{bmatrix}, Q_2 = \begin{bmatrix} 0 & 0 & 0 & 0 & 0 & 0 \\ 0 & 0 & 0 & 0 & 0 & 0 \\ 0 & 0 & 0 & 0 & 0 & 0 \\ 0 & 0 & 0 & 1 & 0 & 1 \\ 0 & 0 & 0 & 0 & -1 & 0 \\ 0 & 0 & 0 & 1 & 0 & 1 \end{bmatrix}$$

Where $= [1, x_1, x_2, x_1^2, x_1 x_2, x_2^2]^T$, $Q_1 \geq 0$ and $Q_2 \ngeq 0$.

The set of such matrices was shown to be an affine subspace Q_p of symmetric matrices [48] as follows –

$$Q_p = Q_0 + \sum_{i=1}^{n_q} \lambda_i Q_i \tag{2.16}$$

Where $p(x) = z(x)^T Q_0 z(x)$ & $z(x)^T Q_i z(x) = 0$. Existence of $Q \geq 0 \in Q_p$ was solved as an LMI problem as proposed by Parrilo [49] through the following theorems.

Theorem 2.6 Given polynomial p, find the relevant affine subspace $Q_p = \{Q_0 + \sum \lambda_i Q_i \,|\lambda_i \in \mathbb{R}\}$. p is SOS iff the following LMI is feasible

$$\exists \lambda_i$$
$$s.t. \, Q_0 + \sum \lambda_i Q_i \geq 0 \tag{2.17}$$

Theorem 2.7 Given $p_i's$, the existence of $\alpha_i's$ such that

$$s.t. \, p_0 + \sum \alpha_i p_i \in \Sigma \tag{2.18}$$

is an LMI feasibility problem.

These can be better understood with the following example [47].

Example 2.2 Let us take any polynomial $p(x)$ of degree 4 with $= [x_1, x_2, x_3, x_4]^T$. We start with any symmetric matrix Q_0 as defined above. Now, in order to find $Q_i's$, we write the equation –

$$\begin{bmatrix} 1 \\ x_1 \\ x_2 \\ x_1^2 \\ x_1x_2 \\ x_2^2 \end{bmatrix}^T \begin{bmatrix} q_1 & q_2 & q_3 & q_4 & q_5 & q_6 \\ q_2 & q_7 & q_8 & q_9 & q_{10} & q_{11} \\ q_3 & q_8 & q_{12} & q_{13} & q_{14} & q_{15} \\ q_4 & q_9 & q_{13} & q_{16} & q_{17} & q_{18} \\ q_5 & q_{10} & q_{14} & q_{17} & q_{19} & q_{20} \\ q_6 & q_{11} & q_{15} & q_{18} & q_{20} & q_{21} \end{bmatrix} \begin{bmatrix} 1 \\ x_1 \\ x_2 \\ x_1^2 \\ x_1x_2 \\ x_2^2 \end{bmatrix} = 0$$

Term	Coefficient	Term	Coefficient
1	q_1	$x_1x_2^2$	$2q_{11} + 2q_{14}$
x_1	$2q_2$	x_2^3	$2q_{15}$
x_2	$2q_3$	x_1^4	q_{16}
x_1^2	$q_7 + 2q_4$	$x_1^3x_2$	$2q_{17}$
x_1x_2	$2q_8 + 2q_5$	$x_1^2x_2^2$	$q_{19} + 2q_{18}$
x_2^2	$q_{12} + 2q_6$	$x_1x_2^3$	$2q_{20}$
x_1^3	$2q_9$	x_2^4	q_{21}
$x_1^2x_2$	$2q_{10} + 2q_{13}$		

Equating terms to 0, we pick each term and write a matrix corresponding to it. For example, for the term x_1x_2, a Q_i matrix with $2q_8 + 2q_5 = 0$ and rest $q_i's = 0$ would be sufficient. So, it can be written as –

$Q_i = 2E_8 - 2E_5$ where E_i has all zero elements except for $i^{th}(q_i) = 1$ and $\dim(E_i) = \dim(Q)$. It is referred to as a basis matrix for matrices $\in \mathbb{R}^{\dim(Q)}$. Thus the subspace of matrices satisfying $z^TQz = 0$ for the given example is –

$$Q$$
$$= \{\lambda_1(2E_7 - E_4) + \lambda_2(E_8 - E_5) + \lambda_3(2E_{12} - E_6) + \lambda_4(E_{10} - E_{13}) + \lambda_5(E_{11} - E_{14}) + \lambda_6(2E_{19} - E_{18})|\lambda_{1\ldots}\lambda_6$$
$$= \sum \lambda_i Q_i$$

We use SOSOPT [50] software package that converts the problem of finding if some polynomials are SOS to a relevant LMI problem and solves it through standard SDP solvers.

2.2.2 Positivstellensatz (P-Satz) Theorem

Definition 2.11 (Multiplicative Monoid) Given functions $\{g_1, g_2 \dots . g_t\}$, Multiplicative Monoid generated by $g_j's$ is

$$M(g_1, \dots g_t) := \{g_1^{k_1} g_2^{k_2} \dots . g_t^{k_t} | k_1, \dots k_t \in positive\ integers\} \tag{2.19}$$

Definition 2.12 (Cone) Given functions $\{f_1, f_2 \dots . f_s\}$, Cone generated by $f_j's$ is

$$C(f_1, \dots . f_s) := \{s_0 + \sum s_i b_i | s_i \in \Sigma, b_i \in M(f_1, \dots . f_s)\ \} \tag{2.20}$$

Definition 2.13 (Ideal) Given functions $\{h_1, h_2 \dots . h_u\}$, Ideal generated by $h_k's$ is

$$I(h_1, \dots . h_u) \coloneqq \{\sum h_k p_k | p_k\} \tag{2.21}$$

Theorem 2.8 (Positivstellensatz) Given polynomials $\{f_1(x), f_2(x) \dots . f_s(x)\}$, $\{g_1(x), g_2(x) \dots . g_t(x)\}$, $\{h_1(x), h_2(x) \dots . h_u(x)\}$ the following are equivalent -

1.
$$\left\{ x \in R^n \left| \begin{matrix} f_1(x) \geq 0\ , f_2(x) \geq 0 \dots . f_s(x) \geq 0 \\ g_1(x) \neq 0, g_2(x) \neq 0 \dots . g_t(x) \neq 0 \\ h_1(x) = 0, h_2(x) = 0 \dots . h_u(x) = 0 \end{matrix} \right. \right\} = \emptyset \tag{2.22}$$

2. There exist polynomials

$F \in Cone\big(f_1(x), f_2(x) \dots . f_s(x)\big)$, $G \in Monoids\big(g_1(x), g_2(x) \dots . g_t(x)\big)$, $H \in Ideals(h_1(x), h_2(x) \dots . h_u(x))$ st.

$$F + G^2 + H = 0 \tag{2.23}$$

The following simple example shows how this theorem can be applied to formulating the problem of checking if a function is non-negative (much less stricter condition that SOS check) which is an NP hard problem as an SOS problem easily solved as an LMI.

Example 2.3 Check if a polynomial $p(x) \geq 0$. We start by writing the corresponding set emptiness equation which would be acted on my P-Satz theorem as introduced before.

$$p(x) \geq 0\ \equiv \{x \in \mathbb{R} | -p(x) \geq 0, p(x) \neq 0\} = \emptyset$$

Using P-Satz, the above equation is equivalent to –

$$C\big(-p(x)\big) + \Big(M\big(p(x)\big)\Big)^2 = 0$$

$$=> s_0 - ps_1 + p^{2k} = 0, s_1 \in \Sigma$$

$$=> ps_1 - p^{2k} \in \Sigma_{n,d}\ , s_1 \in \Sigma$$

Degree of s_1 and value of k need to be carefully chosen such that the corresponding SOS problem is feasible. $d = \max(deg(p) + \deg(s_1), 2k + deg(p))$. For example in the above problem, $p^{2k} \geq 0$ and $s_1 \geq 0$ so as an initial guess, the degree of first term as chosen to be $\geq$ that of the second term for the overall expression to have a chance at being a SOS. While there is surely a lower bound on the degrees, there also exists an upper bound apart from the computational burden. We will now be presenting how SR can be estimated for a general non-linear system using SOS programming. Several important applications of this theorem coupled with LMI formulation of SOS problem in control theory are summarized in [51].

2.2.3 Estimating Region of Attraction (Expanding Interior Algorithm)

Let us first formally define Lyapunov's second method for stability [19].

Theorem 2.9 Consider the system

$$\dot{x} = f(x) \tag{2.24}$$

Let $D \subseteq \mathbb{R}^n$ be a neighborhood of the origin. If there is a continuously differentiable function $V: D \to \mathbb{R}_+$ such that the following conditions are satisfied:

1. $V(x) > 0\ \forall x \in D\backslash\{0\}$ and $V(0) = 0$
2. $-\dot{V}(x) = -\frac{\partial V}{\partial x} f(x) \geq 0\ \forall x \in D\backslash\{0\}$

then the origin is a stable equilibrium. If $\dot{V}(x)$ is negative definite in D then its asymptotically stable. If $D = \mathbb{R}^n$ and $V(x) \to \infty$ as $\|x\| \to \infty$ then result holds globally. Now, given a Lyapunov function V defined in D, the next theorem shows how SR can be estimated from it.

Theorem 2.10 [47] Let $D \subseteq \mathbb{R}^n$ be a domain containing equilibrium $x = 0$ of the system $\dot{x} = f(x)$ with $V(x)$ being a corresponding Lyapunov Function defined in D. Any region $\Omega_\beta := \{x \in D | V(x) \leq \beta\}$ is a positively invariant region contained in the equilibrium's SR.

Proof:

Let us take a trajectory starting at any point $x_1 \in \Omega_\beta$ with value of $V = V_1 \leq \beta$ (by definition). Now since $\dot{V} < 0$, all successive points on trajectory have $V < V_1 < \beta$. Thus, all points on the trajectory $\in \Omega_\beta$ which shows it's a positively invariant set. Now to show that the trajectory converges to origin, since $V \geq 0$ and monotonically decreases along the trajectory, V reaches 0 eventually which is only possible at the origin (as defined). Hence proved that Ω_β is contained in SR.

Thus, we see that Lyapunov function level sets can be used to estimate a portion of the SR. Since there are multiple possible Lyapunov functions, we are in search for the one whose associated Ω_β is the largest or in simple words, the one whose one of the level set approximates largest portion of the SR and is contained in it. The Expanding Interior Algorithm as proposed in [47] which will be discussed in the following section helps solve this problem through SOS programming making the algorithmic construction of Lyapunov Functions to estimate SR possible.

2.2.4 Expanding Interior Algorithm

The aim of the discussed problem is to maximize the level set of an unknown Lyapunov function contained within the SR of the corresponding equilibrium. There are two approaches to this problem that will be considered in our work. The first approach referred to as the expanding D algorithm expands a known semi algebraic set D which contains the origin (equilibrium) and is contained inside the set $\{x | V(x) > 0, \dot{V}(x) < 0\}$ followed by level set of V constrained in it. A major problem with this approach was that it was possible to have a large D with a very small V level set. The second approach, which is more successful expands the V level set from inside and is called the Expanding Interior Algorithm. The two approaches can be visually compared through the following figure where the larger purple ellipse is the Lyapunov level set inscribing

the smaller P_β(blue) for expanding interior while the smaller one (red) circumscribes larger D(yellow) for expanding D algorithm.

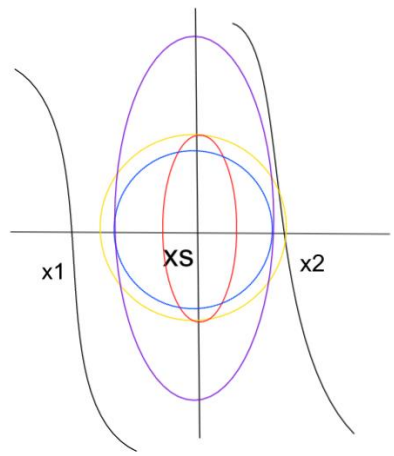

Figure 2.16 Expanding D vs Expanding Interior Algorithm SR Estimates

In this section, the formulation for dynamical systems with equality constraints would be discussed since later on we will see that the polynomial version of the power systems classical model has an inherent equality constraint. Given the following system –

$$\dot{x} = f(x) \qquad (2.25)$$
$$0 = g(x)$$

Here it should be kept in mind that $f(x)$ is defined such that the trajectories starting in the constraint manifold $g(x) = 0$ are restricted to evolve over it. i.e. $\dot{g}(x) = \frac{\partial g(x)}{\partial x} f(x) = 0 \; \forall \{x | g(x) = 0\}$. Let us define a variable sized semi algebraic set $P_\beta = \{x \in \mathbb{R}^n | \beta - p(x) \geq 0, g(x) = 0\}$ where p is a known positive semi definite polynomial. For a given initial Lyapunov Function $V(x)$, the optimization problem in terms of set emptiness constraints (for P-Satz theorem) can be written as –

$$\boldsymbol{max.\ \beta}$$
$$s.t.$$
$$\boldsymbol{V(x)}\ \textbf{cannot be negative:} \{V(x) \leq 0,\ g(x) = 0, x \neq 0\} = \emptyset \qquad (2.26)$$
$$\boldsymbol{P_\beta}\ \textbf{Is contained inside the SR estimate (}\boldsymbol{V(x) \leq 1}\textbf{) :}\ \{p(x) \leq \beta\ ,\ g(x) = 0,\ V(x) \geq$$

$$1,\ V(x) \neq 1\} = \emptyset$$

Inside the SR estimate,$V(x)$ strictly decreases along all trajectories:

$$\{V(x) \leq 1, \dot{V}(x) \geq 0,\ g(x) = 0, x \neq 0\} = \emptyset$$

The first constraint forces V to be > 0 at all points besides the origin (SEP of interest) since in this algorithm the true SR is unknown beforehand. So, using a Lyapunov function that can take a 0 value at points other than origin will mean that $\dot{V} < 0$ will not always mean a movement towards the origin. Writing the SOS formulation using P-Satz theorem,

$$\begin{gathered}
\boldsymbol{max.\ \ \beta} \\
V, V(0) = 0, k_i's \in positive\ integers, s_i's \in \Sigma, \lambda_i's \\
st. \\
s_1 - s_2 V + \lambda_1^T g + l_1^{2k_1} = 0 \\
s_3 + s_4(\beta - p) + s_5(V-1) + s_6(\beta - p)(V-1) + \lambda_2^T g + (V-1)^{2k_2} = 0 \\
s_7 + s_8(1-V) + s_9\dot{V} + s_{10}(1-V)\dot{V} + \lambda_3^T g + l_2^{2k_3} = 0
\end{gathered} \tag{2.27}$$

Here it should be noted that since $\lambda's$ are not SOS functions, the trick is to assume them to be comprised of any terms that simplify the final expression. For example in 2nd constraint, when we assumed $s_3 = s_4 = 0$, the constraint became $s_5(V-1) + s_6(\beta - p)(V-1) + \lambda_2^T g + (V-1)^2$. Now you can assume λ_2 to be of the form $(V-1) \times \gamma(x)$ to take out $(V-1)$ common from the expression to get the final simplified expressions for constraints –

$$\begin{gathered}
V - \lambda_1^T g - l_1 \in \Sigma \\
-s_6(\beta - p) - \lambda_2^T g - (V-1) \in \Sigma \\
-s_8(1-V) - s_9\dot{V} - \lambda_3^T g - l_2 \in \Sigma
\end{gathered} \tag{2.28}$$

where Σ_n denotes sum of squares function of the given n variables. Here it should be mentioned that equality constraints got converted to SOS condition by taking an SOS multiplier to the other side. For example in first constraint equation taking s_1 to RHS would result in the SOS constraint above. Now, the given formulation has bilinear constraints (for e.g. the term $s_9\dot{V}$ for both s_9 & V unknown. However if we fix one, then the resulting constraints can easily be written as a linear combination of functions which can be solved through SOS programming. Using this idea, an iterative scheme was proposed in [47]. There is however one shortcoming to

this approach. The size of the estimate would heavily depend on the choice of expanding region p. To deal with this situation, a scheme was proposed in [52] where once the iteration converges for a given p, the p is replaced by V obtained at the end and algorithm repeats. The overall algorithm is presented below. Here it is important to acknowledge that the LMI formulation of SOS conditions is valid for only polynomial functions. Thus, only systems with polynomial state equations can be handled. That being said, most non polynomial systems can be converted to polynomial ones through variable transformations [53].

Algorithm 2.5 Expanding Interior Algorithm for Region of Attraction Estimation

1. **Initializing degrees for unknown functions :** Choose a maximum degree d_V for V. Also since $V(0) = 0$, the constant term in the expression for V is set to 0 from the start. Also initialize degrees for multiplier polynomials as $d_{s_6}, d_{s_8}, d_{s_9}, d_{l_1}, d_{l_2}, d_{\lambda_1}, d_{\lambda_2}, d_{\lambda_3}$. A rule of thumb for picking these degrees for a given d_V such that the corresponding SOS constraints are feasible yet not of a very high dimensionality is that for every constraint, try to keep the degree of each term same. Using this idea, the following rules can be made –
   a. $s_i's$, l_{i_s} need to have even degrees due to being SOS.
   b. For first constraint, set $d_V \geq \max\left(\deg(\lambda_1^T g), d_{l_1}\right)$
   c. For second constraint, $d_p + d_{s_6} \geq max(d_V, \deg(\lambda_2^T g))$
   d. For third constraint, $d_V + d_{s_8} \geq \max(\deg\left(\dot{V}\right) + d_{s_9}, \deg(\lambda_3^T g)\,, d_{l_2})$
2. j = 1. Initialize with $p^{j-1} = \sum_k |a_k| x_k^2$
3. Set $p = p^{j-1}$, p iteration, outer loop
4. i = 1. expanding interior for a given p, inner loop
5. Fix $V = V^{i-1}$, perform a line search on β starting from β^{i-1} (= 0 if j = 1) till the following SOS is infeasible.

$$V^{i-1} - \lambda_1^T g - l_1 \in \Sigma$$
$$-s_6\left(\beta - p^{j-1}\right) - \lambda_2^T g - (V^{i-1} - 1) \in \Sigma$$
$$-s_8\left(1 - V^{i-1}\right) - s_9 \dot{V}^{i-1} - \lambda_3^T g - l_2 \in \Sigma$$

   Physically it means expanding P_β still it touches boundary of a fixed $V \leq 1$. We get s_8^i, s_9^i, β^i

6. Set $s_8 = s_8^i, s_9 = s_9^i$. Perform the following optimization starting from $\beta = \beta^i$

$$\max \beta$$
$$V, \dot{V}, s_6, \lambda_1, \lambda_2, \lambda_3$$
$$st.$$
$$V - \lambda_1^T g - l_1 \in \Sigma$$
$$-s_6(\beta - p^{j-1}) - \lambda_2^T g - (V - 1) \in \Sigma$$
$$-s_8^i(1 - V) - s_9^i \dot{V} - \lambda_3^T g - l_2 \in \Sigma$$

To get $V^i, \dot{V}^i, \beta^i$

7. If $\beta_i - \beta^{i-1} > 0.01$, i = i + 1. GOTO 5.
8. If $|(\max coeff \quad (p^{j-1} - V^i))| > 0.01$, j = j + 1. $p^{j-1} = V^i, \beta^{i-1} = 1$. GOTO 3.
9. STOP. Stability region estimate = $\{V^i \leq 1\}$

$P_\beta \approx \{V \leq 1\}$ when the outer iteration ends. As seen above, the algorithm needs an initial estimate of V to start which can be obtained easily through a single iteration of expanding D algorithm. For detailed derivation of the algorithm below, please refer to [47]. Once the initial V, c pair is found, we scale down V as $\frac{V}{c}$ to get the initial estimate of SR as $V_{new} = \frac{V}{c} \leq 1$ to take out the variable c from the formulation.

Algorithm 2.6 Initial Estimate of Lyapunov Function for Expanding Interior Algorithm

1. For finding V for a given p

$$\max \beta$$
$$V, \dot{V}, s_2, s_6, \lambda_1, \lambda_2$$
$$st.$$

V cannot be ≤ 0 inside $P_\beta \forall z \neq 0 : -s_2(\beta - p) + V - \lambda_1^T g - l_1 \in \Sigma$

$\dot{V}$ cannot be ≥ 0 inside P_β $\forall z \neq 0$:$-s_6(\beta - p) - \dot{V} - \lambda_2^T g - l_2 \in \Sigma$

2. For finding correct level set ($V \leq c$)

$$\max c$$
$$s_1, s_2, s_3, \lambda$$
$$st.$$

$V \leq c$ contained in P_β: $-s_1(c - V) - s_2(p - \beta) - s_3(c - V)(p - \beta) - \lambda^T g - (p - \beta)^2 \in \Sigma$

2.2.5 Application to Transient Stability Assessment of Power Systems Classical Model

In 2.1, the characterization of stability boundary in terms of the number and types of UEPs on it was presented. A list of assumptions were made regarding the system dynamics and manifold topology thus revealing further details about the stability boundary. The idea of energy functions which can serve as Lyapunov functions was also discussed. Further, the stability boundary of a special category of models, the ones that admit energy functions was discussed which lead to the idea of CUEP and BCU methods. While the assumptions on which the whole theory is based (low loss terms, transversality condition, hyperbolic EPs) hold true for most power systems and the techniques based on those have been proven to be a great success, not much is said about more complex systems like those with other types of limit sets (non-hyperbolic equilibrium, limit cycles, etc), state/output constrained systems, switched systems to name a few. With the grid being operated near the limit with increasing load demand and growing penetration of renewable resources, the possibility of more complex dynamics is not rare [54]. While we acknowledge that there is some work by Alberto et.al [36] [55] [56] on the idea of Generalized Energy Functions in order to deal with some of the assumptions failing to satisfy like having non hyperbolic EPs, it is still based on the assumption that the system has almost negligible loss terms. Besides that, a bigger problem plaguing the current systems is that from inverter based generation which operates at tighter limits. Any deviation from those could result in tripping a large amount of generation with the example of Germany discussed in 1.1.1. Also, the uncertainty in their outputs would require the estimation of a robust stability region. Thus, it is expected that the future systems would have to deal with a lot of constraints making the stability studies more challenging.

While the Lyapunov function approach for transient stability does not rely on any of those system related assumptions, traditionally there was a lack of a computationally feasible systematic methodology to construct one [57] [58]. The Zubov's method [59] however is an exception which in principle can find a Lyapunov function as well as the exact stability boundary.

Its applications to power systems transient stability problem have been explored in the past [60] [61]. It requires solving a partial differential equation which does not have a general closed form solution and is computationally difficult. Also, the presence of conductance (lossy) terms in power systems model has been proven to be a serious difficulty [37] [62]. This led to the dependence on physical insights, intuition, etc to search for similar functions for example the Energy function as discussed before. However, with the advances in SOS concepts, an algorithmic construction of Lyapunov function of any general non-linear system is possible as seen in 2.2.3. Also, it can be seen that using P-Satz theorem makes it a lot simpler to formulate some otherwise difficult problems like stability assessment of complex systems (switched, time delayed, constrained, uncertain). Thus, we plan on pursuing this for formulating the problem of studying transient stability of power systems with operating constraints (as seen in the case of PV). In this section, we will simply be showing how the expanding interior algorithm can be used with a power systems classical model. This direction was first explored in [52] and we will be revisiting those ideas here. Here, it is important to say that analysis of a large scale system is not possible using the technique in its current form due to the prohibitive size of the corresponding SOS problem. This is an active area of research, however outside the scope of this work.

We first start by writing the power systems classical model in one machine reference frame for uniform damping,

$$\dot{\delta}_{in_g} = \omega_{in_g}$$

$$M_i\dot{\omega}_{in_g} = P_{m_i} - \frac{M_i}{M_{ng}}P_{m_{n_g}} - \left(\sum_{j=1:n_g} E_iE_j\left(G_{ij}\cos\left(\delta_{in_g} - \delta_{jn_g}\right) + B_{ij}\sin\left(\delta_{in_g} - \delta_{jn_g}\right)\right) + \frac{M_i}{M_{ng}}\sum_{j=1:n_g} E_{n_g}E_j\left(G_{n_gj}\cos\left(-\delta_{jn_g}\right) + B_{n_gj}\sin\left(-\delta_{jn_g}\right)\right)\right) - D_i\omega_{in_g} \tag{2.29}$$

$$\delta_{in_g} = \delta_i - \delta_{n_g}, \omega_{in_g} = \omega_i - \omega_{n_g}$$

$$i = 1,2 \dots (n_g - 1)$$

Since the system of equations is non-polynomial, we do the following processing to convert it into a polynomial system with equilibrium at the origin–

Algorithm 2.7 Transforming Power Systems Classical Model to Polynomial System

1. Expand the sine and cosine terms of angle differences to get the equations in the following form (treating $E_i's, G, B, M, D$ as constants) –

$$\dot{\delta}_{in_g} = \omega_{in_g}$$

$$\begin{aligned}\dot{\omega}_{in_g} = & \sum_{j=1,j\neq i}^{n_g-1} SC_{ij}\sin(\delta_{in_g})\cos(\delta_{jn_g}) + \sum_{j=1,j\neq i}^{n_g-1} SS_{ij}\sin(\delta_{in_g})\sin(\delta_{jn_g}) + \\ & \sum_{j=1,j\neq i}^{n_g-1} CS_{ij}\cos(\delta_{in_g})\sin(\delta_{jn_g}) + \sum_{j=1,j\neq i}^{n_g-1} CC_{ij}\cos(\delta_{in_g})\cos(\delta_{jn_g}) + \\ & \sum_{j=1}^{n_g-1} C_{ij}\cos(\delta_{jn_g}) + \sum_{j=1}^{n_g-1} S_{ij}\sin(\delta_{jn_g}) + K_i - \frac{D_i}{M_i}\omega_{in_g}\end{aligned} \tag{2.30}$$

For some constant matrices SC, SS, CC, CS, C, S, K

2. Shift the origin to the relevant SEP $(\delta^s, 0)$ by replacing δ_{in_g} with $\delta_{in_g} + \delta_{in_g}^s$.
3. Introduce variables $z \in \mathbb{R}^{3\times(n_g-1)}$ st.

Table 2.1 Variable Transformation for Power System Model

New Variable	Function of Original States
z_i	$\omega_{in_g} - \omega_{in_g}^s(0) = \omega_{in_g}$
z_{n_g+2i-2}	$\sin(\delta_{in_g} - \delta_{in_g}^s)$
z_{n_g+2i-1}	$1 - \cos(\delta_{in_g} - \delta_{in_g}^s)$

It can be seen that the new states $z_{n_g+2i-2}, z_{n_g+2i-1}$ are not independent. The final equations are of the form –

$$\begin{aligned}\dot{z}_i = & \\ & \sum_j a_{ij} z_{n_g+2i-2} z_{n_g+2j-1} + \sum_j b_{ij} z_{n_g+2i-2} z_{n_g+2j-2} + \sum_j c_{ij} z_{n_g+2i-1} z_{n_g+2j-2} + \\ & \sum_j d_{ij} z_{n_g+2i-1} z_{n_g+2j-1} + \sum_j e_{ij} z_{n_g+2j-1} + \sum_j f_{ij} z_{n_g+2j-2} + m_i z_i \\ & \dot{z}_{n_g+2i-2} = (1 - z_{n_g+2i-1}) \times z_i \\ & \dot{z}_{n_g+2i-1} = z_{n_g+2i-2} \times z_i \\ & 0 = z_{n_g+2i-2} + \left(1 - z_{n_g+2i-2}\right)^2 - 1 \\ & i = 1,2 \ldots n_g - 1\end{aligned} \tag{2.31}$$

Thus the system is a constrained quadratic system in the new transformed variables.

$$\dot{z} = f(z) \tag{2.32}$$
$$0 = g(z)$$

Now, we can easily apply the expanding interior algorithm as discussed before to get the estimate of SR. Let us continue the 3-machine system Example 2.1 introduced in 2.1.5 and try finding the CCT through SOS programming as discussed in this section.

Example 2.1 Continued We first start by writing the post fault system's SEP in one machine reference frame which is given by $(\mathbf{0.3487}, \mathbf{0.3451}, \mathbf{0}, \mathbf{0})$. Now, converting the equations in one machine reference frame to an equivalent polynomial system using Algorithm 2.7 with the following variable transformation and final polynomial system given as,

Table 2.2 Example 2.1 Variable Transformation for Polynomial System

New Variable	In terms of Original System State
z_1	ω_{1n_g}
z_2	ω_{2n_g}
z_3	$\sin(\delta_{1ng} - 0.3487)$
z_4	$1 - \cos(\delta_{1ng} - 0.3487)$
z_5	$\sin(\delta_{2ng} - 0.3451)$
z_6	$1 - \cos(\delta_{2ng} - 0.3487)$

$$\dot{z}_1 = 30.003 \times z_4 - 53.75 \times z_3 - 3.99 \times z_1 - 16.26 \times z_5 + 5.01 \times z_6 - 1.57 \times z_3 \times z_5 + 5.35 \times z_3 \times z_6 - 5.35 \times z_4 \times z_5 - 1.57 \times z_4 \times z_6$$

$$\dot{z}_2 = 1.80 \times z_4 - 4.53 \times z_3 - 3.99 \times z_2 - 100.62 \times z_5 + 48.92 \times z_6 - 1.02 \times z_3 \times z_5 - 3.57 \times z_3 \times z_6 + 3.57 \times z_4 \times z_5 - 1.02 \times z_4 \times z_6$$

$$\dot{z}_3 = z_1 - 1.0 \times z_1 \times z_4$$

$$\dot{z}_4 = z_1 \times z_3$$

$$\dot{z}_5 = z_2 - 1.0 \times z_2 \times z_6$$

$$\dot{z}_6 = z_2 \times z_5$$

We choose the following degrees for unknown functions (refer Algorithm 2.5) for expanding interior algorithm with initial value of $p = z^T z$ -

Table 2.3 Example 2.1 SOS Degrees

Function	Degree	Function	Degree
V	2	s_9	0
p	2	λ_{11}	0
l_1	2	λ_{12}	0
l_2	4	λ_{21}	0
s_6	0	λ_{22}	0
s_8	2	λ_{31}	1

The final values of SOS multipliers (refer to Algorithm 2.5) as well as V in terms of z are –

$$V = -7.29 \times z_4 - 8.71 \times z_6 - 0.0012 \times z_1 \times z_2 + 0.037 \times z_1 \times z_3 + 0.012 \times z_1 \times z_4 - 0.002 \times z_2 \times z_3 - 0.004 \times z_1 \times z_5 - 0.003 * z_2 * z_4 + 0.002 \times z_1 \times z_6 + 0.02 \times z2 \times z5 + 0.014 \times z_3 \times z_4 + 0.004 \times z_2 \times z6 - 0.012 \times z_3 \times z_5 + 0.0016 \times z_3 \times z_6 - 0.013 \times z_4 \times z_5 - 0.113 \times z_4 \times z_6 + 0.015 \times z_5 \times z_6 + 0.006 * z_1^2 + 0.003 \times z_2^2 + 4.005 \times z_3^2 + 3.96 \times z_4^2 + 4.71 \times z_5^2 + 4.67 \times z_6^2$$

$$s_6 = 0.999$$

$$s_8 = 0.024 \times z_1^2 - 0.0127 \times z_1 \times z_2 + 0.186 \times z_1 \times z_3 - 0.101 \times z_1 \times z_4 + 0.31 \times z_1 \times z_5 - 0.0108 \times z_1 \times z_6 + 0.016 \times z_2^2 - 0.19 \times z_2 \times z_3 + 0.086 \times z_2 \times z_4 - 0.41 \times z_2 \times z_5 - 0.14 \times z_2 \times z_6 + 14.17 \times z_3^2 + 0.31 * z_3 \times z_4 + 1.58 \times z_3 \times z_5 + 0.106 \times z_3 \times z_6 + 16.42 \times z_4^2 - 0.97 \times z_4 \times z_5 + 3.96 \times z_4 \times z_6 + 13.38 \times z_5^2 - 0.33 \times z_5 \times z_6 + 16.36 \times z_6^2$$

$$s_9 = 9.18, \lambda_{11} = 3.778, \lambda_{12} = 4.50, \lambda_{21} = -0.132, \lambda_{22} = -0.143$$

$$\lambda_{31} = 1.296561593002697 \times z_1 - 0.3401916114317417 \times z_2 + 4.075380695690708 \times z_3 + 139.3131662781847 \times z_4 - 8.674903787587864 \times z_5 + 120.2767258053765 \times z_6$$

$\lambda_{32} =$
$-0.02995529345691922 \times z_1 + 0.8372930511072947 \times z_2 + 4.320506818685569 \times z_3 + 143.4126364668558 \times z_4 - 7.85155215242335 \times z_5 + 159.5752004610657 \times z_6$

The progression of SR estimate is shown in the figure below in angle domain with $\omega_{1n_g}.\omega_{2n_g}$ kept constant.

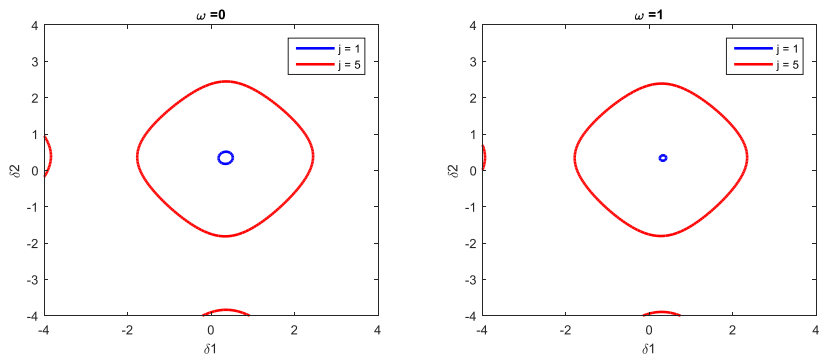

Figure 2.17 Example 2.1 Expanding SR Estimate

Writing the expression in terms of original state variables,

$$V = 0.014 \times \omega_{1n_g} + 0.001 \times \omega_{2n_g} - 0.491 \times \cos\left(\delta_{1n_g}\right) - 0.483 \times \cos\left(\delta_{2n_g}\right) - 0.161 \times \sin\left(\delta_{1n_g}\right) - 0.171 \times \sin\left(\delta_{2n_g}\right) - 0.020 \times \sin\left(\delta_{1n_g}\right) \times \sin\left(\delta_{2n_g}\right) + 3.971 \times \cos\left(\delta_{1n_g}\right)^2 + 4.68 \times \cos\left(\delta_{2n_g}\right)^2 + 3.99 \times \sin\left(\delta_{1n_g}\right)^2 + 4.7 \times \sin\left(\delta_{2n_g}\right)^2 - 0.001 \times \omega_{1n_g} \times \omega_{2n_g} - 0.024 \times \omega_{1n_g} \times \cos\left(\delta_{1n_g}\right) - 0.0008 \times \omega_{1n_g} \times \cos\left(\delta_{2n_g}\right) + 0.003 \times \omega_{2n_g} \times \cos\left(\delta_{1n_g}\right) - 0.010 \times \omega_{2n_g} \times \cos\left(\delta_{2n_g}\right) + 0.031 \times \omega_{1n_g} \times \sin\left(\delta_{1n_g}\right) - 0.005 \times \omega_{1n_g} \times \sin\left(\delta_{2n_g}\right) - 0.0009 \times \omega_{2n_g} \times \sin\left(\delta_{1n_g}\right) + 0.017 \times \omega_{2n_g} \times \sin\left(\delta_{2n_g}\right) + 0.005 \times \omega_{1n_g}^2 + 0.003 \times \omega_{2n_g}^2 - 0.105 \times \cos\left(\delta_{1n_g}\right) \times \cos\left(\delta_{2n_g}\right) - 0.039 \times \cos\left(\delta_{1n_g}\right) \times \sin\left(\delta_{1n_g}\right) - 0.020 \times \cos\left(\delta_{1n_g}\right) \times \sin\left(\delta_{2n_g}\right) - 0.035 \times \cos\left(\delta_{2n_g}\right) \times \sin\left(\delta_{1n_g}\right) - 0.036 \times \cos\left(\delta_{2n_g}\right) \times \sin\left(\delta_{2n_g}\right) - 7.490$$

Now, this can be transformed to COA reference frame using linear mapping given below –

$$\delta_{coa} = [Map_{onemach2coa}] \times \delta_{onemachine}, \omega_{coa} = [Map_{onemach2coa}] \times \omega_{onemachine}$$

$$[Map_{onemach2coa}] \in R^{(n_g-1)\times(n_g-1)} = + \begin{bmatrix} \frac{H_1}{H_{n_g}} & \cdots & \frac{H_{(n_g-1)}}{H_{n_g}} \\ \vdots & \vdots & \vdots \\ \frac{H_1}{H_{n_g}} & \cdots & \frac{H_{(n_g-1)}}{H_{n_g}} \end{bmatrix} + I_{(n_g-1)\times(n_g-1)} \tag{2.33}$$

Where,

$$\delta_{onemach} = \left[\delta_{1n_g}, \delta_{2n_g}, \dots, \delta_{(n_g-1)n_g}\right]^T, \omega_{onemach} = \left[\omega_{1n_g}, \omega_{2n_g}, \dots, \omega_{(n_g-1)n_g}\right]^T, \delta_{coa} = \left[\delta_1^{coa}, \delta_2^{coa}, \dots, \delta_{(n_g-1)}^{coa}\right]^T, \omega_{coa} = \left[\omega_1^{coa}, \omega_2^{coa}, \dots, \omega_{(n_g-1)}^{coa}\right]^T$$

The expression for V in COA reference frame can be obtained through the above transformation is. Finally, we calculate the value of V along fault on trajectory and whenever its value first reaches 1 is denoted as the CCT. From the graph below, we can see that this happens at $t = 0.25\ s$. This estimate is quite close to the estimate of $0.2355\ s$ by BCU, actually better as seen from the time domain simulation estimate of $0.2750\ s$. Here it should also be noted that since the variable transformation used sin and cosine of angles, the Lyapunov function values would be periodic in angle space (repeating every 2π) which is the reason for it crossing 1 multiple times along fault on trajectory. So, we only use the first crossing to determine stability.

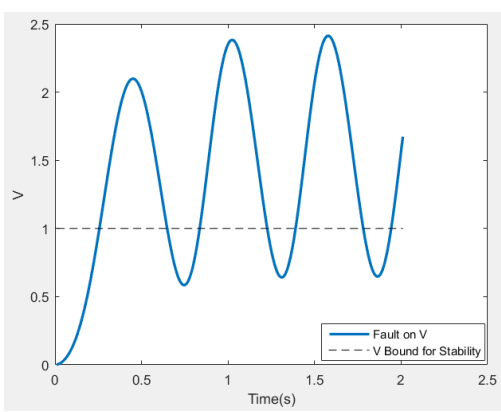

Figure 2.18 Example 2.1 Value of Lyapunov Function along Fault Trajectory

To compare their performance for disturbances in any direction for the same post fault system, we plot the SR estimate by both the techniques. While for Lyapunov approach its

straightforward ($V \leq 1$), BCU estimates it piece by piece using multiple level sets of energy function. So, in order to do that, we need to know all the UEP's on the stability boundary and plotting the constant energy surface passing through each to get relevant stability boundary in each direction. For finding all the EPs, we employ a continuation based technique proposed in [63]. The idea is to use loading at each bus as a separate parameter in the state equations. Now, the value of each parameter is varied in individually which shifts the SEP in a particular direction in state space as well as the UEP's on its stability boundary till a saddle node bifurcation is reached where there's no equilibrium for the parameterized state equation [64] due to maximum power transfer reached. It has been shown in [65] that at this point the SEP and a UEP on its boundary come close, meet and get destroyed. Now the idea is to reverse the change in load to go back to the original system (parameter value same as initial) but not returning to the same SEP, rather to that UEP that the SEP got destroyed with. To do so, a continuation method [66] is used which safeguards against any convergence problems happening around bifurcation. As can be seen from the power angle curve for a single machine infinite bus (as studied before), corresponding to same generator loading there are multiple EPs. Let us change the orientation of the curve and mark the two EPs (SEP on bottom and UEP on top) in the domain $[0, \pi]$. Continuation method will trace this curve starting from the SEP and reach the UEP.

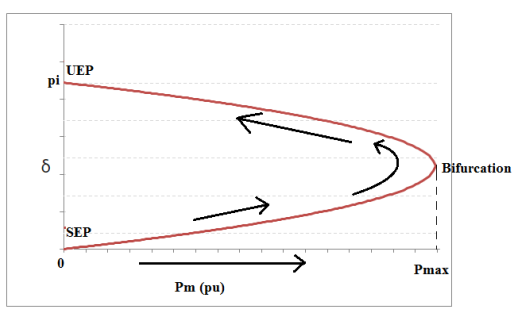

Figure 2.19 Generator Angle vs Loading Curve

Algorithm 2.7 Finding all EPs on the Stability Boundary

Let steady state equations for power system model be of the form $f(x) = \begin{bmatrix} f_1(x) \\ \vdots \\ f_n(x) \end{bmatrix} = 0$ where

for network reduced model, $f_i(x) = P_{m_i} - P_{e_i} - \frac{M_i}{M_{total}} P_{coa}$, $i \in [1, n_g - 1]$, $x = \begin{bmatrix} \delta_1^{coa} \\ \vdots \\ \delta_{n_g-1}^{coa} \end{bmatrix}$

1. Formulate multiple sets of parametric equations where each set corresponds to a continuation parameter α_i and is expressed as –

$F_i(x, \alpha_i) = \begin{bmatrix} f_1(x) \\ \vdots \\ f_i(x) - \alpha_i \\ \vdots \\ f_n(x) \end{bmatrix}$, where α_i is a continuation parameter.

2. Initialize record keeping table as –

EP	$\boldsymbol{\alpha_1}$	$\boldsymbol{\alpha_2}$		$\boldsymbol{\alpha_n}$
x_{ep_1}	×			
x_{ep_2}		×	…	
⋮				

Where first column has all the EPs found. When a continuation trace is started from j^{th} equilibrium x_{ep_j} along $F_i(\alpha_i \; is \; parameter)$, a × is placed on $(j, i)^{th}$ position in table. Each new (not in table) equilibrium encountered in this trace is appended to this table as a new row and the ith column of it is marked with ×. Initialize with $x_{ep_1} = x_{sep}$ (known SEP)

3. Randomly choose a combination of starting equilibrium x_{ep_j} and parameter α_i such that $(j, i)^{th}$ position on table does not have ×. Run continuation trace on $F_i(x)$ starting at x_{ep_j}.
4. Update table rows by appending rows for new EPs found.
5. If no cell in table is blank, STOP else GOTO Step 3.
6. Boundary test (using Algorithm 2.4) on x_{ep_j} $\forall j \neq 1$ and eliminate ones that fail the test.
7. Repeat process replacing α_i with $-\alpha_i$ $\forall i$.
8.

Obtaining Continuation Trace and EPs

For tracing the solution branch along F_i starting at x_{ep_j}, follow these steps –

New states $y = \begin{bmatrix} x \\ \alpha_i \end{bmatrix}$

Formulate Jacobian $[J(y)]_{(n+1)\times(n+1)} = \begin{bmatrix} \frac{\partial F_1}{\partial x_1} & \frac{\partial F_1}{\partial x_2} & \dots & \frac{\partial F_1}{\partial x_n} & 0 \\ \vdots & \vdots & \dots & \vdots & \vdots \\ \frac{\partial F_i}{\partial x_1} & \frac{\partial F_i}{\partial x_2} & \dots & \frac{\partial F_i}{\partial x_n} & -1 \\ \vdots & \vdots & \dots & \vdots & \vdots \\ \frac{\partial F_n}{\partial x_1} & \frac{\partial F_n}{\partial x_2} & \dots & \frac{\partial F_n}{\partial x_n} & 0 \end{bmatrix}$

1. $y_{pre} = \begin{bmatrix} x_{ep_j} \\ 0 \end{bmatrix}_{(n+1)\times 1}$. Initialize step size h. Set continuation parameter index $k = n + 1$, $direction = +1$. Iter = 1.
2. **Predictor**: Tangent vector $t = \begin{bmatrix} J(y_{pre}) \\ e_k \end{bmatrix}^{-1} \times \begin{bmatrix} 0 \\ 0 \\ direction \end{bmatrix}$ where e_k is an all 0 row vector with k^{th} position as 1. $y_{post} = y_{pre} + h \times t$.
3. **Continuation parameter** index $k = argmax([|t_1| \quad \dots \quad |t_{n+1}|])$.
4. **Corrector**: Solve system of equation $\begin{bmatrix} F_i(y) \\ y(k) = y_{post}(k) \end{bmatrix}$ using y_{post} as initial condition to update y_{post} using Newton-Raphson similar to Algorithm 2.3.
5. **Equilibrium Test** If $y_{post}(n+1) = 0$, EP found = $\begin{bmatrix} y_{post_1} \\ \vdots \\ y_{post_n} \end{bmatrix}$
6. If Iter < Itermax AND $y_{post}(1{:}\,n-1)$ within constraints, Iter = Iter + 1 , $direction = y_{post}(k) - y_{pre}(k)$, $y_{pre} = y_{post}$, GOTO Step 2.
7. STOP

Using the above algorithm we find the following UEP's for gradient system (same as original system) and filtering out the ones not lying on the stability boundary of original system. The continuation traces are shown below for understanding the process visually. The parameter α values are in x axis while y axis has state values $\delta_1^{coa}, \delta_2^{coa}$. Each graph has a collection of 2 vertically integrated graphs corresponding to 2 state values respectively for the same continuation trace. The graphs in the top row are for positive direction of $alpha$ while lower

row is for tracing in negative direction. To understand a trace, whenever the trace intersects the y axis, we obtain an equilibrium. The trace is restricted to the state values within $\pm\pi$ of x_{sep}.

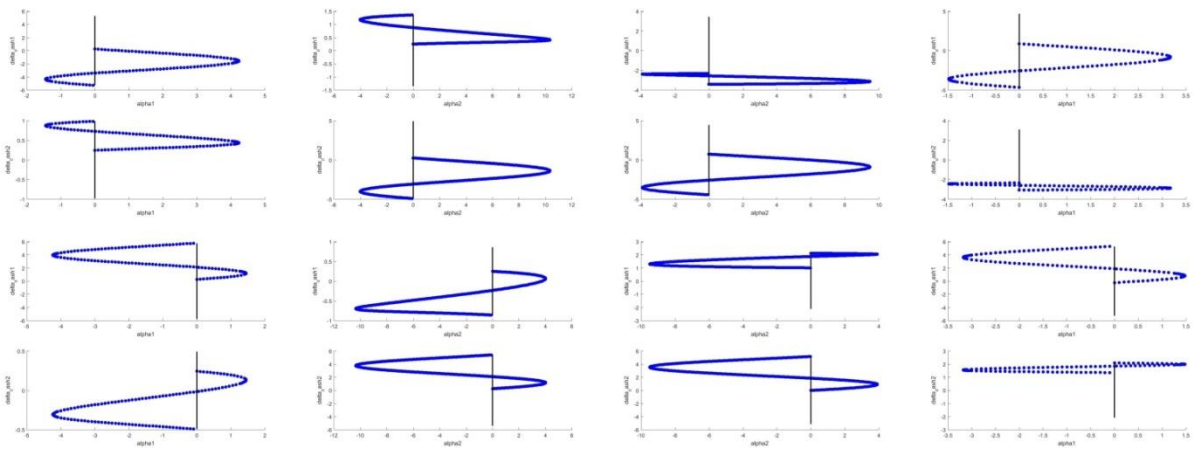

Figure 2.20 Example 2.1 Continuation Traces for Locating All EPs

Now, out of those we select only the ones relevant to BCU (which have stable manifolds in angle domain) to get the following –

Table 2.4 Example 2.1 Type 1 UEP on Stability Boundary

UEP$(\boldsymbol{\delta_1}, \boldsymbol{\delta_2})$	**Energy**
$(-3.4265, 0.7236)$	10.3794
$(0.8729, -3.0869)$	25.2977
$(2.1175, -0.0156)$	1.9279
$(-0.2359, 2.0875)$	5.7426

We now superimpose the intersection of SR estimate from SOS programming and BCU with constant ω_1, ω_2 surface. It can be noticed that SOS programming based Lyapunov approach does a fairly decent job as compared to BCU's piecewise estimate and thus can be used for our work in dealing with more tricky applications due to its flexibility.

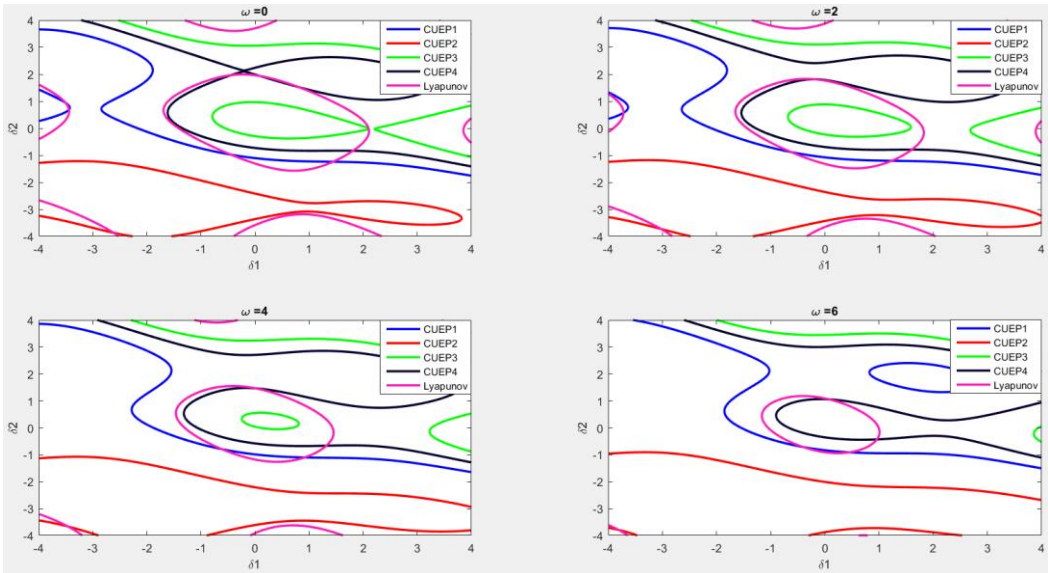

Figure 2.21 BCU vs SOS SR Estimate

2.2.6 Estimating the Relevant Portion of Stability Region for Power Systems Classical Model

The Lyapunov approach using SOS programming discussed as seen before aims at maximizing the interior of the SR estimate. While the knowledge of the overall stability region of a system is essential when carrying stability analysis, in many applications such as power systems transient stability analysis, only the relevant portion of the stability region is needed. During a typical disturbance, power system goes through pre-disturbance, disturbance-on and post-disturbance phase with the stability obviously defined w.r.t post disturbance system. When seen from that perspective, the disturbance-on trajectory usually moves away from the post-disturbance SEP.

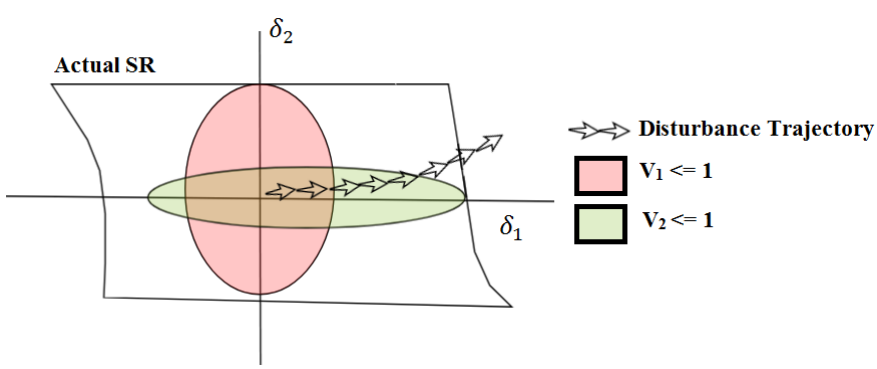

Figure 2.22 Comparing SR Estimates for a Fault Trajectory

Let us take an example of a two machine system whose actual SR is shown in Figure 2.22 along with two different Lyapunov estimates in the $\omega_1 = \omega_2 = 0$ plane. The disturbance trajectory is also shown. Here, the fault seems to have a more local effect on machine 1 thus resulting in a more horizontal trajectory. The Lyapunov estimate V_1 gives a very good overall estimate of the stability region in terms of size. It can be seen that longer the disturbance sustains, closer the system is pushed towards the stability boundary which is usually the case with power system faults. Now, the question that needs to be answered is how long can we sustain the disturbance without going outside the stability region of the post disturbance system which is basically the CCT as discussed earlier. A good stability region estimate in this regard would be the one which contains the disturbance trajectory for the longest time. From that point of view, it can be seen that the estimate from V_2 is better that that from V_1. Thus, the CCT estimate from V_2 will be higher than that from V_1 and needless to say that both the estimates are lower than the actual CCT and therefore reliable.

As mentioned before in 2.1.4, this is the governing idea behind CUEP where the UEP on the portion of the stability boundary that the disturbance trajectory is trying to head towards is found with the constant energy surface passing through it serving as the relevant stability region. There is however a fundamental difference in what can be achieved when trying to estimate the relevant portion of the SR through a single Lyapunov function vs the CUEP idea. While we may be able to choose along what axes the Lyapunov estimate needs to be expanded more relatively, it is tricky to also incorporate the direction in the expansion process. For example, in Figure 2.22, the disturbance trajectory heads towards positive and not negative δ_1 direction but the choice of $p(z)$ will be an ellipse whose axis length along δ_1 axis is longer than δ_2. This however can be overcome by choosing non ellipsoidal $p(z)$ making the strategy more computationally intensive and therefore outside the scope of the current work. Next, we discuss how to algorithmically choose $p(z)$ for the expanding interior algorithm discussed previously given a disturbance trajectory data.

Looking for higher degree Lyapunov functions for multi machine systems is not practical computationally. Thus, we need to find a positive quadratic function $p(z)$ which belongs to a

family of elliptical contours. A good candidate for an ellipse would be one whose axes are aligned in the directions of maximum variances of the disturbance trajectory dataset. The successive level sets of such ellipse would expand more in the direction of disturbance trajectory and less in other directions. We propose a simple candidate for this ellipse using principle component analysis (PCA) [67]. PCA gives a set of orthogonal variables called the principle components with the first component in the direction of maximum variance in the data followed by the second and so on. These principle components are actually eigen vectors of the data covariance matrix with the eigen values giving the variance in data in those directions. Normally the data is centered and normalized before carrying out the PCA which results in principle components centered at the data center and with the eigen values scaled down. However, this is not we are looking for. We are interested in an ellipse centered at the origin (SEP of the post fault system) with axis lengths truly representing the true distances the disturbance trajectory travels in each direction. Thus, we will be working with raw trajectory data. Let X denote the data matrix as represented below.

$$X = [x_1 \quad \cdots \quad x_{nstates}] \tag{2.34}$$

Where x_i is a vector with values of ith state variable at different times along the disturbance trajectory. The PCA on this raw data gives the principle components $e_1, e_2 \dots e_{nstates}$ which are vectors aligned in the direction of maximum variance while the associated eigen values $\lambda_1, \lambda_2 \dots \lambda_{nstates}$ representing the variances in each direction. We propose the following choice of ellipse $p(z)$ for expanding interior algorithm.

$$p(z) = z^T A z$$

$$A = Emat \times \begin{pmatrix} \frac{1}{\sqrt{\lambda_1}} & \cdots & 0 \\ \vdots & \ddots & \vdots \\ 0 & \cdots & \frac{1}{\sqrt{\lambda_{nstates}}} \end{pmatrix} \times Emat^T \tag{2.35}$$

$$Emat = [e_1, e_2 \dots e_{nstates}]$$

There are a few things to note about the proposed matrix. Since PCA is basically eigen analysis of covariance matrix of the data matrix which is a real symmetric matrix, the eigen values are real. Also, the covariance matrix is positive semi definite giving positive eigen values.

Now, we evaluate the choice of square root of λ vs λ itself in the diagonal elements. Usually, a sustained disturbance displaces some states more than the others giving majorly differing λ's. Using λ itself in the A matrix defined resulted in an extremely eccentric ellipse (large major to minor axis lengths) as compared to $\sqrt{\lambda}$ which is a smaller ratio and thus more rounded ellipse. Having such an eccentric expanding region gave a final Lyapunov estimate prone to giving highly conservative CCT estimate in some cases. The problem can be visualized for a hypothetical disturbance trajectory data in the figure below. Here, when expanding the lower ellipse (more eccentric), it quickly hits the stability boundary in the major axis direction with the minor axis still being negligibly small. This increases the chances of the disturbance trajectory leaving this ellipse early on in time yielding a low CCT estimate.

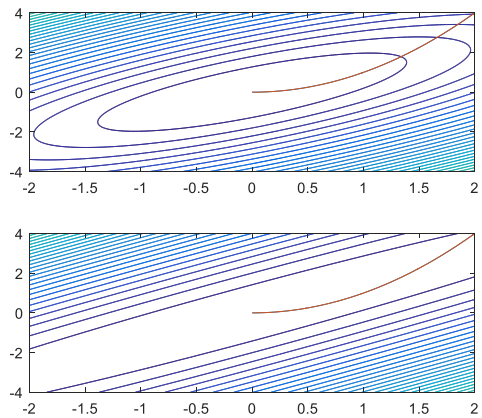

Figure 2.23 p(z) contours using λ_i (lower) vs $\lambda_i^{1/2}$ (upper)

Let us now demonstrate the effectiveness of this initial choice of $p(z)$ for expanding interior algorithm for transient stability assessment of a multi machine system.

Example 2.2 Given 3 machine system with damping coefficient of 2.

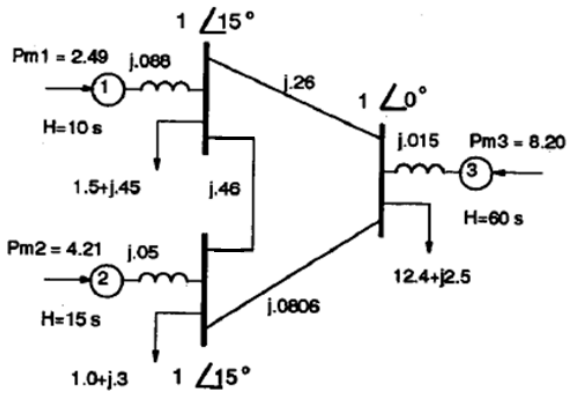

Figure 2.24 Example 2.2 Test Case

The first fault studied in the above system is on line connecting 1-2 on the bus 2 side. This fault is carefully based on the prior knowledge of the Lyapunov estimate shape which has a shorter axis in the direction of machine 2 states (δ_2, ω_2). The SEP of the post fault system is $(0.3487, 0.2070, 0, 0)$. Ideally, the portion of the fault trajectory data lying inside the actual stability region should be used to estimate the start $p(z)$ but since its known beforehand, we use the data from the sustained fault trajectory for 2 seconds. PCA on the transformed variables z yields the following results,

$$\lambda = [37.83, 0.7965, 0.4246, 0.0769, 0.0024, 2.2e-5]$$

$$Emat = \begin{bmatrix} 0.0183 & 0.6410 & -0.0193 & 0.7669 & 0.0143 & 0.0016 \\ 0.9840 & 0.0148 & -0.1703 & -0.0396 & -0.0312 & 0.0075 \\ 0.0494 & -0.0219 & 0.0961 & 0.0026 & 0.9409 & -0.3203 \\ 0.0086 & -0.0066 & 0.0330 & -0.0018 & 0.3185 & 0.9473 \\ 0.0026 & 0.7503 & 0.2258 & -0.6214 & -0.0047 & -0.0022 \\ 0.1702 & -0.1596 & 0.9536 & 0.1554 & -0.1100 & 0.0014 \end{bmatrix}$$

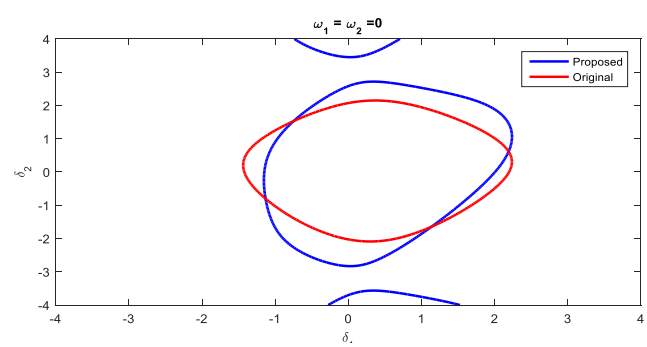

Figure 2.25 Example 2.2 SR Estimate for Fault on Bus 2

A matrix can be found using the earlier discussion. The final SR estimates using the identity matrix for A and the proposed matrix are shown in Figure 2.25 which considerably differ in the shape with the proposed approach covering more area along the δ_2 axis.

Let us now plot the value of the two Lyapunov functions along the fault trajectory. The CCT estimate for this fault as given by the proposed methodology is 0.44 s while original estimate is 0.37 s which shows a significant reduction in the conservativeness of the estimate.

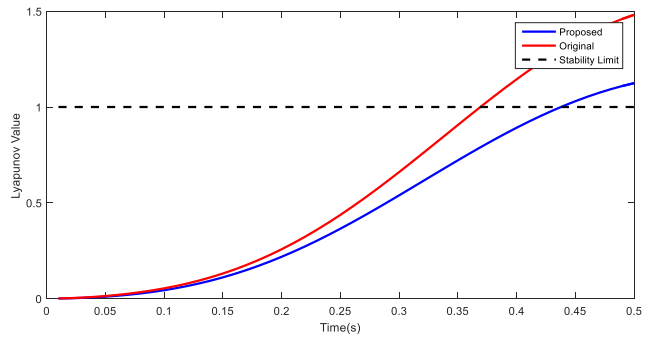

Figure 2.26 Example 2.2 Lyapunov Value Along Fault Trajectory for Fault on Bus 2

We take the previous case with the same line fault but closer to bus 1. This case is chosen since it was previously seen that the SR estimate with $A = I$ was significantly bigger in the δ_1 direction and thus we need to make sure that the proposed technique is able to do as well if not better in terms of the CCT estimate. The SR estimates are as shown below. It can be seen that there is a marginal expansion of the SR estimate along the machine 1 states axes due to the disturbance trajectory taking the system to that region.

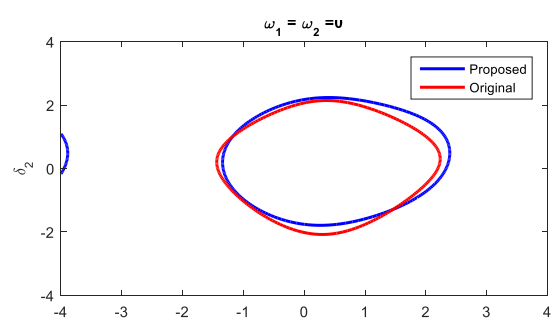

Figure 2.27 Example 2.2 SR Estimate for Fault on Bus 1

Plotting the Lyapunov values along the fault trajectory we can see that there is no improvement in the CCT estimate. This can be attributed to the fact that the default choice of $p(z)$ resulted in the Lyapunov estimate expanding in a similar direction as with the proposed $p(z)$ thus no further scope for improvement.

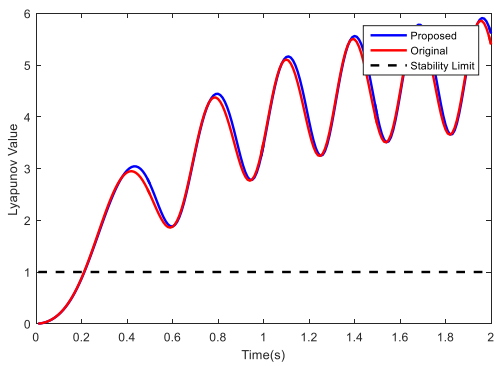

Figure 2.28 Example 2.2 Lyapunov Value Along Fault Trajectory for Fault on Bus 1

Chapter 3 Impact of Inertia Displacement and Generator Redispatch

In this chapter, we will start by studying the impact of locational inertia reduction to power system stability through the BCU method as well as time domain simulations. This would be followed by a visualization of how SR changes with changing the way conventional generators are dispatched when accommodating PV. Here it should be noted that for the studies using BCU/Energy functions, the states (δ, ω) are assumed to be in COA reference frame and so we eliminate the need for using the notation $\delta^{coa}, \omega^{coa}$ and simply use δ, ω unless stated otherwise.

3.1 Inertia Reduction Issues

A majority of the generation in power systems has been through synchronous machines whose simplified dynamics were studied in the previous section. Revisiting the idea of power systems stability, a grid consists of multiple synchronously rotating machines driven by fuel (gas,nuclear, etc) together supply electrical loads. At steady state, there is an input(mechanical)-output(electrical load) balance at each machine and thus machines rotate at fixed speeds. On the electrical side, the power flow between machines is dependent on their relative rotor angles. Any disturbance to the balance results in some machines speeding or slowing down wrt others and beyond certain limit (defined in terms of relative rotor angles and speeds) they become unstable and cannot be synchronized again and have to trip offline. Now, as seen from the swing equation (the equation of motion of a synchronous machine), these machines have inertia which resists these speed changes during an imbalance. The grid frequency is coupled to the generator speeds and thus relies a lot on this inertia. A heavy machine is less likely to reach the instability limit during a disturbance as its slow in responding to responding to disturbances thus giving more time for control. With the increasing penetration of inverter based generation like solar and wind, these normally do not have any inertia though theoretically it has been

shown that with a storage unit, they can simulate inertia [68]. However, there are still practical limitations to it.

3.1.1 Literature Review

The impact of low inertia on the power systems transient stability is a well-studied problem. One of the earliest works in this regard dates back to the 70's where the trends in steam turbine generator design which maximized output per pound was shown to reduce the CCTs by 2-3 cycles [69] [70]. Basu, et al [71] shows the dependence of settling time on the relative inertia of remote machine to rest of the network for a two machine system. The work in [72] showed the importance of having a higher damping in low inertia machines. The first rigorous study in understanding the impact of inertia on transient stability was done by Nakorn [73]. He explored in detail the combined influence of generator coupling and inertia to the overall system dynamic performance during disturbances. Also, the impact of low inertia on remote hydro units on the small signal performance was studied through linearized analysis. This was before the popularity of ideas in SR and direct methods and thus most of these studies used time domain simulations to study the impact. Also, during that period, the inertia reduction problem was negligible due to the absence of inverter based generation and thus was not a prime focus.

With the increasing deployment of renewable resources all over the world leading to a downwards trend in the grid inertia, this area of research was revived and became increasingly popular. Andersson et.al [13] did a parametric study on the inertia and damping of a single machine equivalent system to analyze the changes in the SR obtained using time domain simulations. Since inertia acts as a nullifying agent on the synchronizing torque, for a single machine system, the reduction in inertia was seen to rotate the SR such that for the same starting synchronization torque, lower speeds were allowed. While this work helped giving us an insight into the expected changes in true SR, it is not practical when trying to visualize changes in larger practical systems due to computational limitations. Vittal et.al [74] analyzed the eigen sensitivity to inertia reduction and also assessed the modes excited by large disturbances using time domain simulations under high wind generation penetration. Various

scenarios showed both positive and negative impact of wind generation on mode damping. While important extremely important in its contribution, it did not give an insight into the SR changes and the reason for the particular dynamics observed. Bell et.al [75] did a parametric study on the effect of inertia reduction and fault location on CCTs using closest UEP method. While our work is along on the same lines, the difference is that not only we use a much less conservative approach (BCU) but also develop a way to visualize the problem without extra computations. Also, since the closest UEP estimates the SR according to the minimum energy UEP on the stability boundary, it would be difficult to correlate the amount of impact on the CCT with the estimated SR. Naik [76] did a similar work but using the PEBS method which has been proven to be unreliable in the estimates. Thus, there is a need for a parametric study that gives an insight into the relevant stability boundary changes as well besides the impact on the CCT. Also, this study should be extendable to large scale systems.

3.1.2 Inertia Case Study

We would be using the standard 3 machine system introduced before with PV incorporated at different buses. PV is modeled as a 0 inertia/0 damping synchronous machine. This means that the added PV has reactive support capabilities. For this study, the internal impedance of the 0 inertia PV is set according to that of the synchronous machine connected at the bus it was connected. It is important to view a single generator is being comprised of multiple small identical units connected in parallel. Thus in these studies, switching off a percentage of a generator translates to switching off appropriate number of those small component generators. Effectively in this study, the impact of replacing generators with 0 inertia machines is seen with the study details as shown below,

1. 100 % displacement ratio [77] is assumed i.e. for each PV MW added, a MW of conventional generator is switched off. The size of PV added is varied wrt the amount of generation at that bus. This is a very realistic scenario as due to the absence of associated fuel costs, PV will likely displace the much more expensive conventional units in the system. Let us define $PVratio = \frac{MW\ PV\ Added}{Total\ MW\ injected\ at\ the\ same\ bus}$ which represents

the penetration level. The parameters of the pseudosynchronous PV generator [76] at each bus are assumed to be -

Table 3.1 PV Generator Model Parameters as Pseudosynchronous Machine for Inertia Studies

Parameter	Value
$\boldsymbol{M(inertia\ const)}$	0
$\boldsymbol{D(damping\ const)}$	0
$\boldsymbol{x_d(internal\ impedance)}$	$\frac{x_d}{PVratio}$ where x_d is that of generator connected to same bus
$\boldsymbol{E(emf)}$	Same as E of the generator at that bus.

2. For $PVratio$ as a parameter and 100% displacement ratio, the net equivalent generator parameters become –

$$M_{net} = k \times M_{conventional} \tag{3.1}$$

$$D_{net} = k \times D_{conventional} \tag{3.2}$$

$$x_{d_{net}} = x_{d_{conventional}} \tag{3.3}$$

$$k = (1 - PVratio)$$

This assumption assumes a linear dependence of inertia with PV penetration level which may not always hold true. However, since we are interested in impact of inertia displacement, this study will help us capture it completely.

We start by studying a case with single PV added to the 3 machine system shown in 1.3. In this study the location of this PV as well as the penetration level is varied. As discussed before, the generator present at the same bus is the only one assumed to be impacted. The BCU results for a single PV scenario are as given below.

Table 3.2 Inertia Case Studies BCU Results for Single PV

PV Bus	Fault Bus	Trip Line	Local PV Penetration $\frac{PV}{P_g}$	SEP (δ_1, δ_2)	CUEP(δ_1, δ_2)	Ecr (pu)	BCU CCT (s)	TDS CCT (s)
1	1	1-2	0 %	(0.2468,0.2431)	(2.1175,-0.0156)	2.0062	0.2355	0.2750

			50 %	(0.2622,0.2586)	(2.1987,0.1185)	1.8767	0.1425	0.1650
			90 %	(0.27605,0.27238)	(2.2669,0.23337)	1.7673	0.0538	0.0550
2	2	1-2	0 %	(0.2468,0.2431)	(-0.2359,2.0875)	5.8376	0.2585	0.2850
			50 %	(0.2704,0.2667)	(-0.0420,2.2369)	5.4407	0.1587	0.1750
			90 %	(0.29273,0.28906)	(0.13468,2.3708)	5.0854	0.0605	0.0650
1	2	1-2	0 %	(0.2468,0.2431)	(-0.2359,2.0875)	5.8376	0.2585	0.2850
			50 %	(0.20419,0.26108)	(-0.1341,2.0764)	5.8974	0.2599	0.2850
			90 %	(0.27605,0.27238)	(-0.019355,2.0785)	5.9577	0.2620	0.2950
2	1	1-2	0 %	(0.2468,0.2431)	(2.1175,-0.0156)	2.0062	0.2355	0.2750
			50 %	(0.2704,0.2667)	(2.1305,0.0103)	2.0358	0.2385	0.2850
			90 %	(0.29273,0.28906)	(2.1398,0.040818)	2.0658	0.2444	0.2850

To begin with, in the COA reference frame, there are minor changes in the SEP with changing penetration of PV. Now one might argue that SEP should not change with inertia as seen through the nature of state equations. While it is correct to say so when talking about the relative angle values wrt one machine, the same cannot be said for angles in COA reference. This is because the changing a machine's inertia changes its participation factor (influence) in the center of angle as $\delta_i^{coa} = \frac{(M_{total}-M_i)\delta_i - \sum_{j\neq i} M_j\delta_j}{M_{total}}$. For example let equilibrium in terms of actual rotor angles be (δ_1, δ_2) for both machines with $M = 2\,pu$ in a two-machine system. This gives equilibrium in COA angles as $(\frac{\delta_1-\delta_2}{2}, \frac{\delta_2-\delta_1}{2})$. Now we increase M_1 to ∞. Recalculating the equilibrium in COA reference gives $(0, \delta_2 - \delta_1)$ which is different. Moving on with analyzing the results, it can be seen that as the PV penetration increases at the same bus where the fault happens, the CCT decreases making the system less stable. However, when the displacement is done at a bus electrically far from the fault bus, there is no impact on stability (e.g. fault at bus 2 PV at bus 1). It is also evident that the estimate of CCT by BCU is quite close to that obtained

by time domain simulation but on the conservative side due to the conservativeness associated with the CUEP approach as discussed before. The relative location of the CUEP wrt the SEP is in the direction of the angle of the accelerating generators during the fault. For example in first case (fault at generator 1), the CUEP found has a higher value for δ_1 than δ_2. This means that the CUEP should be able to capture the participation of individual generators in the mode of interest, the one that could result in instability.

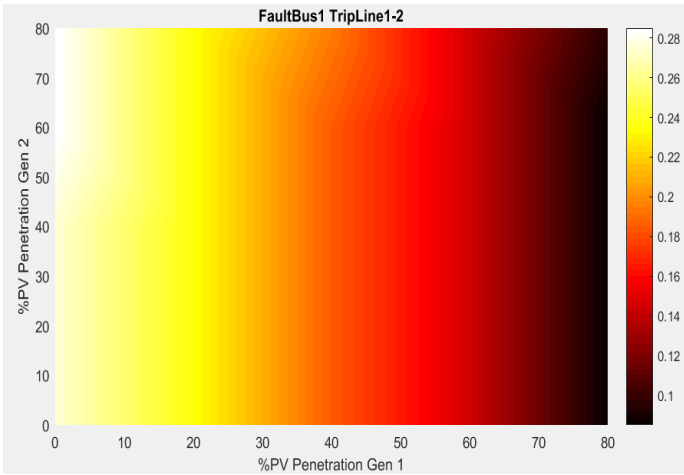

Figure 3.1 Inertia Studies - Fault Bus 1, Trip Line 1-2 CCT changes vs Local PV Penetration

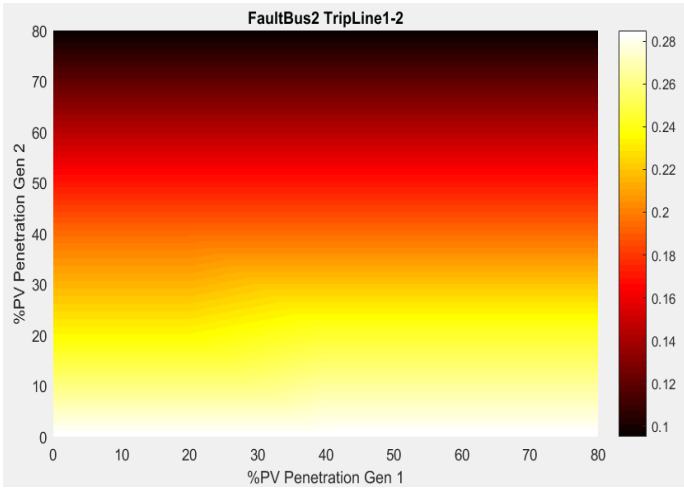

Figure 3.2 Inertia Studies - Fault Bus 2, Trip Line 1-2 CCT changes vs Local PV Penetration

The next set of studies is done to understand the combined impact of multiple PVs resulting in inertia reductions in various locations in the grid. For these, we add a PV each at buses 1 and 2 and obtain the CCT estimates for 3 phase to ground faults at different locations and varying PV

penetrations. The visualization strategy used was proposed in [78] and is a 2 dimensional plot shown in Figure 3.1, Figure 3.2 and Figure 3.3 with the axis representing the percentage PV penetration at each conventional generator location while the color denotes the severity in CCTs (decreasing stability from light to dark).

The trends in the CCT wrt to the relative location of inertia reduction can be seen more clearly. There is effectively no dependence of CCTs for faults electrically far from the areas with PV penetration as seen in Figure 3.1 and Figure 3.2. It is easy to explain in terms of the modes excited due to the disturbance. Since the farther generator does not have any participation in those, its parameters do not influence the risk of instability.

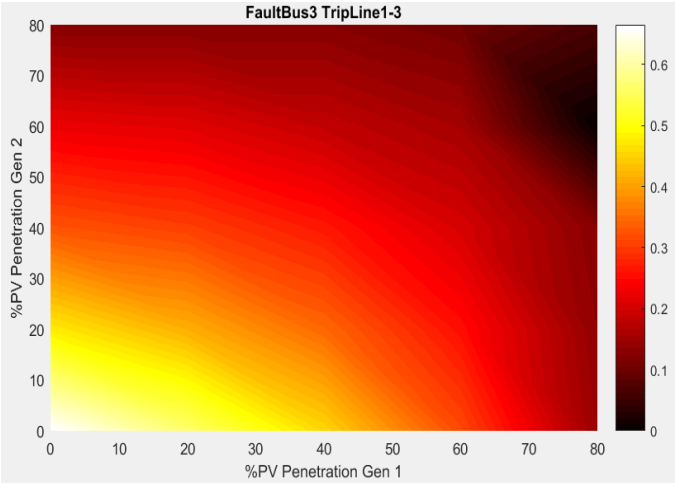

Figure 3.3 Inertia Studies - Fault Bus 3, Trip Line 1-3 CCT changes vs Local PV Penetration

However, the mode of interest for fault at generator 3 has significant participations from generators 1 and 2 due to electrically being close. This is evident in Figure 3.3 in the variation of CCTs for changing inertia at those generators as seen in the figure above.

Now, in order to better visualize the impact of inertia reduction to explain the changes in CCTs, we need to represent the portion of the stability boundary most expected to be breached by the mode of interest (relevant stability boundary) on 2 dimensional planes. According to [79], the best estimate of relevant stability boundary can be obtained using the algorithm discussed below.

Algorithm 3.1 Estimating Relevant Stability Boundary

1. Obtain controlling UEP from BCU method for the disturbance under study.
2. Plot the constant energy surface passing through the controlling UEP found.
3. The SR estimate is the connected component containing the SEP.

Since for an n dimensional system, the stability boundary is $n-1$ dimensional, we need a visualization over relevant lower dimensional (2D) surfaces for varying inertia. Also, the impact of inertia reduction cannot be seen clearly in the angle domain thus requiring ω domain. As discussed before, we use the CUEP to identify the interesting machines from the point of view of stability. Finally, we plot the intersection of the relevant stability boundary with multiple planes for varying PV penetration at each PV bus individually. Each plane corresponds to a unique machine of interest, has δ and ω of that machine as its axes. All other machines δ and ω are set to the values at the SEP.

We start by analyzing the faults at bus 1 and 2. For the first two figures below, the PV is at the same bus as the fault. Based on the CUEPs for these cases (from BCU results table), we see that only the local machine as well as machine 3 participate in these faults. Since we eliminate the machine 3's states anyways, the only machine of interest is the one at which the fault occurs.

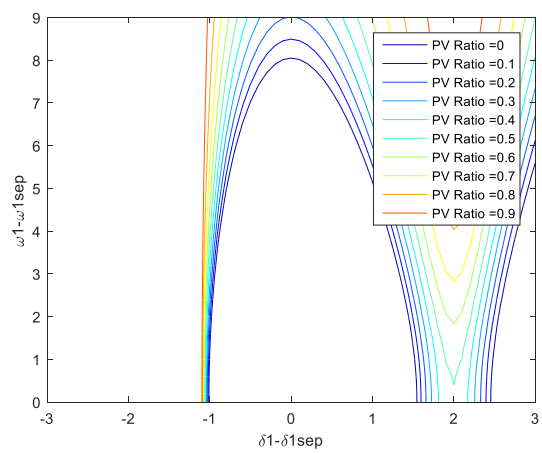

Figure 3.4 Inertia Study – FB = 1, PB = 1, L = 1-2 Estimated Relevant Stability Boundary Projection vs Local PV Penetration

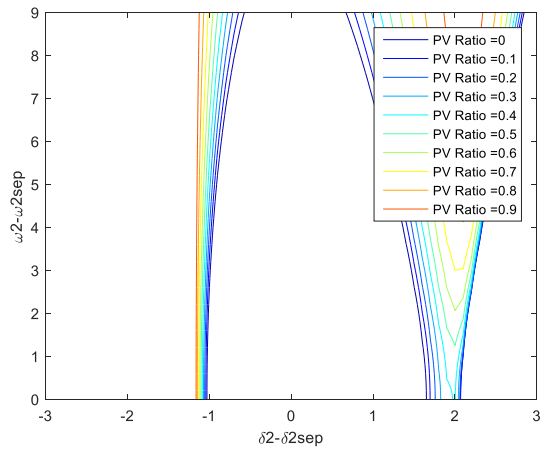

Figure 3.5 Inertia Study – FB = 2, PB = 2, L = 1-2 Estimated Relevant Stability Boundary Projection vs Local PV Penetration

So, plotting the intersection of the relevant stability boundaries with states of machines of interest for varying PV penetration, we get figures Figure 3.4 and Figure 3.5. In these plots, FB = fault bus, PB = PV Bus and L = Tripped Line. We can notice from these figures that the values of ω with which the post fault trajectory can start and still remain inside the SR are higher for the higher penetration case (lower inertia) for local faults. Inertia plays the role of reducing the impact of synchronizing torque (which increases with increasing δ upto a certain extent) as seen through the swing equation. Thus, the same amount of synchronizing torque (same δ_1) has more impact on a lower inertia generator than on a higher one and thus is able to bring back the lighter generator moving at the same speed more easily than heavier one. This can also be also be physically understood as the amount of effort (synchronizing torque) required to stop a heavy body (high inertia machine) is more than that required for a lighter body moving at the same speed (ω).

Moving on, we study cases with PV is introduced at a bus electrically far from the fault bus. As seen in the previous cases, only the local machines are interesting. Plotting the projection of relevant stability boundary with varying PV penetration, we obtain the estimates shown below.

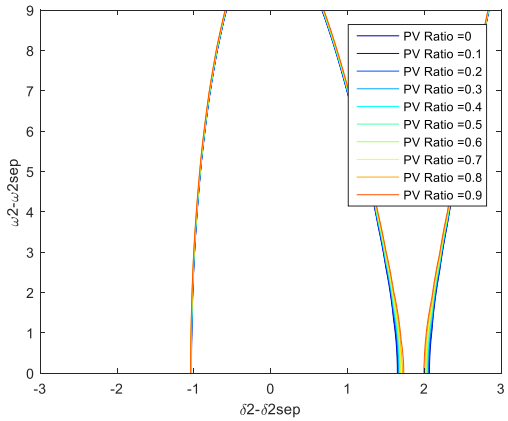

Figure 3.6 Inertia Study – FB = 2, PB = 1, L = 1-2 Estimated Relevant Stability Boundary Projection vs Local PV Penetration

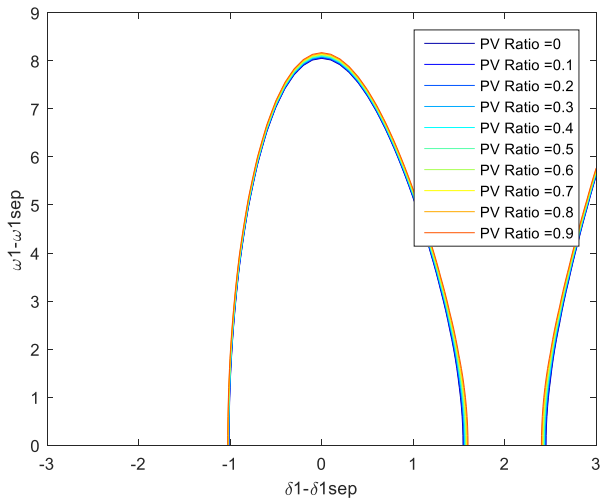

Figure 3.7 Inertia Study - FB = 1, PB = 2, L = 1-2 Estimated Relevant Stability Boundary Projection vs Local PV Penetration

Using the above figures, we can clearly explain the changes in CCTs as seen before. The displacement of inertia in electrically farther regions of the grid has no major influence on the relevant stability boundary thus not influencing the stability for those faults. Finally, we analyze a case where the fault is at a bus electrically close to both the machines with inertias displaced.

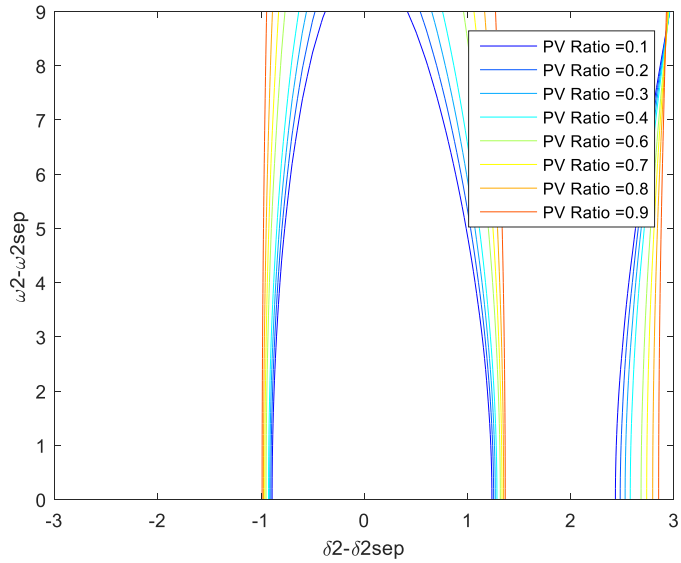

Figure 3.8 Inertia Study - FB = 3, PB = 2, L = 1-3 Estimated Relevant Stability Boundary Projection vs Local PV Penetration

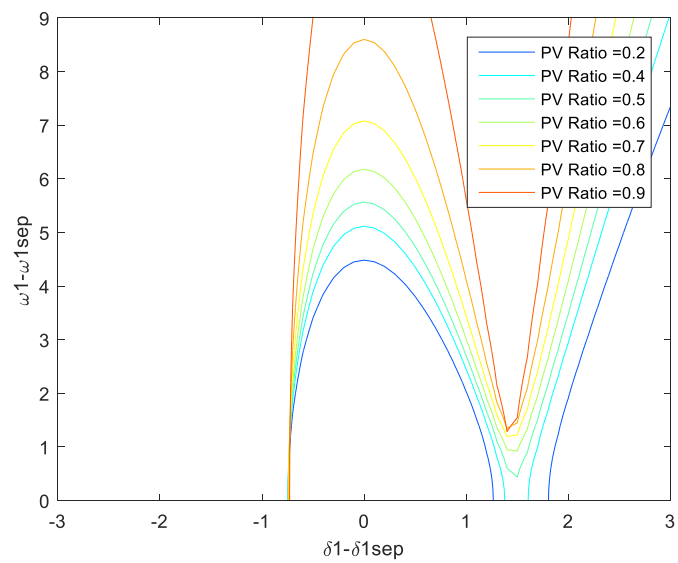

Figure 3.9 Inertia Study - FB = 3, PB = 1, L = 1-3 Estimated Relevant Stability Boundary Projection vs Local PV Penetration

In the above two figures, the fault is at bus 3. Based on the CUEP values as seen before, both machines 1 and 2 had considerable participation in this fault. Now, varying the PV penetration at each of the machines individually we see that the relevant stability boundary is impacted considerably in terms of states of both the machines as expected from our discussion.

3.2 Impact of Generation Dispatch

While inertia reduction is a big threat to stability, another quantity that impacts stability is generation dispatch/loading. Power system operation revolves around maintaining an economical and a reliable generation load balance. Since the generators are not capable to pick up rapid changes in loads, the load is forecasted day ahead to generate the operating schedule for each generator [80] for the whole day which included what periods it would be online and how much power would it produce. Since the forecasts cannot be 100% accurate, in real time some of the units (called peaking units) which are much more capable in picking up loads quickly balance out the net generation to loads while the other heavier/larger units (called the base load units) operate at their max normally and do not adjust their powers. Now with the PV coming into picture which is an unreliable generation, the system operations currently does not treat PV as dispatchable units and thus treated as a load reducer. Now PV is seen to develop in areas with cheaper lands [81] and those areas are not necessarily provided with a good enough transmission networks. Thus there is an increased flows in parts of the network which did not see much before which increases the normal operating angle differences between some regions in the system while decrease between some others. This can be dealt with up to a certain extent by changing the dispatch on units but this is heavily constrained by fuel costs. Increase in angle difference reduces the synchronizing torque between generators of those regions making it more difficult to maintain synchronism between them during disturbances thus threatening the stability.

3.2.1 Generation Dispatch Case Study

In this study, we vary the way a fixed amount of PV at a given location in the system is accommodated by generators through re-dispatch. We try to visualize how the structure of SR changes due to the changes in operating point (SEP) to draw conclusions regarding the impact on stability. The details of the study modeling are as follows –

1. Power generated by PV is 4 pu ~ 30% of total load. It is introduced at bus 3 as a negative real load.

2. % of PV accommodated by generator 1 & 2 are used at parameters (rest absorbed by generator 3). This is modeled for a generator i as a decrease in steady state loading –

$$Pg_{i_{new}} = Pg_{i_{old}} - PVsize \times (\%PV\ accomm\ by\ i^{th} gen) \tag{3.4}$$

The loading and dispatch changes impact the potential energy of the system directly [82]. According to [83], under the BCU assumptions satisfied, the gradient system's stability boundary (also known as the PEBS) is the intersection of original system's SR with the plane characterized by $\omega_i = 0\ \forall i \in [1, n_g]$. Thus, we will be plotting the changes in PEBS to visualize the stability region changes with changing generation dispatch in this study. We are primarily interested in the relative location of the SEP to the PEBS in order to get an insight. For tracing the stability boundary of the gradient system, there are two popular algorithms (dynamic gradient [41] and the ray method [40]) for the same task. Both of these utilize the topological properties of the gradient system's stability boundary and require only the states of the gradient system. The ray method constructs several rays emerging from the SEP while calculating the energy function (potential energy of original system) value along each. The stability boundary is characterized by first local maxima of energy function value along each ray starting from SEP. The drawback of this scheme is that it assumes that each ray is transversal to the stability boundary. An improvement over this scheme was proposed referred to as the dynamic gradient method involves integrating the gradient system trajectory for a few big steps (along the gradient of potential energy) and then evaluating a metric whose value is supposed to be positive everywhere inside the gradient system's SR and negative at least in the immediate neighborhood of the boundary lying outside the SR. The algorithm for it is as shown below.

Algorithm 3.2 Dynamic Gradient for PEBS Estimation

1. Define a meshgrid of points in gradient system's state space (δ).
2. For j = 1:num points
3. **Computing Metric $\boldsymbol{\mu}$-**
    a. Set $\delta_0 = j^{th}\ point\ \delta(j)$. Initialize h as number of steps.
    b. k = 1

c. Calculate distance $d1$ from SEP to δ_0. Set $\delta = \delta_0$

d. Compute normalized unit vector u in direction of potential energy gradient (given by RHS ($f(x)$) of gradient system equation) at δ–

$$u_i = (P_{mi} - P_{ei}(\delta) - \frac{M_i}{M_{total}} P_{coa})/\|u\| \tag{3.5}$$

Where $u = [u_1, u_2 \dots u_{ng}]^T$

e. Advance angle along the gradient –

$$\delta_{new} = \delta + u\left(\frac{d1}{h}\right) \tag{3.6}$$

f. If k < h, k = k + 1. $\delta = \delta_{new}$ GOTO d.

g. STOP. Compute distance $d2$ from SEP to δ. Metric = $\mu(\delta(j)) = d1 - d2$.

4. The connected component made by points with value of μ >= 0 gives the estimate of SR.

Now, we obtain results for the given two parametric studies to study the impact of dispatch–

1. PV accommodated by generator 2 fixed, PV accommodated by generator 1 varied.
2. PV accommodated by generator 1 fixed, PV accommodated by generator 2 varied.

The gradient system SR is plotted in angle domain (δ_1, δ_2) with the SEP shifted to the origin. The UEPs lying on the stability boundary are marked by thick dots (found using Algorithm 2.7).

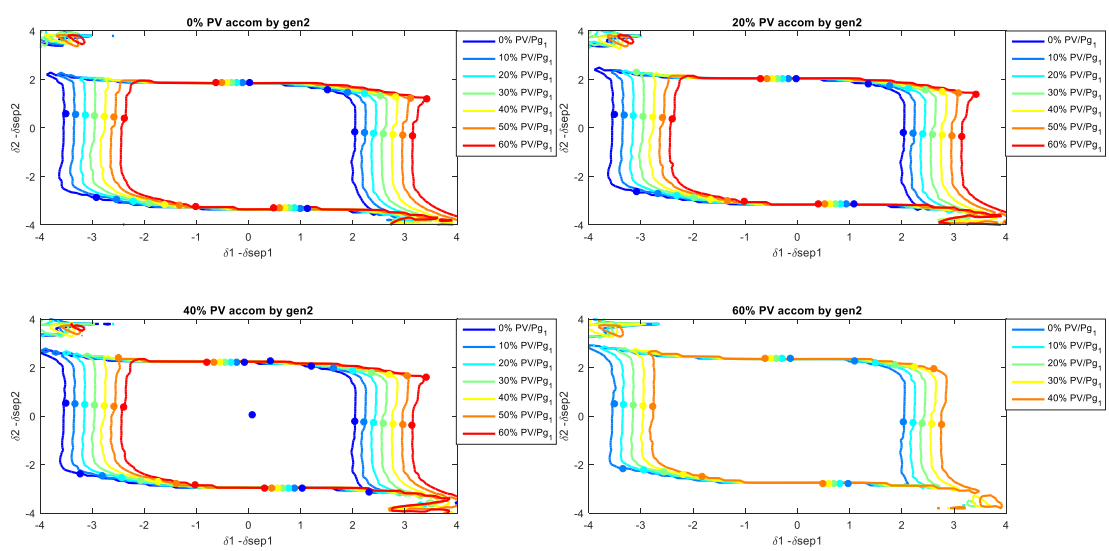

Figure 3.10 PEBS Changes with Increasing PV Accommodated by Generator 1

As seen in the figures above, the stability boundary shifts in the direction of generator 1's angle with increasing under-loading of generator 1 to accommodate PV. This means that the system has more chances of being stable for faults at generator 1. The same can be observed at generator 2. However, it can also be seen that this has a negative impact for negative angle excursions. Loss of generation is one such event for which the dynamics are negatively impacted on increasing under-loading. The number of these types of events is expected to rise if the ride-through requirements are not revised in accordance with the growing inverter based generation.

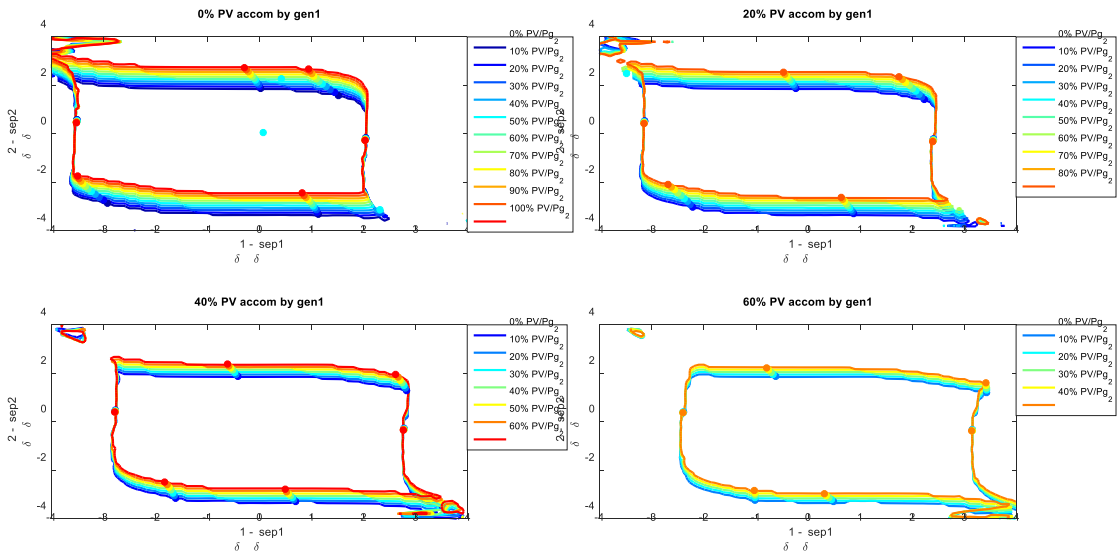

Figure 3.11 PEBS Changes with Increasing PV Accommodated by Generator 2

Chapter 4 Studying the Impact of Low Voltage Ride Through (Inverter Protection) using Direct Methods

Traditionally, the inverter based generators were made to trip offline during major disturbances as they were not treated like regular generation for grid support. Since large amounts of PV are being incorporated into the grids all over the world, this translates into large amounts of generation lost during disturbances. This poses a serious threat of system collapse. Inverter ride through capabilities safeguard against these scenarios. The ride through standards defines operating requirements for PV to not trip offline. These are primarily arrived at keeping the protection of inverter as well as utility preferences in mind. However, these generators still are tripped offline due to various reasons. Firstly, the fault current contribution of these generators is determined by the solar irradiance and current limiter logic unlike conventional generators which can provide extremely high fault currents. Thus, effectively, the internal impedance of the solar PV generator changes a lot throughout the day. Specifically for distribution systems, the protection system is overcurrent based which makes it challenging to design for distribution connected PV systems. Therefore, these need to be deliberately tripped offline during nearby faults in order to stop feeding the fault from the point of view of safety of the personnel. Also, utilities do not have total control over most of these generators because they are mainly privately owned. As for the larger sites, they are a mix of utility owned and privately owned with full control over the former type but these still need to follow the NERC standards for ride through characteristics [84]. There is also a level of uncertainty associated with this type of generation which further puts a doubt over dependability and therefore another reason why the utilities trip them offline during major events. However, the ride through standards for both transmission and distribution connected PV are still under development [85] [84] and not fully adopted yet by inverter manufacturers adding more complexity to the system. These standards are mainly voltage and frequency ride through curves which define the time dependent

operating limits (upper and lower) on voltage and frequency respectively at the point of interconnection to the grid. Power system faults which result in depressed voltages constitute the major portion of the events that threaten the transient stability and therefore will be the focus of our studies. The low voltage ride through (LVRT) curves defined for each inverter which as the name suggests give a lower limit on the voltage as a function of time are the main culprits for tripping PVs during these events. For the remainder of this thesis, we will be treating the tripping of the PV synonymous to its lower voltage limit (from LVRT curve) violated. However, the techniques that will be developed can be easily extended to incorporate other ride through constraints as well. The standard ride through curves vary a lot and are carefully designed based on the characteristics of the grid they are deployed in. For example, a system with a lot of induction motor loads is known to have a much slower voltage recovery than systems with static loads [86]. So, voltage recovering to nominal values in 5 minutes might be normal for the former cases while abnormal for latter. Shown below are LVRT curves defined by various standards. As we can see that these can be quite different from each other.

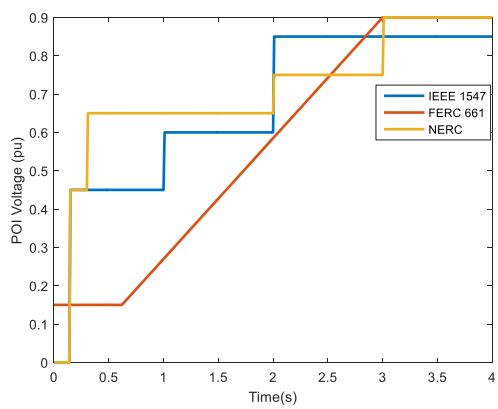

Figure 4.1 LVRT Standards

Thus, with increasing renewable penetration, we will have power systems relying on generation which is made more prone to trip offline. This added complexity makes the problem of studying power system transient stability using direct methods much more complicated. To the best of our knowledge, this problem has not been tackled in its entirety and thus we plan on taking the first steps. In this chapter, multiple approaches will be proposed differing in the way this uncertainty is handled. We will be majorly relying on SOS programming by demonstrating its

effectiveness in dealing with complex systems such as this. It should be kept in mind that in this section of work, the power system model in single machine reference frame (with n_g^{th} machine as the reference) is used as opposed to COA frame in the previous section. Also, PV will be modeled as a negative real load in accordance with the common modeling practices. Thus, the inverter dynamics are totally ignored with no reactive support from them.

4.1 Constrained System Approach

Traditionally, the aim of transient stability assessment used to be to capture the mode that resulted in loss of synchronism of synchronous machines. This was characterized by the post disturbance system trajectory leaving the SR of the corresponding SEP as discussed before. However, another potentially severe scenario that has emerged in systems with prone to tripping renewable generation is a single generation tripping event triggering a cascading sequence. Since the PV location is heavily dependent on the land prices, it is common to see multiple PVs connected in the same region of the grid. This makes increases the chances of cascaded tripping which could potentially lead to system collapse. Thus, in this section, we treat tripping of even a single PV as an instability phenomenon, an idea that was first discussed in [87].

Let us now give a brief background in the type of systems we will be dealing with called the constrained systems. There are mainly two types of commonly present constraints in dynamical systems viz. equality and inequality constraints. Equality constraints when present, force the systems to evolve over a manifold. Thus, if we restrict the starting point of a trajectory to the given constraint manifold, the emerging trajectory will always stay on it. An example is the power system which is constrained to satisfy a balance in nodal injections (Kirchoff's laws). The inequality constraints usually stem from the physical limitations of the system or system designer's preferences. Since we are only focusing on the LVRT, the inequality constraint in our case requires is that the voltage at each PV's point of interconnection should be above the respective LVRT curve. Due to the presence of these inequality constraints, the state space is divided into feasible and infeasible regions. In our problem, the former consists of all those points that do not violate the ride through constraints of any of the connected PVs in the

system. Unlike the equality constraints, the inequality constraints do not influence the system dynamics. What this means is that the system will behave as though it did not have any inequality constraints.

From the point of view of stability, an added characteristic of a stable trajectory is that it should not enter the infeasible region. This requires us to define a CSR vs an SR for the desired SEP. Here the word constrained represents only inequality constraints. This could be thought of as the largest invariant portion of the corresponding unconstrained system's SR that does not intersect the infeasible region. It is important to keep in mind that CSR is smaller than unconstrained SR minus the infeasible region which an be understood from the following figure. The ellipse represents the SR of the unconstrained system for the SEP x_s. Everything lying above the feasibility boundary is infeasible while below it is feasible. Now, one big requirement for the CSR is that it should be invariant. This is because we want the trajectories to always remain in the feasible region as well as the SR (which ensures they converge to x_s). In this case, we can clearly see that the region defined by unconstrained SR minus the infeasible portion (upper sector) is not invariant. This is because the trajectory starting from the marked test point which is still inside the feasible region and SR breaches the feasibility boundary thus not a part of the CSR (shaded grey area).

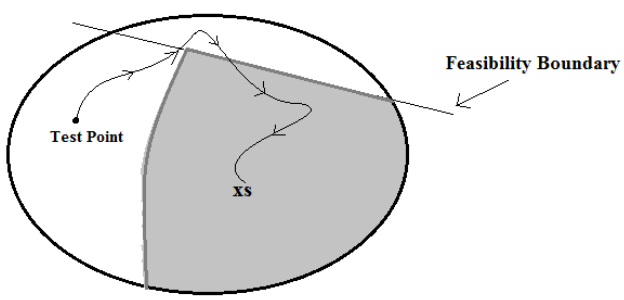

Figure 4.2 Constrained Stability Region (Grey)

4.1.1 Challenges in Analytical Energy Function Based Methods for TSA of Systems with Inequality Constraints

Previously it was discussed in 2.1.1 that the analytical energy function based methods are developed for autonomous non-linear systems and thus are not capable of handling constrained systems. In [88], a way to convert a constrained system to an unconstrained one was shown with the CSR of constrained system same as the SR of the transformed system. This appears to make the applicability of the energy function based methods straightforward for TSA of such systems. The idea was that any given n dimensional constrained system,

$$\dot{x} = f(x) \tag{4.1}$$

$$h_i(x) \geq 0 \; \forall i$$

Can be converted to the following unconstrained system,

$$\dot{x} = (\prod_i h_i(x)) \times f(x) \tag{4.2}$$

4.1.1.1 Critical Points of Transformed Unconstrained System

As evident, there are two types of EPs viz. original system's EPs denoted by $x_{ep-or} \in \{x | f(x) = 0\}$ and points on feasibility boundary (pseudo EPs) denoted by $x_{feas} \in \{x | \prod_i h_i(x) = 0\}$. Linearizing the system around any EP x_{ep} we get,

$$\Delta\dot{x} = \left[\prod_i h_i(x_{ep}) \times \frac{\partial f(x_{ep})}{\partial x} + \sum_j \prod_{i \neq j} h_i(x_{ep}) \times \frac{\partial h_j(x_{ep})}{\partial x} \times f(x_{ep})\right] \times \Delta x \tag{4.3}$$

Let us first try to understand the dynamic properties of the original system's EPs and how they get modified due to this change in vector field. The linearized system becomes,

$$\Delta\dot{x} = \left[\prod_i h_i(x_{ep-or}) \times \frac{\partial f(x_{ep-or})}{\partial x}\right] \times \Delta x \tag{4.4}$$

First thing that's evident is that stable manifold $W^s(x_{ep-or})$ and unstable manifold $W^u(x_{ep-or})$ of x_{ep-or} swap if $\prod_i h_i(x_{ep-or}) < 0$ thus type k becomes type $n-k$. Furthermore, the shape of $W^s(x_{ep-or})$ and $W^u(x_{ep-or})$ are unchanged inside the region

$\prod_i h_i(x) > 0$ due to the vector field transformation being just a mere scaling in the original vector field $f(x)$ with no changes in direction.

Now, let us move on to the points on the feasibility boundary ($\{x| \prod_i h_i(x) = 0\}$) of the original constrained system which serve as pseudo EPs for the transformed system. We are mainly concerned with the feasible region of state space when estimating the CSR. The feasibility boundary is a union of individual sections of maximal dimension $n-1$ [88] where a jth section is characterized by $\{x|h_j(x) = 0, h_i(x) > 0\ \forall i \neq j\}$. The intersection of these sections is an n dimensional manifold.

Firstly, let us focus on the points on an individual section j with $f(x_{feas}) \neq 0, h_j(x_{feas}) = 0$ and $h_i(x_{feas}) > 0\ \forall i \neq j$. The linearized system becomes,

$$\Delta\dot{x} = \prod_{i \neq j} h_i(x_{feas}) \times \begin{bmatrix} f_1(x_{feas}) & 0 & 0 \\ 0 & \ddots & 0 \\ 0 & 0 & f_n(x_{feas}) \end{bmatrix} \times \begin{bmatrix} \frac{\partial h_j}{\partial x_1} & \cdots & \frac{\partial h_j}{\partial x_n} \\ \vdots & \cdots & \vdots \\ \frac{\partial h_j}{\partial x_1} & \cdots & \frac{\partial h_j}{\partial x_n} \end{bmatrix} \times \Delta x \tag{4.5}$$

Since the last matrix on the right has rank 1, we have $n-1$ eigen values as 0. The eigen vectors forming the local center manifold (corresponding to 0 eigen value) are tangential to the feasibility boundary itself. Thus, the vector field for the transformed unconstrained system is 0 on the center manifold. Since trace of a matrix = sum of eigen values, the only possible non 0 eigen value can be $\prod_{i \neq j} h_i(x_{feas}) \frac{\partial h_j(x_{feas})}{\partial x} f(x_{feas})$ whose corresponding eigen vector is not tangential to the feasibility boundary. We can further classify the nature of those points according to the sign of this eigen value, sink if negative, source if positive and saddle if 0 which is when $f(x)$ is tangential to $h_j(x)$. It is important to mention that the dimension of manifold defined by the set of all saddle points is $n-2$. The dynamics around source and sink type pseudo EP surrounded by pseudo EPs of the same type can be understood through the Figure 4.3. For the saddle pseudo EP, we take a closer look at the field lines around it in Figure 4.4. The unidimensional center manifold W^c transverse to the feasibility boundary can be divided into stable (W^s) and unstable (W^u) manifolds marked. Needless to say, on a section of the

feasibility boundary, assuming smoothness, the source and sink EPs are always separated by saddle EPs.

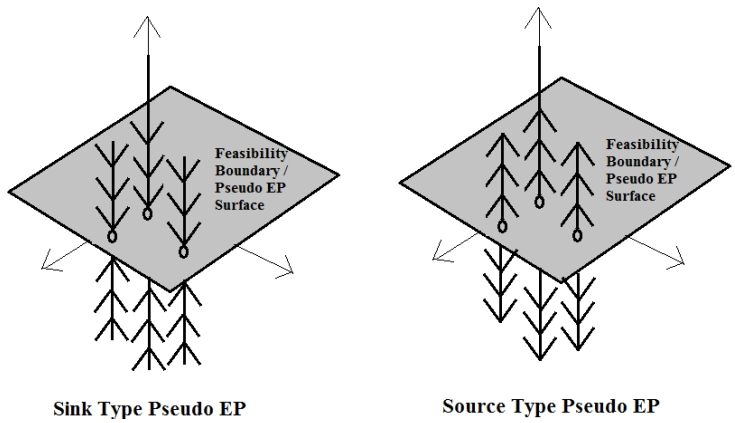

Figure 4.3 Dynamics Around Pseudo EPs

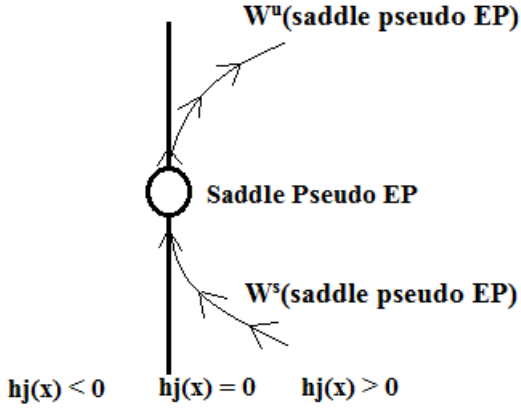

Figure 4.4 Field Lines Around Saddle Pseudo EP

Furthermore, all other points at the intersection of such sections have all 0 eigen values since the state matrix on linearization has all zeros elements.

4.1.1.2 Stability Boundary of Transformed Unconstrained System

Since the characterization of the stability boundary on which the mentioned direct methods rely is only for systems with hyperbolic EPs [34] or limit cycles, there is a need to characterize the constrained system's stability boundary. In [89], the characterization of stability boundary of systems with equality constraints (DAE systems) was discussed which has certain similarities to the system being dealt with in our case. Loparo et.al [88] further went ahead to study the

stability boundary for systems with inequality constraints, the ones we are interested in. We will however be approaching the results from a different direction with the final outcome same as Loparo's results. The general progression of this section starts by drawing comparisons to the DAE systems and deriving the stability boundary for constrained systems using DAE's results [89].

The DAE systems have a singular surface where the dynamics do not exist and thus a transformed unconstrained system is constructed which has dynamics existing everywhere. In those systems, intersecting the singular surface is treated as a phenomenon for instability which is equivalent to intersecting the feasibility boundary in our system. The critical points for that transformed unconstrained representation of DAE systems has original system's EPs, pseudo EPs which lie on the singular surface with at most 2 non zero eigen values and semi singular points which also lie on the singular surface but have non zero vector field tangential to the singular surface. In our system, we do not have an equivalent of semi singular points as all the points on the feasibility boundary (equivalent of singular surface) are pseudo EPs. The W^s and W^u of the pseudo EPs if exist are free to be tangential to the singular surface (those that do not have tangentiality are called pseudo transverse EPs) while in our case they are always transversal to the feasibility boundary.

Now, moving on to the characterization of the stability boundary for DAE systems, it could be thought of as being comprised of parts of stable manifolds of original system's EPs and points from which the emerging trajectories intersect the singular surface. The latter part is actually made up of sections of the singular surface, stable manifolds of some pseudo EPs and semi singular points for the DAE system. Equivalently for our system, it should be comprised of some sections of the feasibility boundary and the stable manifolds of the points on it (pseudo EPs).

It was shown for the DAE systems that the pseudo EPs with both negative eigen values (pseudo sink) cannot lie on the stability boundary while ones with both positive eigen values (pseudo sources) can lie on the boundary but are unimportant for characterization. Only the pseudo EPs which have eigen values of opposite signs (pseudo saddles) were shown to be important for stability boundary characterization. In our case, we do not have those types of points due to

only a single possible non zero eigen value which requires the derivation of sufficient conditions on the invariant manifolds of those critical points necessary for them to lie on the stability boundary. Since the stability boundary is $n-1$ dimensional, the points lying on the intersection of individual sections ie the pseudo equilibrium points having $h_j = 0$ at more than one j cannot lie on the stability boundary. Also, the sink type pseudo EPs on the individual sections cannot lie on the stability boundary. This is because any point in the immediate neighborhood of such point will be attracted to the feasibility boundary if not to the same EP as seen in Figure 4.3. Thus, the only pseudo EPs that can possibly lie on the stability boundary are unstable ones and saddle ones.

Before proceeding with the characterization, it should be mentioned that we take the following assumptions related to the system under question.

(F1) Original system EPs are hyperbolic.

(F2) The intersection of stable and unstable manifolds of original system EPs and pseudo EPs lying on the stability boundary is transversal except for at the pseudo saddle points.

(F3) The trajectory starting on the stability boundary converges to one of the EPs.

Now, it was shown that for the transformed DAE system [89], a critical point x_0 (original system EP, pseudo EP or semi singular) lies on the stability boundary if $W^u(x_0)$ intersects the SR. Due to the maximal dimension of stability boundary being $n-1$, the most important elements for characterizing were expected to be type 1 hyperbolic EPs for original system and connected $n-2$ dimensional component of transverse pseudo saddle EPs and transverse semi singular saddle. Since all our pseudo EPs are transverse and there are no semi singular points, we are mainly interested in individual sections of feasibility boundary which are $n-1$ dimensional connected components of pseudo EPs. Using the result for DAE systems, we can say that only the source type pseudo EPs whose unstable manifold intersects the SR lie on the stability boundary. Furthermore, the following theorem [34] gives the necessary conditions for a connected component of such source type pseudo EPs to make up a portion of the stability boundary.

Theorem 4.1 Let $A(x_s)$ be the stability region of an asymptotically stable equilibrium point x_s of a DAE system. Let $v \in$ connected component of source type pseudo EPs. $v \in \partial\overline{A(x_s)}$ if there exist δ_0 such that $W^u(\delta(v)) \cap A(x_s)$ is dense in $W^u(v)$ for every δ-neighborhood of v in that connected component.

Characterization of the saddle type pseudo EPs is a bit tricky. In [90], the presence of type-0 saddle node EPs ($n-1$ negative eigen values and single 0 eigen value) on the stability boundary was studied. This was possible only if W^u part of the W^c of those points intersected the SR. In the saddle pseudo EP of interest to us, vector field is 0 in the part of the center manifold tangential to the feasibility boundary while non-zero otherwise. Since the feasibility boundary cannot intersect the SR, the only way this point can lie on the stability boundary is if its W^u intersects the SR. On fulfilling this condition, the W^s of this point serves as a part of the stability boundary.

Shown below is a constrained single machine infinite bus system.

$$\dot{\delta} = \omega$$

$$0.1 \times \dot{\omega} = 0.8 - \frac{\sin(\delta)}{0.5} - 0.2 \times \omega$$

$$h_1(x) = 1 - \delta > 0$$

$$h_2(x) = 1 - \omega > 0$$

Here, $n = 2$ and state vector $x = [\delta, \omega]^T$. Firstly, in Figure 4.5, we show the stable trajectories near the section of the feasibility boundary characterized by $\{(\delta, \omega) | \delta = 1\ (h_1(x) = 0), \omega \neq 1\ (h_2(x) > 0)\}$. The pseudo EPs are marked red if source type and blue of sink type. The relevant portion of the stability boundary is highlighted in black. It can be seen that the part of the feasibility boundary on the right ($\delta = 1$) that serves as the stability boundary is comprised of pseudo EPs whose W^u intersects the SR. Also, there are 2 saddle pseudo EPs (marked in green). The W^u of these intersects the SR thus W^s of both of them serves as a part of the stability boundary. We can also see that the sink type pseudo EPs (blue) do not lie on the stability boundary.

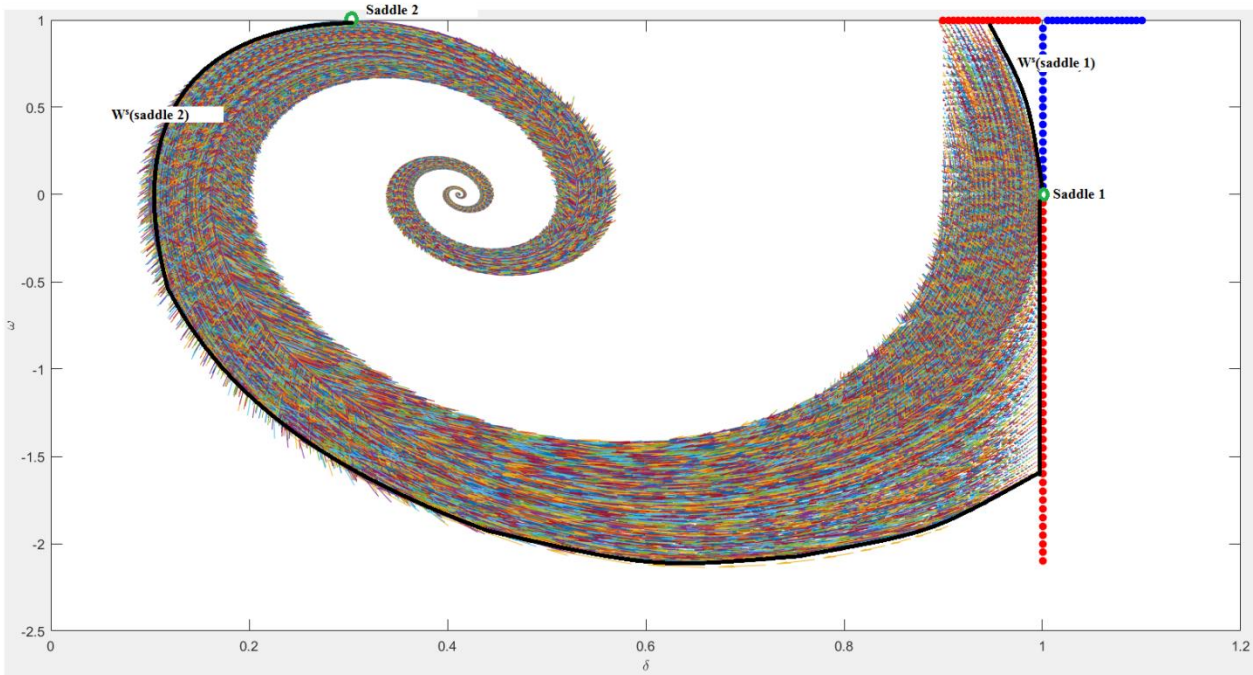

Figure 4.5 Stable Trajectories Around Feasibility Boundary $h_1(x) = 0$

Now, let us plot the stable trajectories emerging from the other connected component of the feasibility boundary $((\delta, \omega)|\delta < 1, \omega = 1)$ in Figure 4.6.

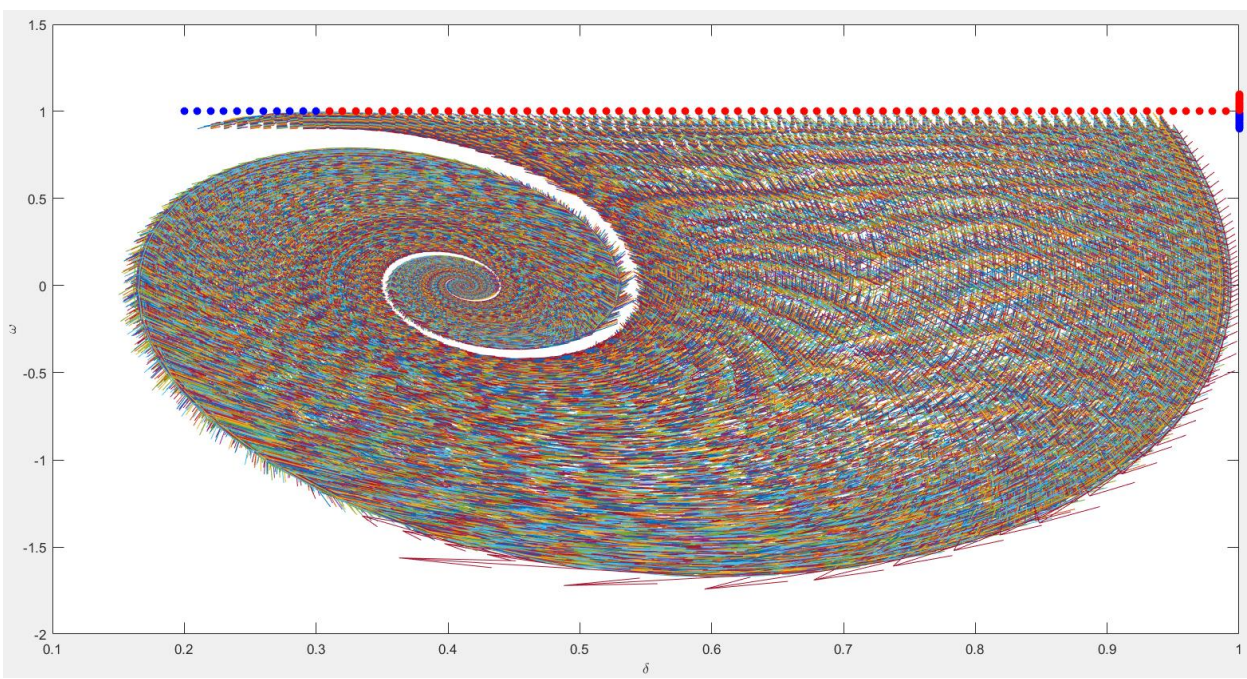

Figure 4.6 Stable Trajectories Around Feasibility Boundary $h_2(x) = 0$

The same thing is observed in these trajectories as well where only the source type pseudo EPs whose W^u intersects the SR lie on the stability boundary.

Now, after the characterization of the original system and pseudo EPs on the stability boundary is done, a need for a direct method arises. Loparo et.al introduced a modification to PEBS method for estimating the critical energy for a given disturbance. If the disturbance trajectory intersected the PEBS first then the potential energy of the intersection point was used as the critical energy as is the case with traditional PEBS which has been shown to be reliable only when this exit point is sufficiently close to the CUEP [35]. As for the case with the disturbance trajectory hitting the feasibility boundary at one of the constraints first say $h_j(x) = 0$, he proposed using the potential energy at that point to get lower bound on CCT and proposed finding the nearby pseudo saddle point with maximum energy using quadratic programming on the same section of the feasibility boundary to get an upper bound on CCT. There are however major problems to this part of the approach. One is that the section of the saddle type pseudo EP whose W^s is intersected by the disturbance trajectory can lie on a completely different section $h_i(x) = 0$ of the feasibility boundary as compared to the section of the feasibility boundary intersected by the sustained trajectory. For example, in Figure 4.5, a disturbance trajectory intersecting $h_2(x) = 0$ near the point of intersection both sections $h_1(x) = 0$ and $h_2(x) = 0$ has the CUEP as saddle1. However, the proposed approach will search for saddle2 point as upper bound and energy at point of intersection as lower bound. Thus, both the bounds obtained could be wrong. Another limitation was that the constraints being dealt with did not contain ω terms which means that the constrained emerging from frequency ride through curves cannot be dealt with using this technique. These problems were mentioned as limitations of that approach but were not addressed leaving a major scope for future research. As for the application of BCU method to this type of a system, one major roadblock is proving the existence of an energy function under all sorts of ride through constraints which is an impossible task. Also, defining a gradient system satisfying the dynamic properties as defined in 2.1.5 is not straightforward. The feasibility boundary can comprise of pseudo EPs with non-zero ω. Furthermore the type of pseudo EPs (on feasibility boundary) is determined by the lie

derivative of the constraint at that point. This means that the EP type is not independent of ω. Thus, simply removing the ω terms as done before does may change the type of those EPs.

That being said, Lyapunov based direct method can be easily employed for constrained systems since SOS programming provides a way to systematically find it and the associated CSR. Thus, we will be using it to directly deal with the original constrained system without any transformation necessary. In this chapter we will be developing techniques to estimate this CSR using various proposed approximations for the LVRT constraints. These would also provide a framework for dealing with several other operating constraints like frequency ride through, line limits, etc commonly found in practical power systems.

4.1.2 Modeling

One issue that might bother us is that in a power system network reduced model, all the buses are eliminated except for the internal generator buses. So the question comes, how to model the tripping of the eliminated PV bus as well as the LVRT constraint. To answer these questions let us go back to Algorithm 1.1 which deals with forming the network reduced model. For the former question, when the PV is first converted to an impedance load connected as shunt, we can remove this shunt and then continue with the elimination process to get the reduced network admittance matrix corresponding to PV tripped system configuration. For the latter question, we will derive the explicit expression for the voltage magnitudes at network buses for any general network in terms of system states δ, ω and network admittances in a single machine reference frame. Here it should be noted that since the loads are modeled as purely impedance types, thus the impasse surface corresponding to no network solution does not exist [91]. Let us write the nodal equation for extended system (network buses + internal generator buses) after converting loads to impedances as done before in Algorithm 1.1 -

$$\begin{bmatrix} 0 \\ I_g \end{bmatrix} = \begin{bmatrix} Y_{bus}^{new} & Y_{12} \\ Y_{21} & Y_{22} \end{bmatrix} \begin{bmatrix} v \\ E_i \end{bmatrix}$$

Where v are voltages at network buses that we are interested in. Here it should be kept in mind that all the variables above are complex numbers. Here the internal emf of generator can be

written in polar form as $E_i = |E_i| < \delta_i$. Thus using the upper block of the matrix equations we get –

$$v = -[Y_{bus}^{new}]^{-1}[Y_{12}]\begin{bmatrix} |E_1|\left(\cos\left(\delta_1 - \delta_{n_g}\right) + jsin\left(\delta_1 - \delta_{n_g}\right)\right) \\ \vdots \\ \left|E_{n_g}\right|\left(\cos\left(\delta_{n_g} - \delta_{n_g}\right) + jsin\left(\delta_{n_g} - \delta_{n_g}\right)\right) \end{bmatrix} \tag{4.6}$$

All the terms are constants in the above expression except for δ which is the state vector. The magnitude of v can easily be represented as a function of δ. Since the SOS formulation requires all the functions to be polynomials, the constraint of $v_{pvbus} - LVRT\ Curve > 0$ requires both v_{pvbus} and $LVRT$ curve chosen to be polynomials in transformed states. Let us show how v can be formulated in terms of transformed variables z defined in [52]. In the above expression, $|E_i| < \left(\delta_i - \delta_{n_g}\right) = (\delta_{in_g})$ can be written as,

$$\left(|1| < \left(\delta_{in_g}^s\right)\right) \times \left(|E_i| < \left(\delta_{in_g} - \delta_{in_g}^s\right)\right) = \left(\cos\left(\delta_{in_g}^s\right) + jsin\left(\delta_{in_g}^s\right)\right) \times |E_i| \times \left(\cos\left(\delta_{in_g} - \delta_{in_g}^s\right) + jsin\left(\delta_{in_g} - \delta_{in_g}^s\right)\right) \tag{4.7}$$

Expressing it in terms of transformed variables z and clubbing together all the constant terms we get the following expression –

$$|E_i| < \left(\delta_i - \delta_{n_g}\right) = (a_i + jb_i) \times \left(1 - z_{n_g+2i-1} + jz_{n_g+2i-2}\right), \forall i \in [1, n_g] \tag{4.8}$$

Substituting in the matrix equation for V and clubbing together all constant matrix terms we get,

$$[v]_{n_{bus}\times 1} = [K]_{n_{bus}\times n_g} \times \begin{bmatrix} 1 - z_{n_g+1} + jz_{n_g+2} \\ 1 - z_{n_g+3} + jz_{n_g+4} \\ \vdots \\ k_1 \end{bmatrix} \tag{4.9}$$

Since the expression for $|v_i|$ will contain square root terms, we define the constraints in terms of $|v_i|^2$ which is a quadratic function of transformed states z.

Since the LVRT constraint is time dependent, in order to make the problem tractable, we need to make it time dependent. We use the following two ways –

1. Representing the LVRT curve by a constant value equal to the maximum of it.
2. Introducing an artificial system with a state c with state equation $\dot{c} = f(c)$. A particular trajectory $\varphi(c_0, t)$ of this system starting from some value c_0 will be used to approximate the LVRT curve by being above it at all times. This approach was proposed in [87].

Let us now discuss the applications of SOS programming to estimate the CSR for the above two approximations to the LVRT curve.

4.1.3 Using Max LVRT Curve

The system under study can be written in the following form,

$$\begin{gathered} \dot{z} = f(z) \\ 0 = g(z) \\ h(z) \geq 0 \, , LVRT\ Constraint \end{gathered} \tag{4.10}$$

Where $h(z)$ is a vector function of length = number of PV's where it's i^{th} element can be written as –

$$h_i(z) = v_{pv_i}(z)^2 - \max_t \left(LVRT_i(t)\right)^2 \ , \forall i \in [1, n_{pv}] \tag{4.11}$$

Let us write the optimization problem for the expanding interior algorithm–

$$\begin{gathered} \boldsymbol{max.\ \ \beta} \\ s.t. \end{gathered}$$

$$\begin{aligned} &\boldsymbol{V(z)}\ \textbf{cannot be negative except at the origin (SEP)}: \left\{V(z) \leq 0,\ g(z) = 0, z \neq 0\right\} = \emptyset \\ &\boldsymbol{P_\beta}\ \textbf{Is contained inside the SR estimate}\ (\boldsymbol{V(z)} \leq \mathbf{1}): \left\{p(z) \leq \beta\ ,\ g(z) = 0,\ V(z) \geq 1,\ V(z) \neq 1\right\} = \emptyset \\ &\textbf{Inside the SR estimate,}\boldsymbol{V(z)}\ \textbf{strictly decreases along all trajectories:} \\ &\qquad \left\{V(z) \leq 1, \dot{V}(z) \geq 0,\ g(z) = 0, z \neq 0\right\} = \emptyset \end{aligned} \tag{4.12}$$

Inside the SR estimate, $h_i(z)$ is never < 0: $\{V(z) \leq 1, -h_i(z) \geq 0, -h_i(z) \neq 0,\ g(z) = 0\} = \emptyset$

The SOS formulation for first three constraints has been derived before and therefore directly shown,

$$V - \lambda_1^T g - l_1 \in \Sigma \tag{4.13}$$

$$-s_6(\beta - p) - \lambda_2^T g - (V - 1) \in \Sigma \tag{4.14}$$

$$-s_8(1 - V) - s_9\dot{V} - \lambda_3^T g - l_2 \in \Sigma \tag{4.15}$$

For the last constraint, we will derive the SOS equation here. Using P-Satz theorem,

$$s_{1i} + s_{2i}(1 - V) - s_{hi}(1 - V)h_i - s_{4i}h_i + \lambda_{hi}^T g + (-h_i)^{2k} = 0 \tag{4.16}$$

For simplification assume $s_{1i} = s_{2i} = 0, k = 1, \lambda_{hi} = -h_i \times \lambda_{hi}$ and taking $-h_i$ common we get,

$$s_{hi}\,(1 - V) + s_{4i} + \lambda_{hi}^T g - h_i = 0$$

Taking everything besides s_{4i} to RHS and representing multipliers by unique names gives us the final SOS formulation of the constraint –

$$-s_{h_i}(1 - V) - \lambda_{h_i}{}^T g + h_i \in \Sigma \tag{4.17}$$

Let us demonstrate the effectiveness through an example.

Example 4.1 Given 3-machine system with a single PV at bus 1 with a shown LVRT curve,

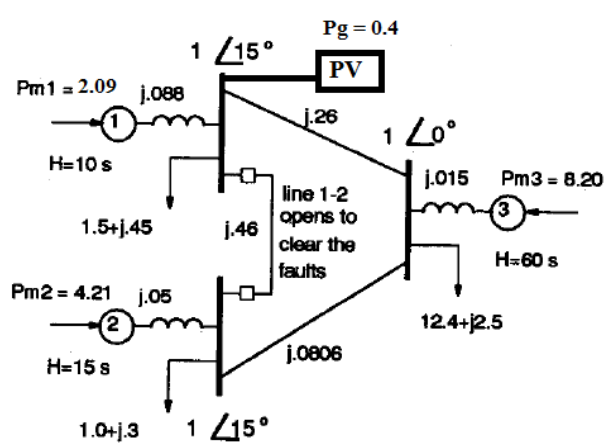

Figure 4.7 Example 4.1 Test System

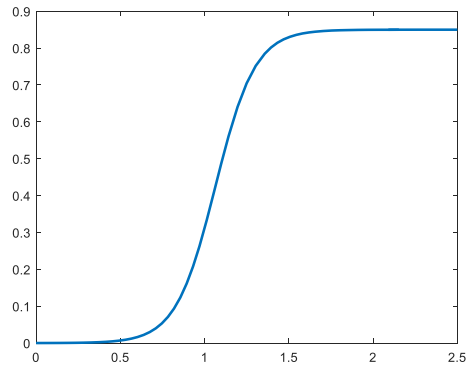

Figure 4.8 Example 4.1 LVRT Curve

The max of the LVRT curve is at 0.85 pu meaning that the non tripping of PV translates to its voltage being above 0.85 pu. The pre PV trip system's post fault SEP in one machine reference frame is at $(0.3165, 0.3451.0, 0)$. Thus, the variable transformation for this system is given as –

Table 4.1 Example 4.1 Max LVRT Approach Variable Transformation

New Variable	In terms of Original System State
z_1	ω_{1n_g}
z_2	ω_{2n_g}
z_3	$\sin(\delta_{1ng} - 0.3165)$
z_4	$1 - \cos(\delta_{1ng} - 0.3165)$
z_5	$\sin(\delta_{2ng} - 0.3451)$
z_6	$1 - \cos(\delta_{2ng} - 0.3451)$

Here we will only mention the degrees chosen for the new multiplier functions (not present in standard unconstrained system formulation in 2.2.5) with rest of the degrees chosen to be the same as Table 2.3 (quadratic Lyapunov) –

Table 4.2 Example 4.1 Max LVRT Approach SOS Multiplier Degrees

Function	Degree
s_h	0
$\lambda_{h_{11}}$	0

$\lambda_{h_{12}}$	0

We get the following quadratic Lyapunov Function in terms of the transformed states –

$$V(z) = 0.019 \times z_1^2 - 3.7e-3 \times z_1 \times z_2 + 0.025 \times z_1 \times z_3 - 0.019 \times z_1 \times z_4 - 0.018 \times z_1 \times z_5 + 0.012 \times z_1 \times z_6 + 3.3e-3 \times z_2^2 + 2.4e-3 \times z_2 \times z_3 - 4.4e-3 \times z_2 \times z_4 + 0.021 \times z_2 \times z_5 + 4.8e-3 \times z_2 \times z_6 + 1.0 \times z_3^2 + 0.21 \times z_3 \times z_4 - 0.14 \times z_3 \times z_5 - 4.0e-3 \times z_3 \times z_6 + 0.65 \times z_4^2 - 0.018 \times z_4 \times z_5 - 0.19 \times z_4 \times z_6 + 0.21 \times z_4 + 0.74 \times z_5^2 - 0.024 \times z_5 \times z_6 + 0.7 \times z_6^2 - 0.73 \times z_6$$

Here, the expression in terms of the original system states in single machine reference frame can be easily obtained by substituting the expression for $z's$ given in Table 4.1 and is therefore not mentioned here. In order to do a time domain validation of obtained results, we start various trajectories from the estimated constrained system stability boundary $\{V = 1\}$. Plotting their projection on the angle plane in Figure 4.9 shows us that they converge to the relevant SEP. On the other hand, plotting the PV bus voltage for each trajectory will validate if these are restricted to the feasible region. It is easy to see that the voltage at bus 1 in Figure 4.10 is never under the max of LVRT curve marked by black dotted line and also the trajectories converge to the SEP (marked in black).

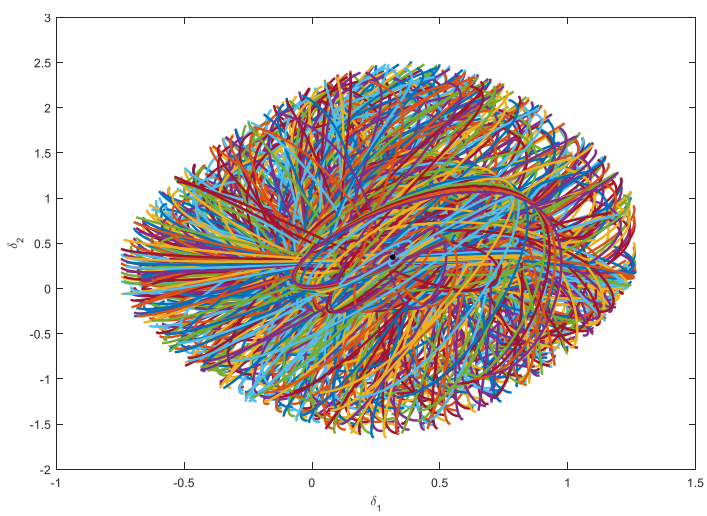

Figure 4.9 Example 4.1 Max LVRT Approach Trajectories on Angle Plane Starting from Estimated SR Boundary

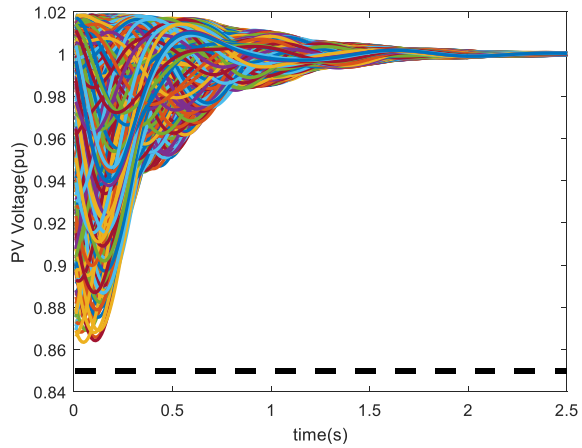

Figure 4.10 Example 4.1 Max LVRT Approach PV Bus Voltage Trajectories Starting from Estimated SR Boundary

We also obtain the unconstrained SR (green) comparing it against the CSR (red) in the figure below. It is easy to see that the Lyapunov level set stops expanding as soon as the feasibility boundary (blue) is hit. However, since the loads are impedance types, recovery of voltage is quick post fault thus resulting in a relatively large enough CSR.

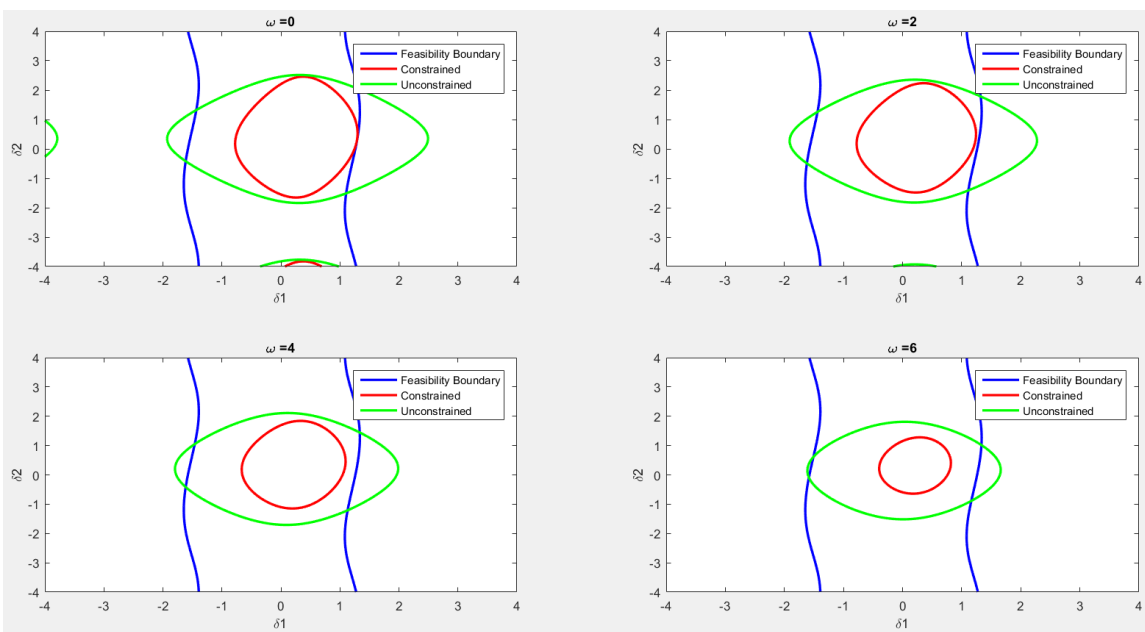

Figure 4.11 Example 4.1 Max LVRT Approach Unconstrained vs Constrained Stability Region

Let us now compare the estimated CSR against actual one (obtained through time domain simulation). It is important to note that the constraint here is the max LVRT approximation.

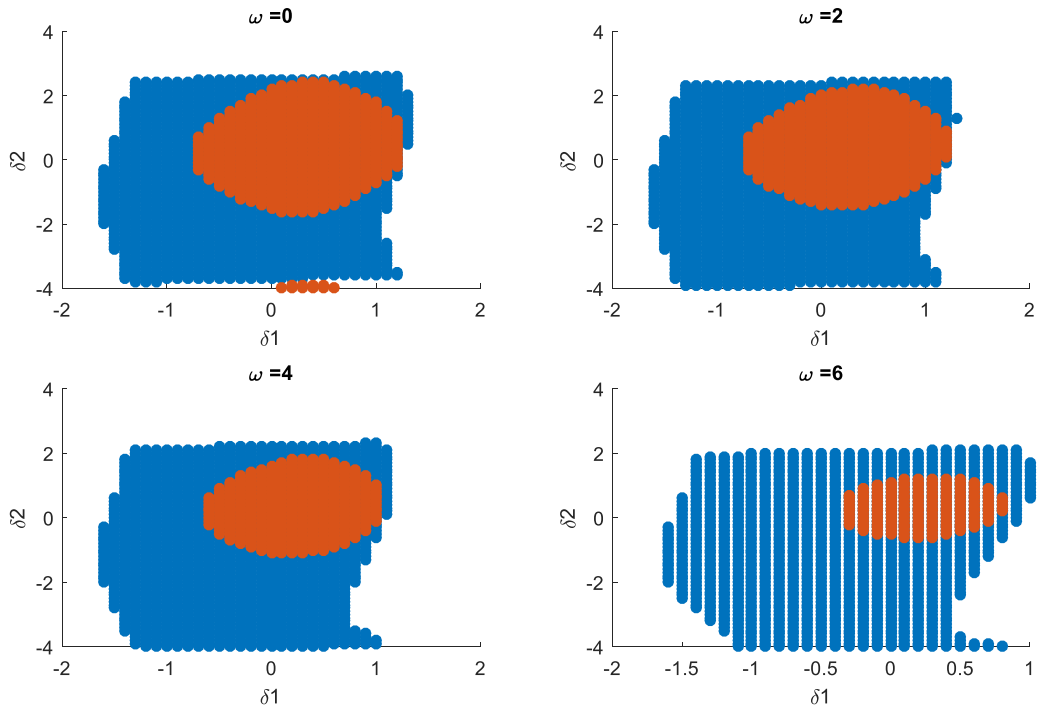

Figure 4.12 Example 4.1 Max LVRT Approach Estimated vs Actual Constrained Stability Region

We can notice in Figure 4.12 that the region estimated is conservative as compared to the true one. This is because the SEP is skewed towards the right and thus when expanding the estimate, the feasibility boundary on the right is intersected and expansion stops.

While the discussed approach is effective, it could prove to be highly conservative for systems with slower voltage recovery. For a system with a large penetration of the induction motor load, expecting the voltage to immediately jump to such a high value (max of LVRT curve) post fault is being highly optimistic. This leads us to the next approach.

4.1.4 Using Augmented State to Envelop LVRT Curve

As we mentioned before, we will be using a particular trajectory of an artificial system to represent the LVRT curve. Basically, we are mapping the time elapsed to this system's state value. This is because in the presence of time dependent constraints, not only do we need the

state values of the power system at the time of fault clearing, we also need the time at that instance to know starting point on the LVRT curve. Here, we will not be focusing on approximating the LVRT curve accurately. Rather, as long as this approximation is above the LVRT curve and close to it, it should work. We understand that this error will give us conservative results but this conservativeness is preferred for transient stability assessment. Now, we need a polynomial system $\dot{c} = f(c)$ having a trajectory starting from some initial point c_0 that approximates the LVRT curve.

Based on the shape of the LVRT curves as seen in Figure 4.1, we can broadly classify them into two categories– staircase type (IEEE, NERC) and linear type (FERC). For the second category, in [87], a complicated arctan function was proposed. However due to the polynomial restriction for SOS, we plan on keeping it simpler and polynomial type of a restricted degree. Based on visual inspection, the first category of curves can be reconstructed by a linear combination of sigmoid functions in time while the second category should require a single sigmoid. Sigmoid function in time can we written as follows,

$$x(t) = par_1 + \frac{par_2 - par_1}{1 + 10^{par_4 \times (par_3 - t)}} \tag{4.18}$$

We would then require a parametric state equation for a system whose one particular trajectory has a sigmoid shape in time which can then be tuned to approximate the respective LVRT curve.

$$\dot{c} = -K\left(c - c_{uep}\right) \times \left(c - c_{sep}\right), c_{sep} > c_{uep} \tag{4.19}$$
$$c_{uep} < c_0 < c \leq c_{sep}$$

For this system, $c_{uep} = par_1$ is an UEP which repels the trajectory to the SEP $c_{sep} = par_2$. This however is only possible if the trajectory starts at a value $c_0 = x(0) > c_{uep}$. $K = -par_4 \times \frac{\log(10)}{par_1 - par_2}$ influences the slope of the sigmoid. Based on the dynamics of this system, closer the starting point is to the c_{uep}, longer is the initial flat portion of the curve.

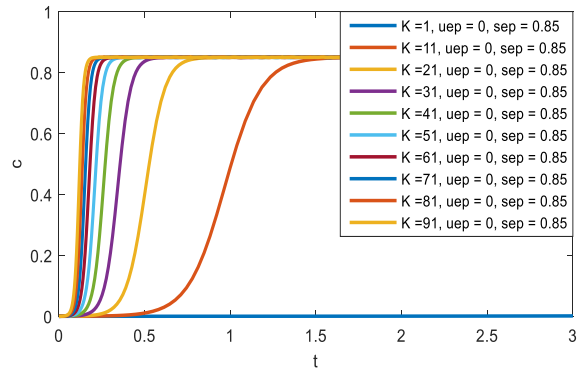

Figure 4.13 Sigmoid Response for Different Values of K

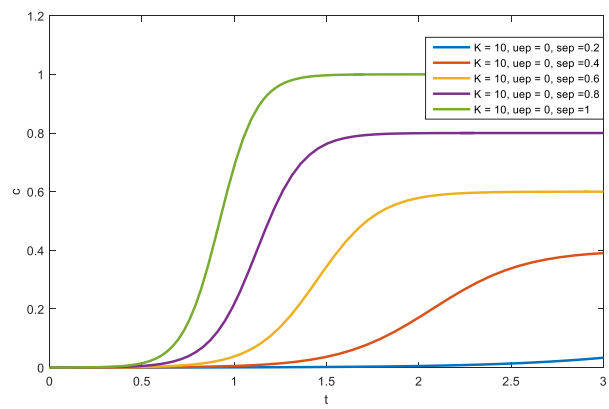

Figure 4.14 Sigmoid Response for Different Values of c_{sep}

The response for different values of parameters (c_{sep}, K) and $c_0 = 0.0001$ are shown above with $c_{uep} = 0$. However, this can also be adjusted by simply changing c_{uep}.

It is important to state that a similar system will be defined for each PV with an LVRT curve. For a given LVRT curve, to get the desired curve shape, a careful selection of c_0, K, c_{sep} & c_{uep} is necessary. The desired characteristics of the final sigmoid fit are as follows,

1. Minimum overall error between the resultant trajectory and the actual LVRT curve.
2. The c_{sep} value is equal to the final value of the LVRT curve. This is necessary as we will see later that the size of the estimated CSR becomes smaller with high value of c_{sep}.

3. The result system trajectory is never below the actual LVRT curve. If this requirement is not fulfilled, the resulting CSR may flag some trajectories that result in some PV tripping as tripping which will pose reliability concerns to the stability assessment.

Thus, the constrained optimization problem can be formulated as an unconstrained one by adding a penalty term as follows,

$$\mathbf{min}_{(par_1,par_2,par_3,par_4)}\, \boldsymbol{f_{obj}} = \sum_i (\boldsymbol{err_i})^2 + \boldsymbol{penaltycoeff} \times (\mathbf{min}(\boldsymbol{err_i}, \mathbf{0}))^2$$
$$err_i = par_1 + \frac{par_2 - par_1}{1 + 10^{par_4 \times (par_3 - t_i)}} - d_i \tag{4.20}$$
$$d_i = LVRT(t_i)$$

Since this needs to be done only once offline, the tuning speed is not an issue which paves the way for meta-heuristic techniques to fit the sigmoid function(s) to the given LVRT curve. We use Particle Swarm Optimization (PSO) [92] with the overall algorithm and implementation details given below.

Algorithm 4.1 Tuning Artificial System to Approximate LVRT Curve

1. Obtain the LVRT curve data of the form $tdat = [t_1, t_2 \dots t_n], lvrtdat = [d_1, d_2 \dots d_n]$.
2. Find number of discrete changes in the data. Each change is modeled as a sigmoid where $n_{sigmoids}$ is the minimum number of sigmoids required to fit the data. As an example, the LVRT data given below can be modeled as a summation of two sigmoids.

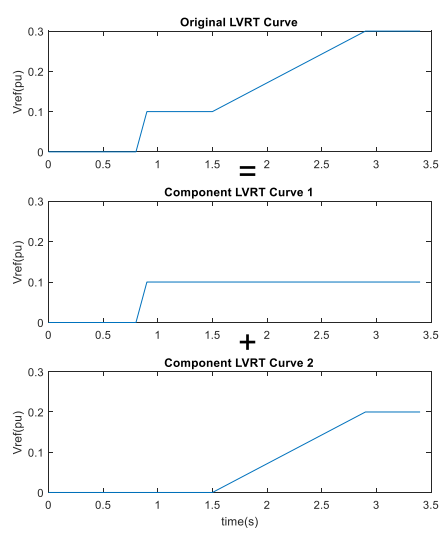

3. For $j = 1$
4. Extract data points to be fit by j^{th} sigmoid (as shown above) denoted by dat^j.
5. Find par^j (set of parameters for j^{th} sigmoid) using PSO. The details are as follows $par_2 = max_t\, LVRT(t) = constant, Particle\ =\ [par_1, par_3, par_4], penaltcoeff, = 100, population\ size\ =\ 50, c1\ =\ c2\ =\ 2, maximum\ iterations\ = 500, inertial\ weight\ w\ varied\ linearly\ from\ 0.9\ to\ 0.4.$
6. $j = j + 1$. If $j \leq n_{sigmoid}$ GOTO Step 4.
7. Stop

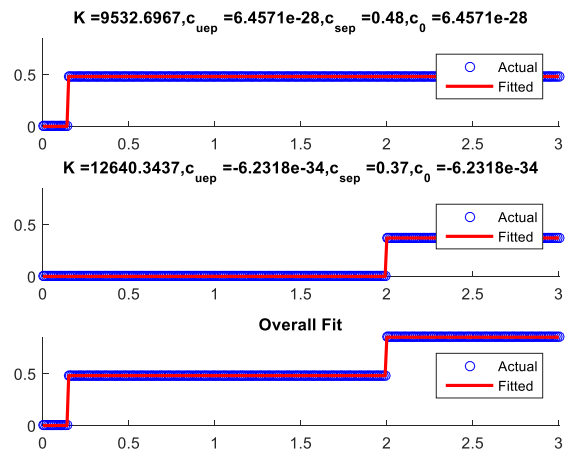

Figure 4.15 IEEE 1547 LVRT Curve Sigmoid Fit

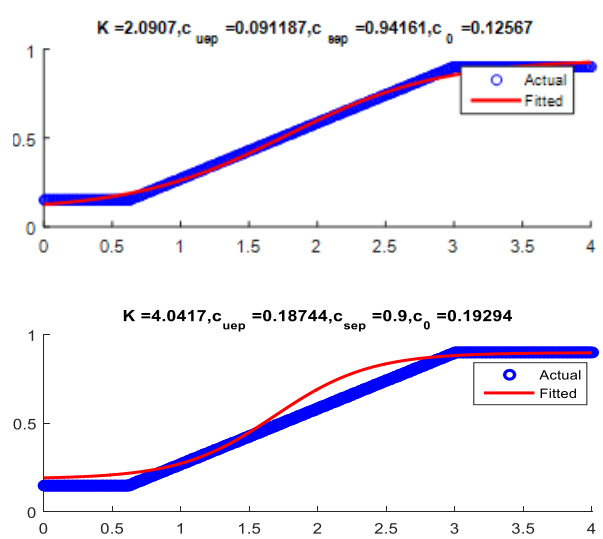

Figure 4.16 FERC LVRT Curve Sigmoid Fit Negative Error Penalty (0 (above) vs 100 (below))

Let us now test the tuning methodology for a few standard LVRT curves. While the tuning performance is excellent of LVRT curves with discrete steps (Figure 4.15), for curves having a more gradual slope (Figure 4.16), the penalty term opposes the minimization of the mean square error. We can see in the above figure that while we are able to get rid of the negative errors, there are now larger positive errors as compared to the previous fit. This introduces conservativeness to the eventually estimated CSR but as discussed before, it is a necessity. Exploring other artificial systems is an option to reduce these errors.

The assessment of systems with PVs having LVRT curves of the first category has an inherent difficulty. As we saw, those curves will be comprised of multiple artificial systems. Now, since the LVRT curve is taken to be the sum of states of the individual artificial systems, there are multiple combinations of state values resulting in the same sum. Each combination of values will result in a different resultant trajectory. Only one combination will result in the trajectory of interest that approximates the LVRT curve as we had planned. The problem is with those trajectories that are above the LVRT curve as they will introduce conservativeness by forcing the voltage trajectory to be above a higher curve than the actual required. One trivial way of dealing with it is using only a single sigmoid that envelopes the LVRT curve which is what we will pursue in the present work which is inherently conservative. An alternative way of modelling is having an artificial system with piecewise vector field. However, this approach is outside the scope of the current work and thus a possible direction for future research.

Once the tuned artificial system (assumed to be a single sigmoid) is satisfactory, we move onto the original problem of transient stability in systems with LVRT. Let us assume there are n_{pv} PV generators in our system each having distinct LVRT curve. Assuming the SEP at origin, we shift the sigmoid equation's origin defining a new state $z_{c_i} = c_i - c_{sep_i}$ governed by the state equation

$$\dot{z_{c_i}} = f_{c_i}(z_{c_i}) = -K(z_{c_i} + c_{sep_i} - c_{uep_i}) \times z_{c_i}, \forall i \in [1, n_{pv}] \tag{4.21}$$

We augment this state to the original power system states, $z_{new} = \begin{bmatrix} [z]_{3(n_g-1)\times 1} \\ [z_c]_{n_{pv}\times 1} \end{bmatrix}$ where z is the state vector corresponding to the power systems model to get the following system –

$$\dot{z}_{new} = \begin{bmatrix} f(z) \\ f_c(z_c) \end{bmatrix}$$
$$0 = g(z) \tag{4.22}$$
$$h(z_{new}) \geq 0$$

Where $h(z_{new})$ is a vector of functions defined for each PV –

$$h_i(z_{new}) = \left|v_{pv_i}(z)\right|^2 - \left(z_{c_i} + c_{sep_i}\right)^2 > 0 \tag{4.23}$$

There is an additional constraint on the value of each state variable z_{c_i} in accordance with restricting to the relevant portion of trajectory $c_{uep_i} < c_{0i} \leq c_i \leq c_{sep_i}$. Writing in terms of z_c we get-

$$u_i(z) = -\left(z_{c_i} + c_{sep_i} - c_{0i}\right)\right) \times z_{c_i} \geq 0 \; where \; \varepsilon \to 0^+ \tag{4.24}$$

This constraint is really important for two reasons. First, as discussed before, initial value will determine the shape of the trajectory. Second, because the feasibility region is defined in terms of z_c^2 rather than z_c and c_{uep} is a source type UEP, for all $c_0 < c_{uep}$, trajectories become unbounded due to absence of any equilibrium there. This will result in expanding interior algorithm stopping prematurely. So, we assume that our system dynamics are constrained on a region defined by–

$$\{z_{new} | u_1\left(z_{c_1}\right) \geq 0, u_2\left(z_{c_2}\right) \geq 0, \dots, u_{n_{pv}}\left(z_{c_{n_{pv}}}\right) \geq 0, g(z) = 0\} \tag{4.25}$$

Lemma 4.2 $\{V(z_{new}) \leq 1\} \cap u(z_c)$ is an invariant set if we can find $\dot{V}(z_{new}) \leq 0$ in it.

Proof Let us take a point $z_0 \in \{V(z_{new}) \leq 1\} \cap u(z_c)$ and a trajectory starting from it say $\varphi(z_0, t)$. Now, since $z_c's$ dynamics are dynamically decoupled with z and $u(z_c) \geq 0$ is an invariant set (based on sigmoid response) as well a part of the SR of $z_c = 0$, φ is constrained to $u(z_c) \geq 0$ as long as z_0 belongs to it. Given $\dot{V}$ is negative inside $\{V(z_{new}) \leq 1\} \cap u(z_c)$, V along φ can never be > 1. Thus, φ never leaves $\{V(z_{new}) \leq 1\} \cap u(z_c)$ making it an invariant set.

So, all the Lyapunov equations need to hold true in this region of state space as before. Now, writing the equations for expanding interior –

$$\boldsymbol{max.\ \ \beta}$$

$$s.t.$$

$\boldsymbol{V(z_{new})}$ cannot be negative:

$$\left\{V(z_{new}) \leq 0,\ u_1(z_{c_1}) \geq 0, u_2(z_{c_2}) \geq 0, \dots, u_{n_{pv}}\left(z_{c_{n_{pv}}}\right) \geq 0, \qquad g(z) = 0, \right.$$
$$\left. z_{new} \neq 0\right\} = \emptyset$$

$\boldsymbol{P_\beta}$ Is contained inside the SR estimate ($\boldsymbol{V(z_{new}) \leq 1}$) :

$$\left\{p(z_{new}) \leq \beta\ ,\ u_1(z_{c_1}) \geq 0, u_2(z_{c_2}) \geq 0, \dots, u_{n_{pv}}\left(z_{c_{n_{pv}}}\right) \geq 0, g(z) = \right.$$
$$\left. 0,\ V(z_{new}) \geq 1,\ V(z_{new}) \neq 1\right\} = \emptyset \tag{4.26}$$

Inside the SR estimate,$\boldsymbol{V(z)}$ strictly decreases along all trajectories:

$$\left\{V(z_{new}) \leq 1, \dot{V}(z_{new}) \geq 0,\ u_1(z_{c_1}) \geq 0, u_2(z_{c_2}) \geq 0, \dots, u_{n_{pv}}\left(z_{c_{n_{pv}}}\right) \geq 0, g(z) \right.$$
$$\left. = 0, \qquad z_{new} \neq 0\right\} = \emptyset$$

Inside the SR estimate, $\boldsymbol{h_i(z)}$ is never $\boldsymbol{< 0}$:

$$\left\{V(z) \leq 1, -h_i(z_{new}) \geq 0, -h_i(z_{new}) \neq 0,\ u_1(z_{c_1}) \geq 0, u_2(z_{c_2}) \geq \right.$$
$$\left. 0, \dots, u_{n_{pv}}\left(z_{c_{n_{pv}}}\right) \geq 0, g(z) = 0\right\} = \emptyset$$

Writing the SOS formulation using P-Satz theorem which is the same as the one introduced in max LVRT case but with $\sum_i s_{u_i 1} u_i$ added to each constraint to represent the state constraint on z_c to restrict to the trajectory of interest as discussed before.

$$\boldsymbol{max.\ \ \beta}$$

$$V \in R_n, V(0) = 0, k_i's \in \mathbb{Z}_+, s, s_{Vh}, s_u \in \Sigma_n, \lambda, \lambda_h \in R_n^{n_g}$$

$$st.$$

$$V - \lambda_1^T g - \sum_i s_{u_i 1} u_i - l_1 \in \Sigma$$
$$-s_6(\beta - p) - \lambda_2^T g - \sum_i s_{u_i 2} u_i - (V - 1) \in \Sigma \tag{4.27}$$
$$-s_8(1 - V) - s_9 \dot{V} - \lambda_3^T g - \sum_i s_{u_i 3} u_i - l_2 \in \Sigma$$

$$-s_{Vhj}(1-V) - \lambda_{hj}^{T} g - \sum_{i} s_{u_i(j+3)} u_i + \; h_j \in \Sigma \,, \forall j \; \in [1, n_{pv}]$$

Now, continuing the previous example,

Example 4.1 Continued In the given example, we assume the same LVRT curve on which the following sigmoid system is fit -

$$\dot{c} = -10 \times c \times (c - 0.85) \rightarrow \dot{z}_c = \; -10 \times z_c \times (z_c + 0.85)$$

$$c_0 = 0.0001$$

The curve was chosen to perfectly fit a sigmoid which may not be the case. However, in this example our focus is on demonstrating the implementation strategy. One thing to note is that here we would be using z_7 instead of z_c. The variable transformation is as given in Table 4.1 with an additional variable $z_7 = c - 0.85$. Let us start by writing down expression for constraints in transformed variables –

$$h(z) = 0.002 \; \times \mathrm{z}_5 - \; 1.55 \; \times \mathrm{z}_4 - \; 0.15 \; \times \mathrm{z}_3 - \; 0.04 \; \times \mathrm{z}_6 - \; (\mathrm{z}_7 + 0.85)^2 + \; 0.03 \; \times \mathrm{z}_3 \times \mathrm{z}_5 + \; 0.005 \; \times \mathrm{z}_3 \times \mathrm{z}_6 - \; 0.005 \; \times \mathrm{z}_4 \times \mathrm{z}_5 + \; 0.03 \; \times \mathrm{z}_4 \times \mathrm{z}_6 + \; 0.61 \; \times \mathrm{z}_3^2 + \; 0.61 \; \times \mathrm{z}_4^2 + \; 0.0005 \; \times \mathrm{z}_5^2 + \; 0.0005 \; \times \mathrm{z}_6^2 + \; 1.00006$$

The degrees for the newly added multiplier functions –

Table 4.3 Example 4.1 SOS Multiplier Degrees

Function	Degree
$s_{u_i k} \forall k \neq 3$	0
$s_{u_i 3}$	2
$s_{Vh_j} \; \forall j$	0

The estimated quadratic Lyapunov Function in terms of transformed variables is,

$$V = \; 0.019 \; \times z_1^2 - \; 3.9e-3 \; \times z_1 \times z_2 + \; 0.024 \; \times z_1 \times z_3 - \; 0.013 \; \times z_1 \times z_4 - \; 0.022 \; \times z_1 \times z_5 + \; 0.012 \; \times z_1 \times z_6 - \; 8.6e-4 \; \times z_1 \times z_7 + \; 3.7e-3 \; \times z_2^2 + \; 4.7e-3 \; \times z_2 \times z_3 - \; 7.3e-3 \; \times z_2 \times z_4 + \; 0.022 \; \times z_2 \times z_5 + \; 1.8e-3 \; \times z_2 \times z_6 + \; 2.2e-4 \; \times z_2 \times z_7 + \; 0.86 \; \times z_3^2 + \; 0.17 \; \times z_3 \times z_4 - \; 0.12 \; \times z_3 \times z_5 - \; 6.5e-4 \; \times z_3 \times z_6 + \; 9.7e-3 \; \times z_3 \times$$

$z_7 + 0.44 \times z_4^2 - 0.052 \times z_4 \times z_5 - 0.22 \times z_4 \times z_6 + 0.14 \times z_4 \times z_7 + 0.68 \times z_4 + 0.15 \times z_5^2 - 0.034 \times z_5 \times z_6 - 9.4e-5 \times z_5 \times z_7 + 0.07 \times z_6^2 - 0.018 \times z_6 \times z_7 + 0.53 \times z_6 + 7.4e-3 \times z_7^2$

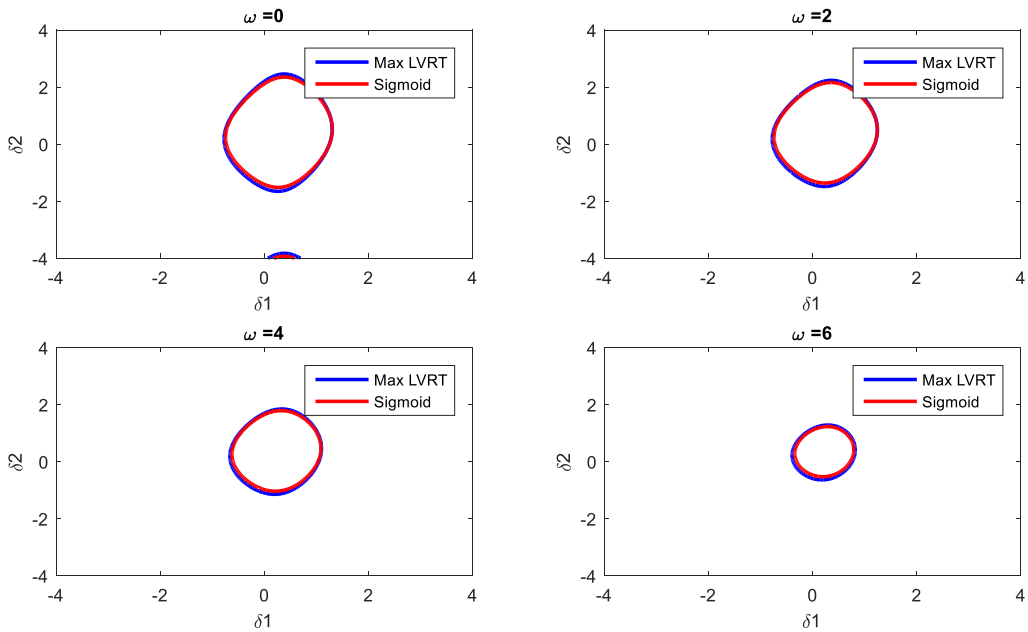

Figure 4.17 Example 4.1 Augmented State Approach vs Max LVRT Approach SR

Let us plot the estimated constrained SR obtained in this approach vs max LVRT approach in terms of the power system states with its intersection with $c = c_0$ in Figure 4.17. This gives us from what initial values of δ, ω at $t = 0$ can we start the post fault trajectory and not see any PV trip on the way. Effectively, no improvement is noticed over the max LVRT approach. Let us now plot it for different values of c (starting point on LVRT curve).

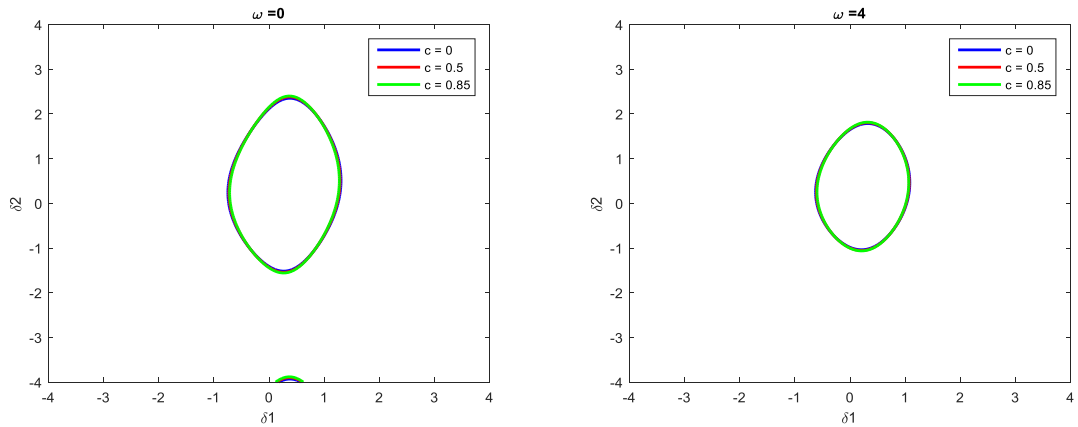

Figure 4.18 Example 4.1 Augmented State Approach Lyapunov Level Set vs Starting Point on LVRT

We see that there is practically no difference between the estimates. In order to explain this, let us plot the true CSR level sets for different starting values of c in Figure 4.19. We can see that the size increases with decreasing value of c (think of it as time) which is obvious due to increasingly binding constraint on the voltage at PV bus. Now, for the artificial system chosen for the LVRT curve, the SEP corresponds to the region which is most restricting ($c = 0.85$). However since our aim is to maximize the size of an invariant set to get the best estimate of SR, we know that the only invariant set for the artificial system is the SR for its SEP which is at 0.85.

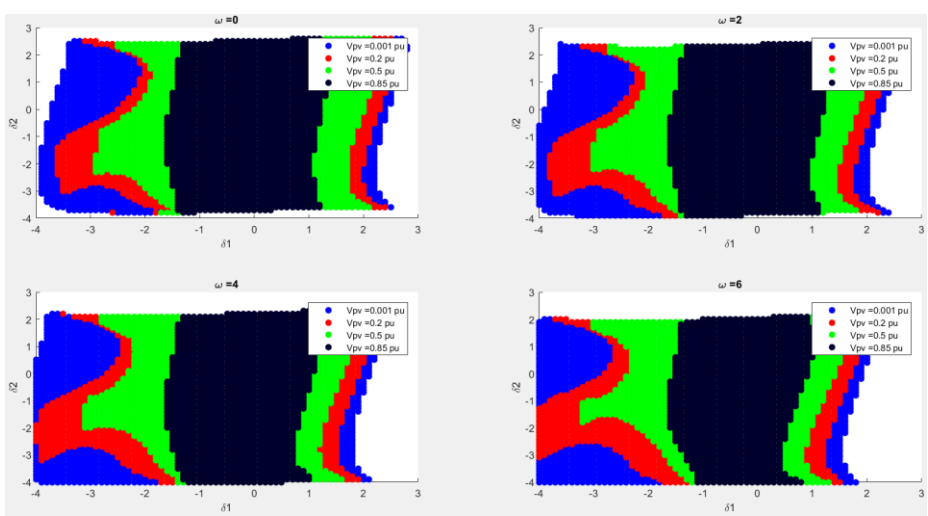

Figure 4.19 Example 4.1 Augmented State Approach True Constrained Stability Region

So, when we start expanding the Lyapunov level sets, the feasibility boundary is quickly met since feasibility region is the narrowest here (in terms of power system states) resulting in an estimate the same as the previous approach. An elliptical invariant set in the augmented state space may not be the best choice for estimating the CSR in this case due to an inverted funnel like shape of the true CSR.

There are two ways out of this situation –

1. Using a combination of Lyapunov level set and parts of the feasibility boundary to get the desired invariant set.
2. Using a higher dimension Lyapunov function. While this approach is attractive, it is impractical due to the increased dimensionality of the SOS problem that will have to be solved to realize it. While a Composite Lyapunov function can perform as well, it requires solving bilinear matrix inequalities which are not convex and there are limited tools available that can formulate the SOS conditions to BMI [93]. So, we decided to pursue the first option.

4.1.5 Using Lyapunov Level Set + Barrier Functions

This idea was proposed in [94]. When trying to estimate a CSR, the first thing that automatically comes to the mind is looking for the largest invariant set containing the SEP using Lyapunov level sets contained inside the feasibility region. We have seen previously that this technique yields conservative results due to the limitation of the shape that can be estimated using a fixed degree Lyapunov function. As seen in 4.1.1, the stability boundary for CSR can include sections of the feasibility boundary itself which is the inspiration for this approach.

Let us first define a function or a set of functions called the barrier functions that together characterize the feasible region. These are not to be confused with the Barrier certificates [95] used in safety verification that have some other properties as well besides separating feasible region from the infeasible. When the exact infeasible region is difficult to represent using polynomial barrier functions, approximations to barrier function can be constructed using Support Vector Machines [94]. For the current problem, the function $h(z)$ which gives us the

LVRT voltage constraint at PV bus serves as the Barrier Function. Let the feasibility set defined with the help of $h(z)$ for a system with n_{pv} number of PVs –

$$F = \{z \,|h_1(z) \geq 0, h_2(z) \geq 0, \dots h_{n_{pv}}(z) \geq 0\} \tag{4.28}$$

The idea is to use parts of the feasibility boundary along with the Lyapunov level set for estimating the CSR which can help obtain a more complex shaped final CSR estimate thus dealing better with tricky shaped feasibility regions. Now, the question to be answered is which parts of the feasibility boundary can serve as the stability boundary for the CSR ? It was shown in 4.1.1 that the non-zero eigen value associated with a point on the feasibility boundary with $h_j(z) = 0$ was proportional to $\frac{\partial h_j(z)}{\partial z} f(z)$ which means it is unstable (source type) if it pushes the system trajectory to the feasible side. The saddle type points ($\frac{\partial h_j(z)}{\partial z} f(z) = 0$) were also important for characterizing the stability boundary. Thus, we only choose these 2 types of points to possibly lie on the boundary of our final CSR estimate.

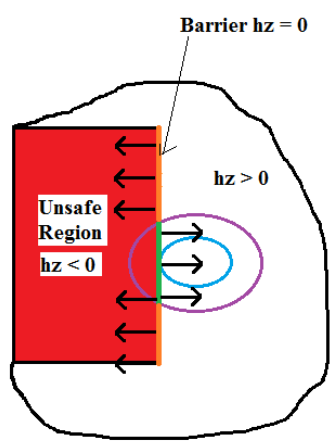

Figure 4.20 Expanding Interior Using Barrier Functions

To understand the expanding interior process with this new formulation, let us see the figure above. The red region is the infeasibility region. When trying to expand the Lyapunov estimates using the previous approach, the expansion process will stop as soon as it hits the barrier (feasibility boundary) giving us the SR estimate as the blue ellipse. Here, the boundary of this estimate is given by $V_{blue} = 1$. However, if we keep expanding this estimate and let it intersect the red region (infeasible), there is a part of feasibility boundary highlighted in green which

pushes nearby trajectories into the feasibility region. This can be formulated as $\{h = 0,\ \dot{h} > 0\}$. The orange part of the feasibility is the one that attracts trajectories into the infeasible region which we need to avoid. Thus we can define the final estimate of CSR having a boundary comprised of green feasibility boundary on the left and purple Lyapunov function to the right. Let us present a proof to show the invariant nature of the given region.

Lemma 4.3 Given $V(z)$ is a Lyapunov function st. $\dot{V}(z) \leq 0\ \forall\ z \in \{V(z) \leq 1\}$ and a continuous and differentiable barrier function h. If $\dot{h}(z) > 0\ \forall\ z \in \{V(z) \leq 1\} \cap \{h(z) = 0\}$ then the set $\{V \leq 1\} \cap \{h \geq 0\}$ is invariant.

Proof Let $z_0 \in \{V(z) \leq 1\} \cap \{h(z) \geq 0\}$. Let a trajectory starting from it be denoted by $\varphi(z_0, t)$. We need to show that φ remains inside the same set. Now, since $\dot{V} \leq 0$ inside $V \leq 1$, $V\big(\varphi(z_0, t)\big) \leq 1$. We also know that $h(z_0) \geq 0$. Given h is continuous and differentiable, $h(\varphi(z_0, t))$ has to cross $h = 0$ in order to become negative and lead the given set. Since $\dot{h}(z) > 0\ \ \forall z \in \{V(z) \leq 1, h(z) = 0\}$, $h\big(\varphi(z_0, t)\big) \geq 0$ implies $\varphi(z_0, t)$ is contained inside $\{V(z) \leq 1\} \cap \{h(z) \geq 0\}$.

Let us now formulate the expanding interior problem using this approach for the state augmentation scheme (LVRT approximation). All the functions and variables are as defined in 4.1.4.

$$\boldsymbol{max.\ \ \beta}$$

$$s.t.$$

$V(z_{new})$ cannot be negative:

$$\Big\{V(z_{new}) \leq 0,\ u_1\big(z_{c_1}\big) \geq 0, u_2\big(z_{c_2}\big) \geq 0, \dots, u_{n_{pv}}\Big(z_{c_{n_{pv}}}\Big) \geq 0, \qquad g(z) = 0, \qquad z_{new} \neq 0\Big\} = \emptyset \tag{4.29}$$

P_β Is contained inside the SR estimate ($V(z_{new}) \leq 1$) :

$$\Big\{p(z_{new}) \leq \beta\ ,\ u_1\big(z_{c_1}\big) \geq 0, u_2\big(z_{c_2}\big) \geq 0, \dots, u_{n_{pv}}\Big(z_{c_{n_{pv}}}\Big) \geq 0, g(z) = 0,\ V(z_{new}) \geq 1,\ V(z_{new}) \neq 1\Big\} = \emptyset$$

Inside the SR estimate,$V(z)$ strictly decreases along all trajectories:

$$\left\{V(z_{new}) \leq 1, \dot{V}(z_{new}) \geq 0,\ u_1(z_{c_1}) \geq 0, u_2(z_{c_2}) \geq 0, \dots, u_{n_{pv}}\left(z_{c_{n_{pv}}}\right) \geq 0, g(z) = 0, \quad z_{new} \neq 0\right\} = \emptyset$$

Inside the SR estimate, $\dot{h}_i(z)$ is never ≤ 0 when $h_i(z) = 0$:

$$\left\{V(z) \leq 1, \dot{h}_i(z_{new}) \leq 0, h_i(z_{new}) = 0,\ u_1(z_{c_1}) \geq 0, u_2(z_{c_2}) \geq 0, \dots, u_{n_{pv}}\left(z_{c_{n_{pv}}}\right) \geq 0, g(z) = 0\right\} = \emptyset$$

The SOS formulation using P-Satz theorem is same as the previous one with a slight modification in the last constraint

$$\begin{gathered}
\boldsymbol{max.\ \beta} \\
V \in R_n, V(0) = 0, k_i's \in \mathbb{Z}_+, s_i's \in \Sigma_n, \lambda_i \in R_n^{n_g} \\
st. \\
V - \lambda_1^T g - \sum_i s_{u_i 1} u_i - l_1 \in \Sigma \\
-s_6(\beta - p) - \lambda_2^T g - \sum_i s_{u_i 2} u_i - (V - 1) \in \Sigma \\
-s_8(1 - V) - s_9 \dot{V} - \lambda_3^T g - \sum_i s_{u_i 3} u_i - l_2 \in \Sigma \\
-s_{Vhj}(1 - V) - \lambda_{ghj}^T g - \lambda_{h_j} h_j - \sum_i s_{u_i(j+3)} u_i + s_{\dot{h}_j} \dot{h}_j \in \Sigma, \forall j \in [1, n_{pv}]
\end{gathered} \tag{4.30}$$

For plotting purposes, the final constrained SR estimate given by $\{V \leq 1, h \geq 0\}$ in original states x can be realized as $\{V_{final} \leq 1\}$ –

$$V_{final}(x) = V \times \prod_{i=1:n_{pv}} \left(1 + \frac{1000}{1 + e^{1000 h_i(x)}}\right) \tag{4.31}$$

Example 4.1 Continued Using the same artificial system for representing LVRT and variable transformations,

$\dot{h}(z) = -0.005907810300775496 \times z_1 \times z_3 \times z_5 + 0.03753426401432929 \times z_1 \times z_3 \times z_6 - 0.03753426401432929 \times z_1 \times z_4 \times z_5 - 0.005907810300775496 \times z_1 \times z_4 \times z_6 + 0.005907810300775496 \times z_2 \times z_3 \times z_5 - 0.03753426401432929 \times z_2 \times$

$z_3 \times z_6 + 0.03753426401432929 \times z_2 \times z_4 \times z_5 + 0.005907810300775496 \times z_2 \times z_4 \times z_6 + 20 \times z_7^3 - 0.3340546573335919 \times z_1 \times z_3 + 0.1567633423437699 \times z_1 \times z_4 + 0.03753426401432929 \times z_1 \times z_5 + 0.005907810300775496 \times z_1 \times z_6 + 0.03753426401432929 \times z_2 \times z_3 - 0.005907810300775496 \times z_2 \times z_4 - 0.04738388956813192 \times z_2 \times z_5 - 0.002703672889869679 \times z_2 \times z_6 + 34 \times z_7^2 - 0.1567633423437699 \times z_1 + 0.002703672889869679 \times z_2 + 14.45 \times z_7$

We can see that $\dot{h}$ is of degree 3 and thus accordingly choosing degrees for SOS multipliers for the last equation given in the table below.

Table 4.4 Example 4.1 Lyapunov Level Set + Barrier Functions Approach SOS Multiplier Degrees

Function	Degree
$s_{\dot{h}_j}$	0
s_{Vh_j}	2
$s_{u_{j+3}}$	2
$\lambda_{gh_{j_{11}}}$	2
$\lambda_{gh_{j_{12}}}$	2

It is unnecessary to provide the Lyapunov function V_{final} here due to a very large number of terms. The SR estimate set for this approach for $c = 0$ is compared to the previous approaches and a marked improvement in the size of estimate can be seen from the figure below. This increase is mainly in the left direction in the angle plain since the SEP is closer to the infeasible region on the right making the right boundary more binding as seen before in Figure 4.19. Now, one change that might occur to the reader is shifting the center of P_β from the SEP to another point where it can expand bigger. This approach was adopted by adding a step to the expanding interior with V and p fixed keeping the center as a variable. Since the constraints are in the form of set emptiness conditions, the algorithm keeps shifts the center to points outside the feasible part of the state space where either the $g(z) = 0$ or $u_i(z) \geq 0$ are not met. Also, the problem becomes unbounded.

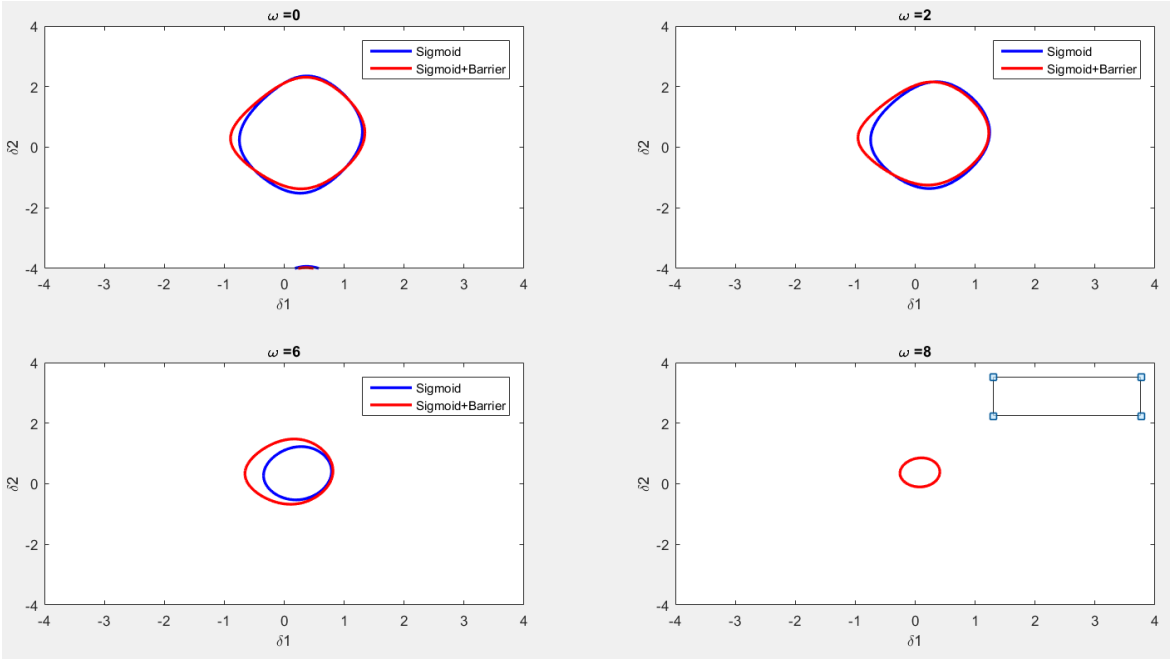

Figure 4.21 Example 4.1 Comparison of Constrained SR Estimates using Different Approaches

Also, plotting the estimated SR vs *c* in Figure 4.22, we notice that due to the more relaxed constraint in this approach, we can see some dependence on the starting point on the LVRT curve. Thus, we can conclude that the best approach to get more out of the CSR for LVRT constraints is using augmented states to approximate LVRT coupled with barrier functions approach.

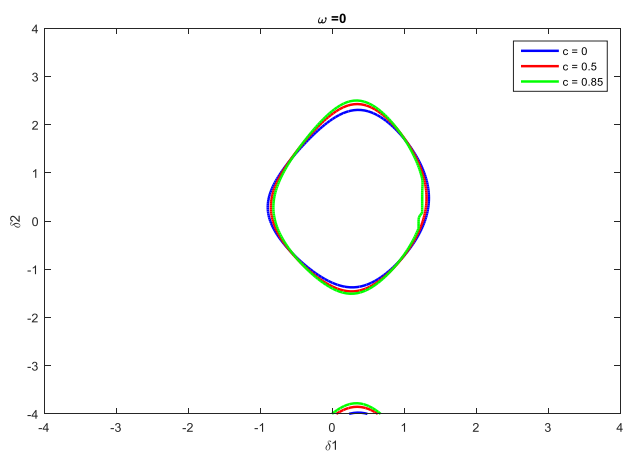

Figure 4.22 Example 4.1 Barrier Function Approach Lyapunov Level Set vs Starting Point on LVRT

4.2 Switched System Approach

One major drawback is the previous approach was that the tripping of PV was considered as an instability phenomenon. However, in reality, the loss of synchronism would totally depend on the size of MW lost where it has been seen that practical systems can usually take up to several hundred MW loss without having any stability issues [96]. Also the location of the tripped PV plays an important role. For the case where it is electrically closer to the accelerating machines, tripping of it transfers the load to the speeding machines (the idea governing generation shedding as a part of emergency control [97]) helping it resynchronize. This can be seen through a small study on the familiar 3 – machine system by comparing CCTs for the two different scenarios in Figure 4.23. The first one allows PV to trip while the second one does not allow PV to trip. The faults are studied at the bus with PV connected. From the plots below, we can see that tripping of PV (dotted curves) up-to a certain penetration has a positive impact (increased CCT) on the accelerating generator. This reflects in a higher CCT. However, beyond a certain penetration level, the CCT is lesser indicating the negative impact of the trip.

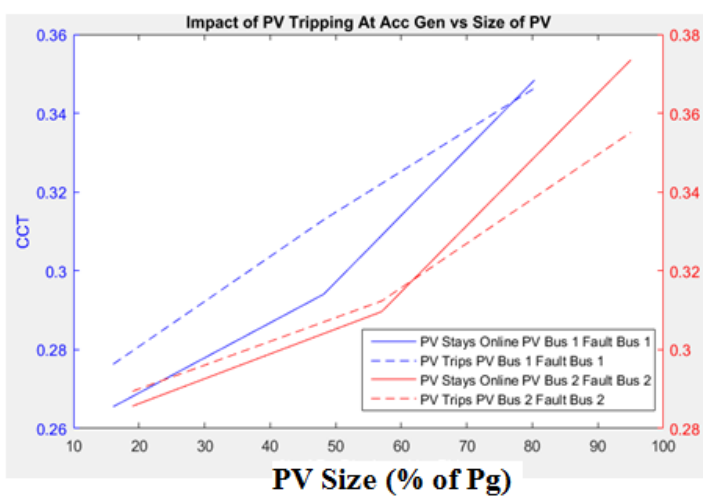

Figure 4.23 Impact of PV Trip at Accelerating Generator vs PV Size

Also, according to the standard LVRT curves seen before, the period from 0 to ~0.1 s is such that none of the PV's would be allowed to trip after which the curve rises and then PV's may trip. What this means is that the constrained systems approach would inherently impose an upper limit on the CCT equal to the time to first PV trip which could be quite conservative. For

example, for Dominion VA Power, the CCTs are seen in the ranges of 0.15 s and above. This would result in an underutilization of a utility's resources as well as unnecessary upgrades in system protection which are economically harmful.

When PVs trip in the system, the system dynamics change in terms of the vector field $f(x)$ where $\dot{x} = f(x)$ represents the state equation. This means that the system is not actually a single system but comprised of multiple systems, each having different dynamics. At a particular time, only a single system is active and governs the overall dynamics. The overall system switches between these individual systems through some logic governed by the LVRT curves and voltage values in our case. Thus, for a system with the number of PVs connected as n_{pv}, there are $2^{n_{pv}}$ possible system statuses where the system status is defined by the combined connection status of all those PVs. The overall dynamics can be written as –

$$\dot{x} = f_{\sigma}(x) \tag{4.32}$$

Where σ is the switching signal, a piecewise constant function taking values among possible system statuses with the overall phenomenon as shown in the figure below.

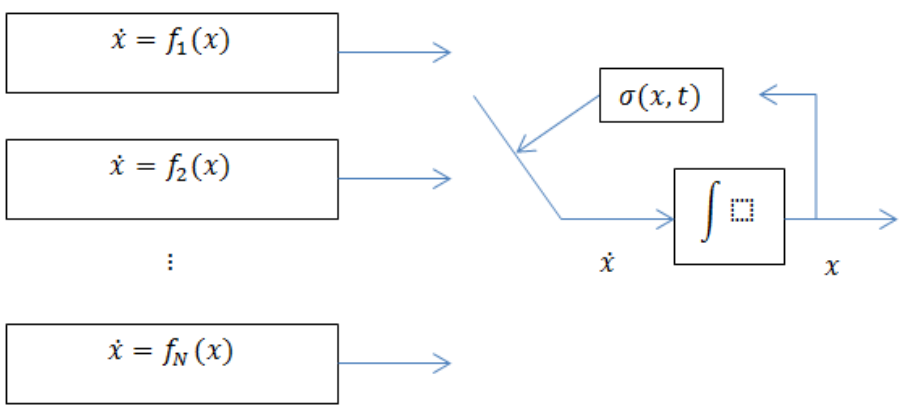

Figure 4.24 Switched System

Here it is important to mention that the system has distinct EPs corresponding to each status. The concept of stability for such systems is different from the non-switched systems which is how the power system has been modelled traditionally. Here, we define stability wrt a set of EPs rather than a single one.

Theorem 4.4 For a switched system defined by $\dot{x} = f_\sigma(x)$ with the switching signal σ resulting in finite number of switchings, given a set Ω, the SR $A(\Omega)$ is defined as a set $\{x \in R^n | x(0) = x \rightarrow \lim_{t\rightarrow\infty} dist(x(t), \Omega)\} \rightarrow 0$ where $dist$ metric between a set and a point can be defined as the Euclidean distance to the closest point inside the set.

Here it is important to mention that the stability for such power systems may not monotonically decrease with fault clearing time. This can be observed in cases where the SRs for individual system statuses do not largely overlap. Take for example a system with a single PV and the SRs of pre-PV Trip and post-PV trip status and a given fault on trajectory shown below. If fault clears at t1 (system state is inside both SRs) and PV trips immediately or never trips, system will remain stable. However if the fault is cleared at t2 > t1 and PV does not trip, system is unstable since its outside SR of Pre-PV trip status. Thus, the nature of switching plays a major role in stability which has no direct correlation with fault clearing time. That being said, there exists a minimum fault clearing time at which the system is already driven outside SRs for each system status.

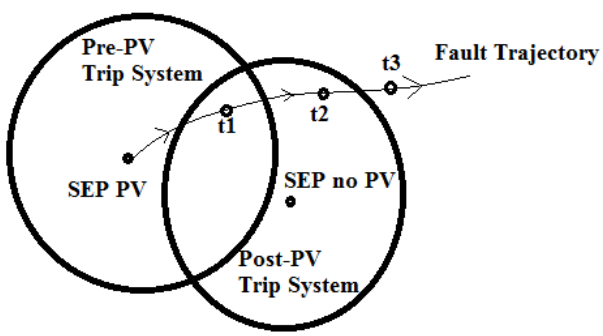

Figure 4.25 Absence of CCT for Switched Systems

In the current work, we are particular interested in the SEP's corresponding to all possible PV connection statuses in the post fault configuration.

4.2.1 Network Reduced Classical Model for Switched Systems

As mentioned before, the connection status across all PVs would correspond to a unique system status. For example, for a system with 2 PVs, the system statuses can be defined as $[1,1], [0,1], [1,0], [0,0]$. Since there are multiple statuses involved, the network reduced model

and the corresponding state equations for each has to be defined. Since we model the PV as a negative load (modelled as a shunt impedance element), this can be done by removing the shunt elements from Y_{bus}^{new} in Algorithm 1.1 corresponding to the PVs that are out of service for the particular status (shown in above table). Rest of the process is the same. For example, in the above system, for making the model with PV status $[0,1]$, the shunt impedance element in the admittance matrix corresponding to PV at bus 1 is set to 0. Let us now try to see what information we can get from BCU.

4.2.2 Multistep BCU

The aim here is to see if knowing the SRs or their estimates corresponding to each individual system status encountered along a fault trajectory and the system state at the time of fault clearing is enough to assess the stability of the overall switched system. In this study, for a given length of fault duration, BCU would be run for every system status encountered (whenever PV trips) individually to estimate the CCT for each. The overall process which we will refer to as a Multistep BCU is explained below. A thing to keep in mind is that for a system with n_{pv} PV generators, there $2^{n_{pv}}$ statuses in the fault phase, $2^{n_{pv}}$ in post-fault but a single one for pre-fault (corresponding to the starting connection status for PVs). Let us denote the fault dynamics by $\dot{x} = f_i^{fault}(x)$, post fault dynamics by $\dot{x} = f_i^{post}(x)\ \forall i \in [1,2^{n_{pv}}]$. Also, for each system status in post fault phase, there will be a corresponding gradient system as defined in 2.1.5.

Algorithm 4.2 Multistep BCU

1. Define all possible system statuses based on the number of PVs in the system.
2. Find SEP ${x_{sep}}_i^{post}$ of each system status in post fault phase by solving $f_i^{post}(x) = 0$ using Algorithm 2.3.
3. Create an encountered status stability table for recordkeeping as shown below –

Status	**Fault Clearing Time**			
	$tstep$	$2 \times tstep$	...	T_{max}
1	×	×		
3	×	×	×	×
4	×			

Here each row corresponds to what statuses were encountered during the fault trajectory (due to PV's tripping). The symbol × in $(i, j)^{th}$ position means that if the fault is cleared at $2 \times j \times tstep$ seconds and at that time the system has status corresponding to row i and no further switching happens then the system is stable. Initialize this table with 1 row corresponding to the status having the initial connection status of PVs.

4. Initialize $t = 0, x(t) = x_{sep}^{pre}, activestatus = initialstatus, f(x) = f_{activestatus}^{fault}(x)$.
5. Integrate $f(x)$ by $tstep$ seconds starting from $x(t)$ to get $x(t + tstep)$.
6. Trip all the PVs with their voltages lesser than the corresponding LVRT curves. Update $activestatus$ according to the current connection status of PV's. Also add a row in the encountered status table corresponding to the new $activestatus$.
7. $t = t + tstep$. If $t < T_{max}$, GOTO Step 5.
8. Obtain the CCTs individually for all the system statuses in post fault phase encountered using the obtained fault trajectory (which includes PV's tripped along the way) with BCU as discussed in 2.1.5.
9. Mark × in the encountered status stability table using the CCTs obtained in the previous step.

Let us take up an example for a better understanding of the process.

Example 4.2 Given the following 3-machine system with a PV of size 2 pu connected at bus 1 with 0% displacement. To maintain generator load balance, the output of generator at bus 3 is reduced by 2 pu. The fault at bus 1 followed by tripping of line 1-2 is studied. The LVRT curve for the PV is also shown. The state values are in the COA reference frame.

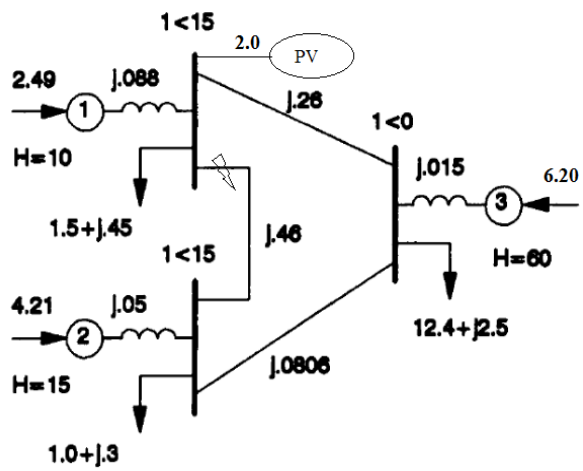

Figure 4.26 Example 4.2 Multistep BCU Test Case

The prefault SEP as well as the post fault SEP's for different statuses are as given below –

Table 4.5 Example 4.2 Post fault SEP for All Statuses

Status	**PV Status**	**Network Configuration**	**SEP**$(\delta_1^{coa}, \delta_2^{coa}, \omega_1^{coa}, \omega_2^{coa})$
1	1	Pre fault	(0.5840,0.2657,0,0)
1	1	Post Fault	(0.8622,0.1782,0,0)
2	0	Post Fault	(0.2630,0.2817,0,0)

The fault was simulated for 1 second with PV tripping at 0.15 s. The BCU results for both the statuses encountered are as shown –

Table 4.6 Example 4.2 Multistep BCU Results

Status	**Encountered At**	**CUEP**	**BCU CCT**	**Time Domain Simulation CCT**
1	0.0	(1.672,0.0743,0,0)	0.0515	0.1350
2	0.15	(2.0923,0.0306,0,0)	0.1797	0.2150

Writing the encountered status stability table,

Table 4.7 Example 4.2 Encountered Status Stability Table

Status	**Fault Clearing Time**								
	0	0.01	…	0.05	0.06	…	0.17	…	∞

1	×	×	×	×					
2	×	×	×	×	×	×	×		

Since starting at $0.15\ s$ when the PV trips, status 1 seizes to exist, the stability of the overall system should only be decided by stability for the statuses that lie ahead in the timeline. With that logic, since after $0.15s$ of the fault, only status 2 is valid (no other PV is left to trip so system never switches to any other status) and thus the overall stability is given by status 2 which says that the system is stable in $[0.15,0.17]$.

Now, for the fault clearing times before PV trips, we will show that nothing can be said about the stability of the overall switched system. Let us study fault clearing at $0.14\ s$. Post fault system in status 2 is stable at this time while status 1 is not as seen from Table 4.7. One might be tempted to say that clearing fault at $0.14\ s$, the post fault system will settle to SEP of status 2 if PV trips. This is not always the case and depends on the time it takes to trip. We can say with surety that if the PV were to trip the same time as the fault clears and then no other PV trips, the system will settle to the SEP of post fault system in status 2. Let us plot the post fault trajectories in angle domain for different fault clearing times. Here the trajectories colored red are the ones along which PV never trips while those colored orange have PV tripping. The bold dots (colored red/orange) are the starting points for post fault trajectory lying on the fault trajectory i.e. if red that means PV has not tripped till then along the fault trajectory and orange means it has. The SEPs for post fault system status with PV connected is marked x_{s_1} and that for PV disconnected is x_{s_2}. We can see that the post fault trajectories starting from the first few dots (marked red) do not see any PV trip(red colored trajectory) and are also stable. Same goes for trajectories that start with orange color and remain orange. However one particular trajectory analyzed which highlighted in black has red starting dot meaning at the time of fault clearing PV hasn't tripped but the emerging trajectory color is orange means eventually the PV trips. This trajectory does not settle to the equilibrium x_{s_2} and goes away meaning the system became unstable which BCU wasn't able to predict.

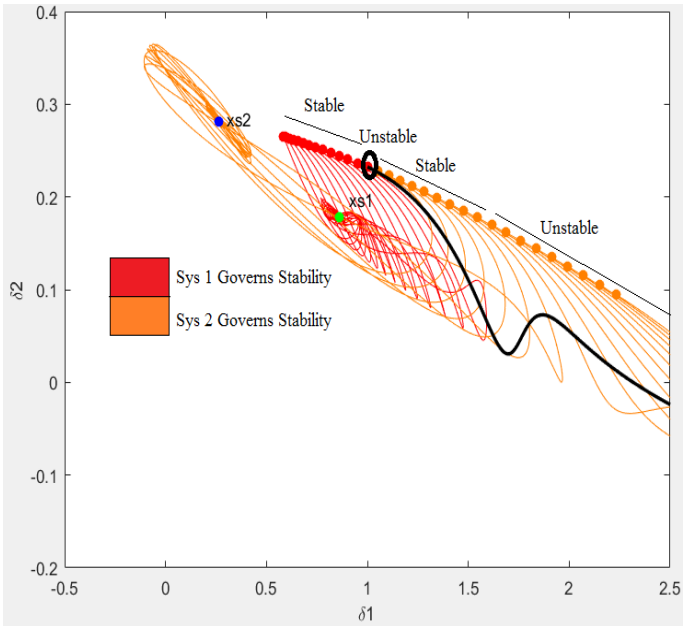

Figure 4.27 Example 4.2 Actual System Trajectory in Angle Domain

Let us look into what exactly happened. The system started outside the SR for status 1 but inside that for status 2 (from BCU results) with the PV still connected. Now, the post fault system vector field ($f(x)$) is that corresponding to status 1 which takes the system outside the SR for status 2. Around 2 seconds, when system is already outside, PV trips and is obviously unstable. This is seen from the voltage plot at PV vs LVRT curve in Figure 4.28.

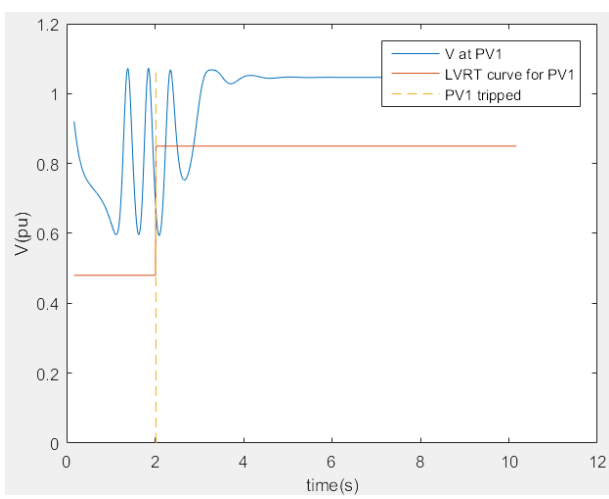

Figure 4.28 Example 4.2 V_{pv} vs LVRT Curve

Let us plot the energy function value for post fault system status 2 along with the corresponding critical energy (from BCU) for the unstable post fault trajectory in Figure 4.29. We can clearly see that in the initial period with status 1's vector field active, the energy increases beyond the critical value which means system leaves SR of x_{s_2}.

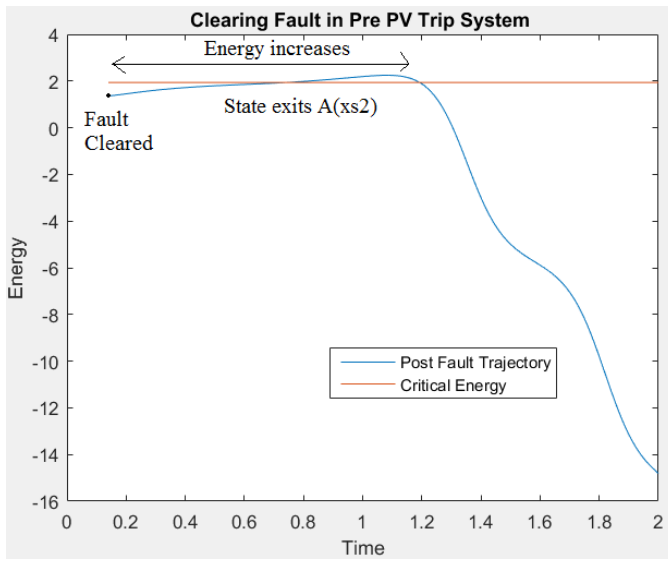

Figure 4.29 Example 4.2 Energy Plot of Unstable Trajectory

Thus, the location of post fault trajectory state after the final PV has tripped along it needs to be known to estimate the overall system stability. Now, guessing the time beyond which no other PV will trip requires simulation of the whole trajectory. However, there seems to be a relationship between the fault and the PV's that are expected to trip (along all fault and post fault trajectories).

4.2.3 Stability Under Cascading Tripping of PVs

Taking a step back, let us try understanding the impact of cascading outages of PVs on a system. Based on the industry's experience, the development of PV plants is mostly concentrated in certain parts of the system mainly driven by land availability and prices. This results in a degree of electrical coherency among many such plants. Also, utilities are driven towards standardizing the ride through settings across their territory which directly maps the electrical coherency to a coherent tripping, a perfect setting for cascading failures. It is important to note that these cascading events happen in a matter of seconds not giving any time to the system operators to

react. This warrants studying the impact of such scenarios on transient stability. These events are further exacerbated by false tripping of these generators which is not uncommon. Thus, there is a need to understand the consequences of certain unforeseen cascading events. Here, we will try to address a broader problem of understanding the impact of likely switching scenarios on transient stability. A given switching signal is characterized by what switching happens at what time giving us infinite combinations of scenarios to study. However, if we could remove the time element from the switching signals, the scenarios become finite and are simply given by which PVs trip and in what sequence. For n_{pv} number of PVs, the possible switching signals become $\sum_{r=0}^{n_{pv}} n_{pv}C_r \times r!$. Even if the time element were to be included in stability assessment, making sense out of such results would be extremely difficult for system planners. For example, if PV 1 were to trip after 1 second and PV 2 trips after 2 seconds is stable but PV 1 tripping after 2 seconds and PV 2 tripping after 1 second is unstable doesn't help much vs a simpler information saying that both PV 1 and 2 tripping has high risk. Making the analysis independent of time requires choosing the worst timings for a given order of events which requires running all possible switching times for every change in system bringing us back to the previous problem. However in this regard, direct methods can possibly help by characterizing an SR independent of switching times for a fixed cascading sequence.

Utilities keep a record of various PV tripping events which would help estimate the relative frequency of each cascading sequence in a broader sense. Let p_i be the probability of ith switching/cascading trip sequence σ^i, the risk of instability for a trajectory starting at x_0 in state space can be defined as –

$$Risk(unstable|x_0) = \sum_i p(unstable|x_0|\sigma^i) \times p_i \tag{4.33}$$

The first term being multiplied on the right hand side will be 1 if x_0 is outside the estimated SR for σ^i. It is important to mention that $p_i's$ can be chosen according to the preference of the operator. At times, he may not to consider only a handful of cascading scenarios or weighing all possible scenarios equally. This could help gain an insight into the impact of RG tripping and identify key chain of considerably likely events that put the system under risk. These events

could then be blocked by choosing strategies like – RG 1 and 2 cannot be offline simultaneously. The initial points in state space from which the emerging trajectories are stable in most of the switching scenarios will truly represent the region of interest pertaining to a minimum threat. In systems with highly impactful switching events (in terms of the magnitude of changes to the SEP as well as the associated SR), having a region in state space having a 100% chance of being stable is rare. One thing to mention again is that each switching scenario/signal is defined by what switching events happen and in what order and is independent of the time elapsed between the successive switchings.

4.2.3.1 Estimating SR Under Fixed Cascading Sequence

Now, in order to evaluate the value of $p(unstable|x_0|\sigma^i)$ in the risk of instability, we need an estimate of the SR for a fixed cascading sequence σ^i. The idea of practical stability [98] which can help analyze switched systems offers a way to achieve that.

Definition 4.1 A switched system is considered practically stable in the time interval $[t_0, T]$ with respect to sets Ω_1 and Ω_2 with $\Omega_1 \subseteq \Omega_2$ if $x(t_0) \in \Omega_1$ implies $x(t) \in \Omega_2 \ \forall \ t \in [t_0, T]$.

There is a popular approach referred to as the dwell time [99] approach when dealing with switched systems with distinct EPs. In this approach, the stability is defined in terms of dwell time which represents the minimum time lapse between two successive switching. This means that the system has to remain at least for dwell time amount of time in each status it encounters before it can switch to another one. This approach was demonstrated on a system to study the stability resulting from load changes [100]. However in our system, this would mean forcing the PVs to remain online thus changing the ride through curves on the fly which is not possible. So, we cannot impose a dwell time constraint. In our problem, we want the state at time t denoted by $x(t)$ to remain inside the SR corresponding to whatever status is active at that time $\forall t$. This condition on a given trajectory can ensure its stability for the given switching which leads us to our next theorem.

Theorem 4.5 Let Ω_1 denote a positively invariant set for the system $\dot{x} = f_1(x)$ st. $\Omega_1 \subseteq A(\mathrm{x}_{\mathrm{sep}_1})$ where x_{sep_1} is the relevant SEP for system status 1. Similarly define Ω_2 for the system

$\dot{x} = f_2(x)$. If $\Omega_1 \subseteq \Omega_2$, then the trajectories starting in Ω_1 at any time t with status 1 active at that moment converge to the set $\{x_{sep_1}, x_{sep_2}\}$ as $t \to \infty$ for the switched system $\dot{x} = f_\sigma(x)$ for the following switching signals-

a. $\sigma(t) = \begin{cases} 1, & t < T \\ 2, & t \geq T \end{cases} \forall T$. System switches from status 1 to 2 with no further switching.

b. $\sigma = 1$. System remains in status 1 with no further switching.

Proof The proof for this theorem is fairly simple. We know that all trajectories starting in Ω_1 for the system $\dot{x} = f_1(x)$ will converge to x_{sep_1} since $\Omega_1 \subseteq A(\mathrm{x}_{\mathrm{sep}_1})$. Also, since Ω_1 is invariant, trajectories will remain inside it. Now, since $\Omega_1 \subseteq \Omega_2$, those trajectories always stay inside Ω_2. Switching from status 1 to 2 at any time will change the dynamics to a system defined by $\dot{x} = f_2(x)$. Since $\Omega_2 \subseteq A(\mathrm{x}_{\mathrm{sep}_2})$, trajectories constrained to Ω_2 will converge to x_{sep_2}. Hence proved.

Next, the task is to find the invariant sets Ω_1 and Ω_2 for the above mentioned switching signals. The idea of multiple Lyapunov like functions as proposed in [101] is used to obtain functions V_1 and V_2 for the systems $\dot{x} = f_1(x)$ and $\dot{x} = f_2(x)$ respectively with their corresponding level sets $\{V \leq 1\}$ satisfying the following constraints.

1. Set $\Omega_2 = \{V_2 \leq 1\}$ is the SR estimate for the system $\dot{x} = f_2(x)$.
2. Set $\Omega_1 = \{V_1 \leq 1\}$ is the portion of the SR estimate for the system $\dot{x} = f_1(x)$ constrained to be inside $\{V_2 \leq 1\}$.

We serially estimate both these sets starting from V_2 then V_1. While the first step can be easily done as discussed in 2.2.4, the second step has a constraint forcing Ω_1 to remain inside Ω_2. One important thing to keep in mind is that the origin is assumed to be the SEP of interest for the expanding interior formulation discussed in 2.2.4. Since SEP's can be distinct for both the system statuses, the V_2 obtained in step 1 has to be transformed accordingly to the new origin at x_{sep_1}. For clarity, we will represent states of post fault system with status 1 with the origin at x_{sep_1} as x_1 and those for status 2 as x_2 with origin at x_{sep_2}.The expanding interior formulation for the second step starting with $V_2(x_1)$ obtained from first step is as shown below.

$$\boldsymbol{max.\ \ \beta}$$

$$s.t.$$

$\boldsymbol{V_1(x_1)}$ **cannot be negative:**$\{V_1(x_1) \leq 0,\ g_1(x_1) = 0, x_1 \neq 0\} = \emptyset$

$\boldsymbol{P_\beta}$ **Is contained inside the SR estimate** $\boldsymbol{(V_1(x_1) \leq 1)}$ **:** $\{p(x_1) \leq \beta\ ,\ g_1(x_1) = 0,\ V_1(x_1) \geq 1,\ V_1(x_1) \neq 1\} = \emptyset$ (4.34)

Inside the SR estimate,$\boldsymbol{V(x_1)}$ **strictly decreases along all trajectories:**

$$\{V_1(x_1) \leq 1, \dot{V}_1(x_1) \geq 0,\ g_1(x_1) = 0, x_1 \neq 0\} = \emptyset$$

Inside the SR estimate,$\boldsymbol{V_2(x_1)}$ **cannot be** $\boldsymbol{> 1}$**:**

$$\{V_1(x_1) \leq 1, V_2(x_1) \geq 1, V_2(x_1) \neq 1,\ g_1(x_1) = 0, x_1 \neq 0\} = \emptyset$$

The problem can be written as an SOS optimization using P-Satz,

$$\boldsymbol{max.\ \ \beta}$$

$$s.t.$$

$$\begin{aligned} V_1 - \lambda_1^T g_1 - l_1 &\in \Sigma \\ -s_6(\beta - p) - \lambda_2^T g_1 - (V_1 - 1) &\in \Sigma \\ -s_8(1 - V_1) - s_9\dot{V}_1 - \lambda_3^T g_1 - l_2 &\in \Sigma \\ -s_{10}(1 - V_1) - (V_2 - 1) - \lambda_4^T g_1 &\in \Sigma \end{aligned} \tag{4.35}$$

The proposed methodology can be easily extended to a sequence of any length.

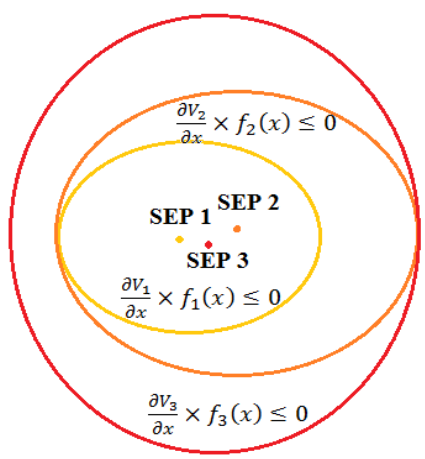

Figure 4.30 Stability Under Fixed Switching using Nested SRs

It can be visualized with the help of the Figure 4.30 for a case with 3 system statuses starting in status 1 and stable under the cascading sequences - $[1], [1 \rightarrow 2]$ & $[1 \rightarrow 2 \rightarrow 3]$.

4.2.3.2 Estimating the Risk of Instability Region

The previous discussion leads us to the following algorithm for estimating the risk of instability for different starting points in state space is shown below.

Algorithm 4.3 Estimating Risk of Instability

1. Enumerate all possible switching scenarios. As an example, shown below are those for a system with two trippable PVs and no other form of switching.

Cascading Sequence	PV Status				
1	11		11		11
2	11		10		10
3	11		01		01
4	11		10		00
5	11		01		00

2. Define a d dimensional grid in state space where d are the number of power system states resulting in N points in state space.
3. $j = 1$.
4. Estimate nested SRs for j^{th} cascading sequence using the technique proposed in 4.2.3.1.
5. $k = 1$. $Risk(unstable|x_k) = 0$.
6. If k^{th} point on the grid lies outside the innermost region in the nested SRs, $Risk(unstable|x_k) = Risk(unstable|x_k) + p(\sigma^i)$
7. If $k < N$, $k = k + 1$,GOTO Step 6.
8. If $j < N_{sw}, j = j + 1$, GOTO Step 4.
9. STOP.

Let us now move onto studying the impact of blocking certain chain of cascading tripping on risk of instability. In this work, only simple blocking signals are studied, defined as a list of online PVs not allowed to stay offline simultaneously. For example, a blocking signal denoted by (1,3) means that only one out of PV 1 and PV 3 are allowed to trip but not both. While the blocking

signals will reduce the probabilities of certain cascading events to 0, they will increase the chances of occurrence of some others which is difficult to know beforehand and depends on the system behavior due to the state and time dependent nature of switching. Therefore, we assume the following simplified changes to the probabilities –

On implementing the blocking signal, if σ^i transforms to σ^j then,

1. $p^{new}(\sigma^j) = p^{old}(\sigma^j) + p^{old}(\sigma^i)$
2. $p^{new}(\sigma^i) = 0$

Let us take up an example to understand the value of this analysis.

Example 4.4 Given the network below with 3 PVs, ~50% penetration. Uniform damping $\frac{D}{M}$ of 4.

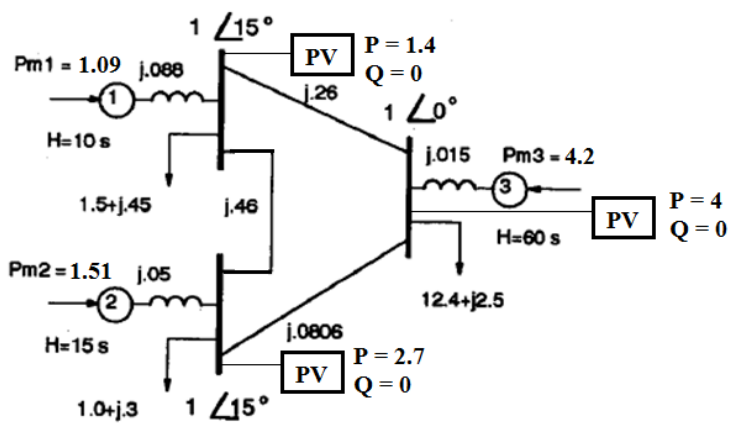

Figure 4.31 Example 4.4 Test System

There are $2^3 = 8$ switching states with each's SEP given below.

Table 4.8 Example 4.4 SEPs for All Switching States

Switching State	PV Connection Status	SEP $(\delta_{13}, \delta_{23})$
1	111	(0.2916,0.2741)
2	110	(0.4000,0.3362)

3	101	(0.2885,0.1124)
4	100	(0.3976,0.1714)
5	011	(0.0767,0.2567)
6	010	(0.1790,0.3177)
7	001	(0.0731,0.0950)
8	000	(0.1754,0.1532)

Let us now enumerate all possible cascading scenarios.

Table 4.9 Example 4.4 Cascading Sequences

Switching Signal	PV Trip Order	Switching State Order (refer previous table)
1	No trip	1
2	1	1 5
3	2	1 3
4	3	1 2
5	2 1	1 3 7
6	1 2	1 5 7
7	3 1	1 2 6
8	1 3	1 5 6
9	3 2	1 2 4
10	2 3	1 3 4
11	3 2 1	1 2 4 8
12	3 1 2	1 2 6 8
13	2 3 1	1 3 4 8

14	2 1 3	1 3 7 8
15	1 2 3	1 5 7 8
16	1 3 2	1 5 6 8

Here it is important to mention that there can be cascading sequences where it is not possible to find such nested regions which may pose a great risk of system collapse. A planner would want to avoid encountering such scenarios by cleverly blocking some trippings from happening. Next, plotting the SR estimate for all switching signals.

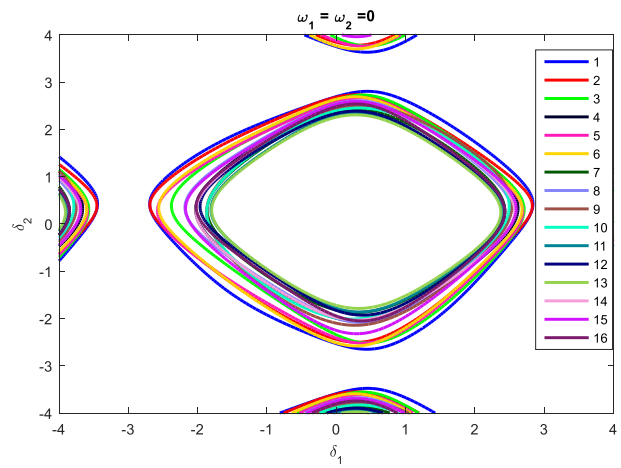

Figure 4.32 Example 4.4 SR Estimate for all Cascading Sequences

A few observations can be made from the graph above –

- The largest SR (blue color) corresponds to the switching scenario with no switching happening. This is obviously true since the SRs of pre and post switching system are not the same.
- The SR estimate for any switching scenario involving switching between largely differing systems (in terms of SEP and SR size) will be small due to less overlapping. Furthermore, the cases with all 3 PVs eventually tripping will have the smallest SRs due to a naturally decreasing intersecting region with increasing number of distinct regions.

- There is a region in the middle which is the intersection of the SRs of all the cascading sequences. Usually such regions rarely exist as beyond a certain cumulative size of PVs tripping, the equilibrium seizes to exist.

Let us now combine these estimates probabilistically. Due to a lack of data, let us assume all these sequences to be equally likely ($p_i = \frac{1}{16}$) . In that case, the risk of instability as discussed before is plotted below.

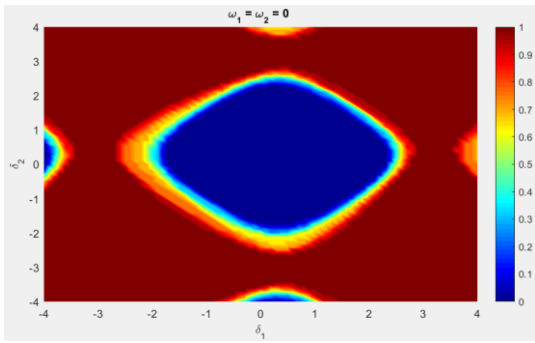

Figure 4.33 Example 4.4 Risk of Instability Region

Here, the risk of instability for different starting points in state space increases from blue to red with blue being the lowest. Let us now visualize the impact of blocking some tripping sequences.

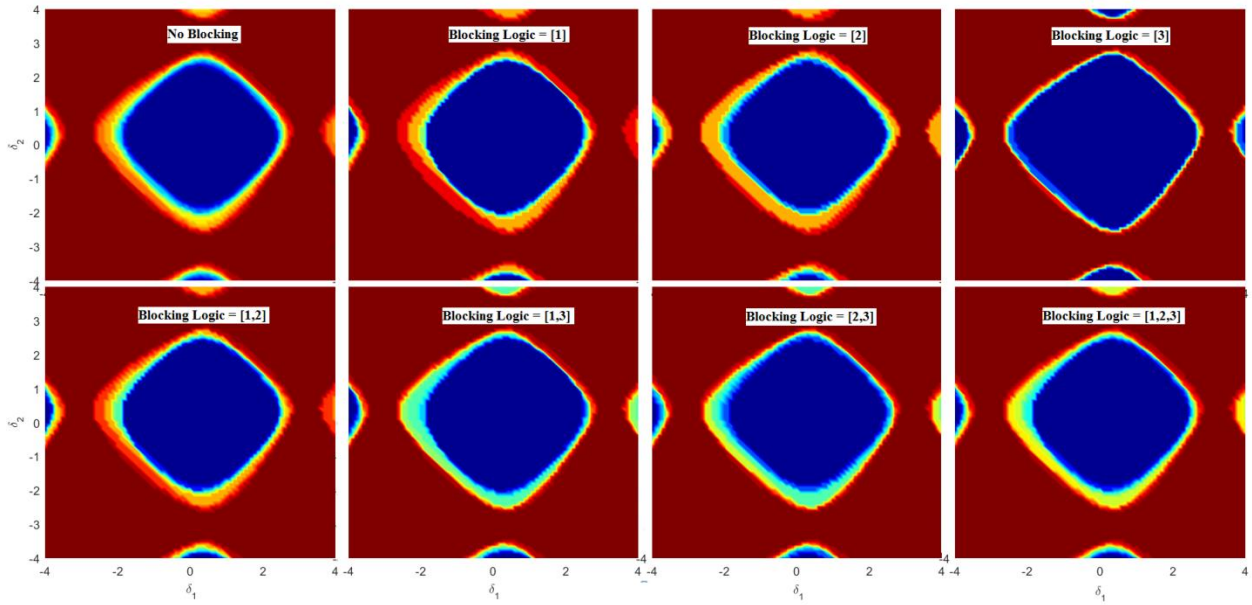

Figure 4.34 Example 4.4 Risk of Instability Under Trip Blocking

Here, one can see that blocking the tripping of PV 3 has the best reduction in the risk of instability marked by a bigger blue region as compared to other options. The region with 100% chances of being stable is colored dark blue and is seen to be considerably sized. This region also happens to cover the majority of the area which is comprised of starting points which are stable in even a single switching scenario (mainly lack of switching). This hints towards large similarities between SRs of across various switching scenarios. The region comprising of starting points resulting in unstable trajectories for any of the switching scenarios majorly consists of the area in state space outside the SR for non- switching scenario.

4.2.4 Multiple CSR Approach

It was seen in the previous section from the SR estimates obtained under cascading tripping that the conservativeness in the estimate relied on the amount of overlap between SRs corresponding to the individual system statuses. It was not rare to see cases with some statuses having no SEP depending on the size and locations of PV(s) tripped or only having a tiny overlap between unconstrained stability regions for each encountered status. In those cases, as we saw, finding a nested SR was not possible. Even if the nested regions exist for a given tripping order, the size of the innermost one would heavily depend on the number of the nested regions being considered for the given disturbance under study. This estimate would continue to shrink if the number of such nested regions were to increase which is possible in networks with a lot of PVs located electrically close. Needless to say, there is also an inherent conservativeness in the SOS based Lyapunov approach.

When assessing the stability for a given disturbance, considering all possible switching scenarios is extremely conservative. Only the ones that are likely to be encountered due to the given disturbance should be considered which is difficult to know beforehand. For example, studying a fault electrically far from any of the PVs will result in none of them violating their LVRT curves thus no tripping. This brings us back to the original problem of transient stability assessment under LVRT based tripping using switched systems approach

Let us try understanding the possible number of switching scenarios that can be encountered. Based on the ride through standards and typical power system characteristics, the following can be said about switching resulting from PV tripping :-

(O1) The system cannot pass through the same status more than once. This stems from the fact that once a PV is tripped will not be allowed to reconnect until several minutes of normal operation is seen [85] [84]. This also means that tripping of a single PV reduces the possible candidates for future status encountered by half. This can be understood with the following example and the assumption above- A 3-PV system with currently all 3 connected i.e. status is [111]. Let an event happen and PV 1 trips i.e. status now becomes [011]. This means that now, there is no possibility of the system passing through statuses with PV 1 having connection status as 1 say the ones defined by connection statuses [**1**01],[**1**00] and so on.

(O2) The influence of a fault, especially at lower kV levels is very local which means that the voltage decline during a fault may not be seen by many PV's in the network. This paired with the previous observation heavily reduces the number of statuses encountered for a particular fault.

We know that the stability depends on the order and the timings of the PV trips. This is difficult to estimate without actually integrating a trajectory which limits the applicability of direct methods. Since the fault trajectory is integrated anyways, we know the sequence of PVs tripping along it beforehand. The trippings along the post fault trajectories are uncertain. It will be easy in theory to estimate the stability of such system if the order of PVs tripping became deterministic as seen from the previous sections. The BCU based idea shown in 4.2.2 faced a similar issue, it was difficult to predict which status's SR to use when making stability decisions for the post fault trajectories. With that being said, we do have a way to identify the post fault trajectories that will definitely not see any PV tripping as discussed in 4.1. Thus, instead of using the unconstrained SR estimates for each status as done in 4.2.2, using CSRs could help achieve that reliability for the results. Thus, we will make stability decisions for those clearing times that lead to trajectories that do not see any tripping. We will flag all other clearing times as

uncertain since we cannot estimate the stability of the emerging trajectory. Conservatively we will call them unstable.

Now, during a sustained fault event, PVs will trip at certain times which are separated by intervals of no tripping. Thus, the starting status of post fault system for each such interval is different.

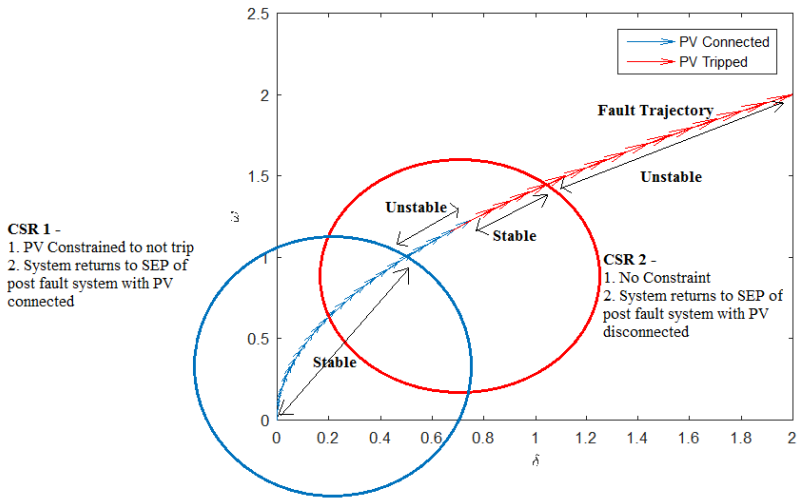

Figure 4.35 Multiple CSR Approach

This can be best understood from the figure above for a single PV system. The part of the fault trajectory during which PV stayed connected is colored blue while the red part corresponds to PV disconnected resulting in two intervals. Now, for the first interval, since PV is connected, we estimate the CSR (blue ellipse) with the constraint that voltage at PV is above its LVRT. This CSR will be used to assess the stability for the blue portion of the trajectory. Similarly for the red portion, since the PV is already disconnected, there is no constraint and the system is simply an unconstrained system with the SR (red ellipse) estimated accordingly. Here we see that there is a portion of the blue part of the trajectory that lies outside the blue ellipse and the thus the corresponding clearing times will be called unstable. Once it becomes red, the stability is governed by the red ellipse making it stable.

The maximum fault clearing time to be studied is based on the preference of the user and/or reliability standards defined for protection systems. As mentioned before, there is a maximum

fault clearing time after which the trajectory exits the SRs for all statuses regardless of the PV tripping. This is where we would want to stop the analysis and mark all higher clearing times as unstable. In this process, since the estimation of constrained SR for one interval is not a function of the other's, we can parallel the estimation process. However, here we will simply present a serial implementation of the proposed approach.

Algorithm 4.4 Switched Systems Approach to LVRT Constrained PV using Constrained SR

1. Obtain state equations and SEP's for each possible status ($2^{n_{pv}}$ in number) as discussed in 4.2.1 and 4.2.2.
2. Simulate fault trajectory for a suitable period of time (T_{max}^{fault}). Let the value of state variables along this trajectory be denoted by $x_{fault}(t)\ \forall\ t \in [0, T_{max}^{fault}]$.
3. Store the timeline of statuses encountered (refer 4.2.1) and LVRT constraint pair similar to the one shown below for a 3 PV system example with maximum fault time studied is 0.2 s.

Fault Interval Number	**Fault Time Interval**	**Active Status**	**PV Status**	**Constraint**
1	[0,0.15]	1	111	$PV1 \geq LVRT1, PV2 \geq LVRT2, PV3 \geq LVRT3$
2	[0.15,0.20]	5	011	$PV2 \geq LVRT2, PV3 \geq LVRT3$

4. $j = 1$
5. For j^{th} fault interval, compute the Lyapunov Function for the post fault system in the active status in that interval, V_j and corresponding constrained SR estimate $\{V_j \leq 1\}$ using any of the techniques proposed in 4.1.
6. If $j < Last\ Fault\ Interval\ Number$, Set $j = j + 1$, GOTO Step 5.
7. STOP

Stability Assessment of States Along Fault Trajectory

8. $t = 0$
9. Fault interval number $k(t)$ at time t can be obtained from the table similar to Step 3. If $V_{k(t)}\left(x_{fault}(t_1)\right) < 1\ \forall t_1 \leq t$, clearing fault at time t will result in a stable trajectory else an uncertain or conservatively unstable one.

$$t = t + t_{step}$$

Let us now apply the proposed methodology to multiple scenarios in order to analyze the effectiveness as well as shortcomings of the approach.

Example 4.5 Let us consider a system below.

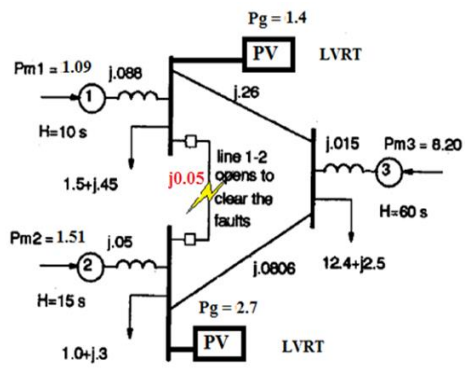

Figure 4.36 Example 4.5 Test System

Let us assume the LVRT curves are same for both generators and given by the artificial system state equation as $\dot{c} = -10 \times (c - 0) \times (c - 0.85)$, $c_0 = 0.001$. Based on voltage values along fault trajectory (see figure below), the following are the encountered statuses –

Table 4.10 Example 4.5

Fault Interval Number	**Fault Time Interval**	**Active Status**	**PV Status**	**Constraint**
1	[0,0.67]	1	11	$PV1 \geq LVRT1, PV2 \geq LVRT2$
2	[0.68,0.79]	3	01	$PV2 \geq LVRT2$
3	[0.80,∞]	4	00	None

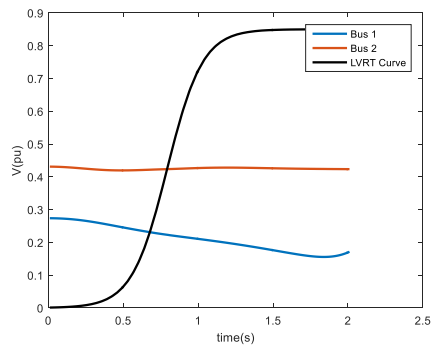

Figure 4.37 Example 4.5 Fault Voltages

We can see from the lookup table that 3 constrained SRs need to be estimated, one for each fault interval. This will depend on the number of tripping events and not necessarily the number of devices tripping. Thus, if 2 PVs were to trip together in this case, we will just have to study 2 intervals as opposed to 3. More the number of PVs at voltage coherent buses, lesser the number of intervals to be studied. The SEPs of interest for the post fault systems in individual intervals are as given below for which constrained SRs are estimated.

Table 4.11 Example 4.5 SEP

Fault Interval Number	**SEP ($\delta_{1n_g}, \delta_{2n_g}$)**
1	0.2342,0.2174
2	-0.0957,0.2363
3	-0.01,0.0463

We use the same state variable transformation as before. The CSR for each is found out through the technique discussed in 4.1.5. The final Lyapunov functions as well as the SRs for each interval are as shown below.

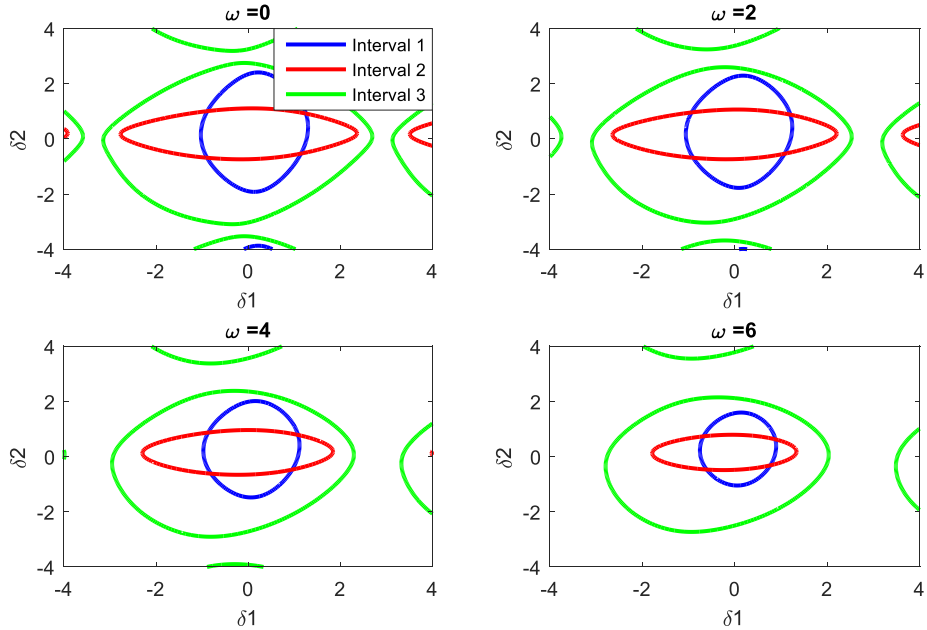

Figure 4.38 Example 4.5 Constrained SR Estimates

The value of Lyapunov function of the active interval along fault trajectory is plotted below based on which the stability results are as shown.

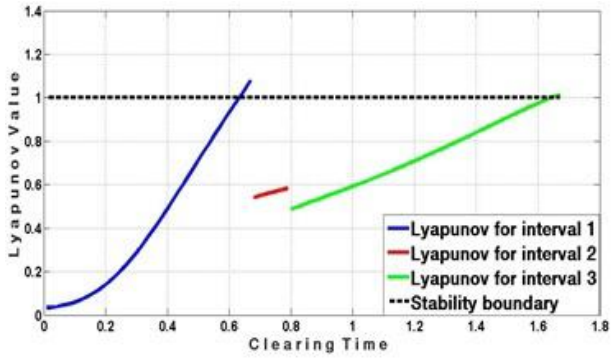

Figure 4.39 Example 4.5 Active Lyapunov Function Value Along Fault Trajectory

We further do the time domain simulation to find the actual stability of the system. It can be seen that the proposed technique is able to accurately capture the stability for most clearing time though a bit on the conservative side. The reasons for conservativeness in this approach are due to the inherent limitations in Lyapunov based approaches and deeming the post fault trajectories expected to see any trippings as unstable.

Table 4.12 Example 4.5 Stability Results

Fault Int. #	1	1	2	3	3	3
Clearing Time	0-0.63	0.64-0.67	0.68-0.79	0.80-1.64	1.65-1.67	>1.67
Proposed	S	U	S	S	U	U
Actual	S	S	S	S	S	U

Example 4.6 Let us study a system with loss of equilibrium on PV tripping. A large PV (~ 40% penetration) is connected to a load rich area (bus 3). The power from generator 1 and 2 feed the local loads with the majority of the power supplying the load at bus 3. The governing LVRT characteristics are $K = 10, c_{uep} = 0, c_{sep} = 0.85, c_0 = 0.001$.

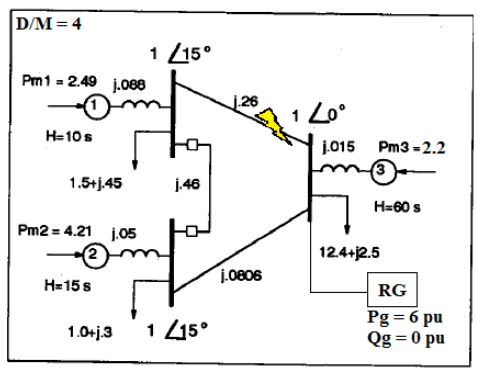

Figure 4.40 Example 4.6 Test System

The fault being studied is at bus 3 and trips the line 2-3 in which case the excess power generated from generator 1 is redirected to a radial path through generator 2 to supply load at 2 and 3. Now, when the PV trips at 0.69 s of the fault due to LVRT as seen below, there is an increase in load at bus 3 which cannot be supplied by the post fault transmission network thus the equilibrium vanishes. The post fault SEP for pre PV trip status is ($\delta_{1ng} = 1.0211, \delta_{2ng} = 0.51597$) while for PV disconnected there is none as mentioned before. Thus, only the pre PV trip post fault system's SR needs to be estimated under the constraint of not letting PV trip.

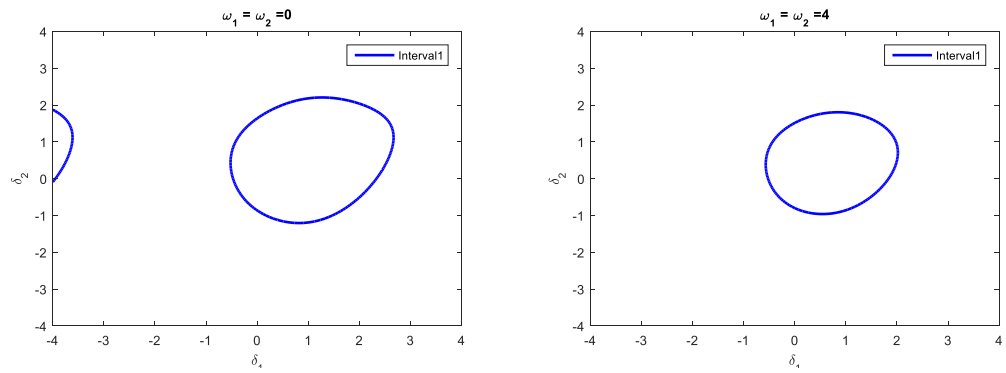

Figure 4.41 Example 4.6 CSR Estimate

Here, since the tripping of PV is truly synonymous to system instability, the approach in [87] would not be conservative. Here, again we can see that while the proposed technique captures the stability reliably, there is still a level of conservativeness. This requires an improvement in obtaining the CSR estimate.

Table 4.13 Example 4.7 Stability Results

Clearing Time (s)	**0.01-0.52**	**0.53-0.68**	**0.68-2.01**
Proposed Approach	S	U	U
Time Domain Simulation	S	S	U

Example 4.7 In this system, there are multiple PVs with the disturbance only seen by few of them which is a common occurrence in large interconnected systems.

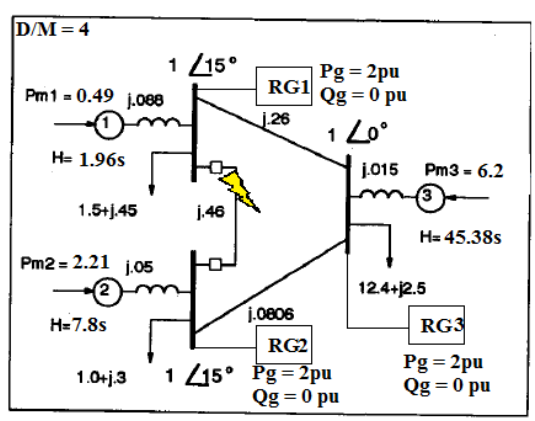

Figure 4.42 Example 4.7 Test System

There is 1 PV connected near each synchronous generator. The MW output, inertia and damping at each generator is are linearly scaled down to reflect the displacement by asynchronous PVs as done in 3.1. The studied fault is on line 1-2 close to bus 1.

The SEPs and the unconstrained SRs for the post fault systems corresponding to each possible PV statuses are shown.

Table 4.14 Example 4.7 SEPs

PV Status	SEP	PV Status	SEP
111	(0.2126,0.2793)	011	(-0.3130,0.2947)
110	(0.2150,0.2946)	010	(-0.3131,0.3106)
101	(0.2138,0.1249)	001	(-0.3113,0.1389)
100	(0.2163,0.1389)	000	(-0.3114,0.1532)

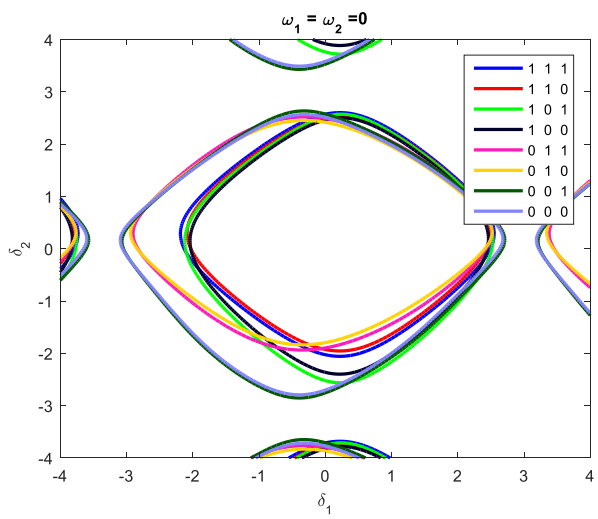

Figure 4.43 Example 4.7 Unconstrained SR Estimates

It can be seen that there is a significant difference in the SRs with changing PV statuses especially with PV 1 status change which widens the stability region along δ_1 axis. This could be attributed to the fact that adding an PV at bus 1 increases the power being exported to buses 2 and 3 thus increasing the relative rotor angle of generator at bus 1 to the others as seen in 3.2. It is known that the SR does not simply move with a moving SEP but also the shape changes. In

this case, with the PV connected, the SEP could have been close to the stability region boundary on the right but moving it to the left increases the stability margin in the positive direction. The largest SRs is seen for the cases with PV 1 and 2 offline which means that for a fault that the system becomes more stable when they trip which shows the issue with treating the tripping as instability.

Now, a sustained fault is introduced and the voltages seen by the PVs are plotted against their respective LVRT curves which shows that only the PV at bus 1 trips. Thus, CSR needs to be estimated for post fault systems for only 2 PV statuses (pre PV 1 trip and post PV 1 trip) out of the possible 8 PV statuses.

Table 4.15 Example 4.7 Constraints

Fault Int. #	1	2
Active Time	[0,0.21]	[0.22,2]
PV Status	111	011
Constraint	$v_{inv1} \geq LVRT_1, v_{inv2} \geq LVRT_2, v_{inv3} \geq LVRT_3$	$v_{inv2} \geq LVRT_2, v_{inv3} \geq LVRT_3$

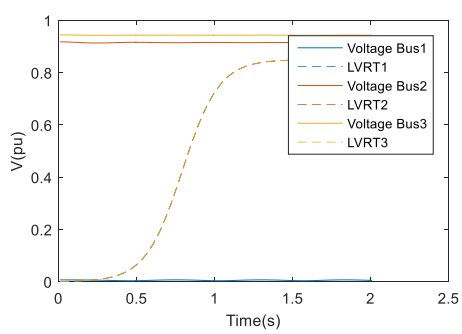

Figure 4.44 Example 4.7 Fault Voltage

The CSR estimates are as shown in Figure 4.45 with the final stability estimates shown in Table 4.16.

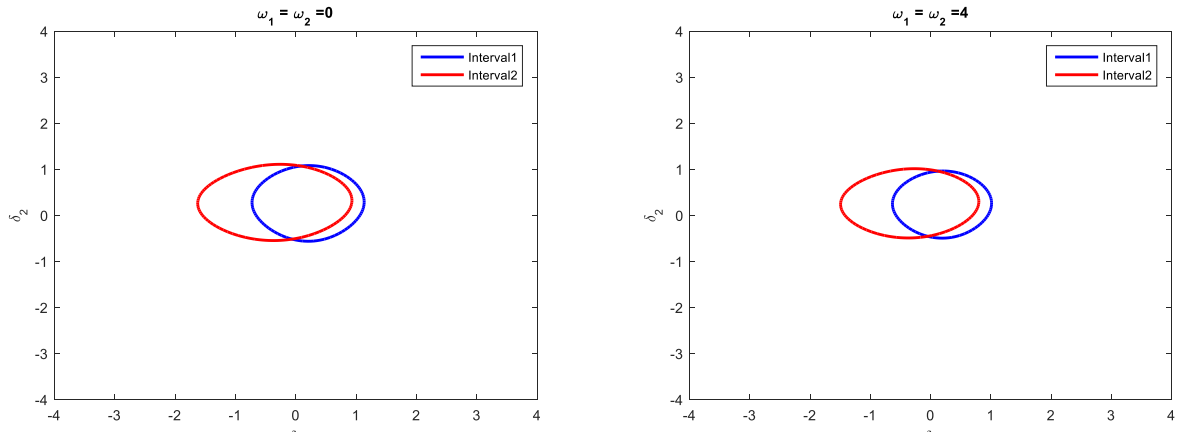

Figure 4.45 Example 4.7 CSR Estimates

Table 4.16 Example 4.7 Stability Results

Clearing Time (s)	0.01-0.21	0.22-0.41	0.42-2.01
Proposed Approach	S	U	U
Time Domain Simulation	S	S	U

Now, in scenarios like these, we know that PVs at buses 2 and 3 are electrically far and therefore not likely to trip. Thus, when estimating each CSR, imposing the LVRT constraints corresponding to all the PVs online brings conservativeness. This can be seen by comparing the size of the CSR plots in Figure 4.45 vs the unconstrained SR plots in Figure 4.43 with a clearly large size for the former. If there is a guarantee that for all the post fault trajectories emerging from the maximum studied fault clearing time which is 2s in this case, those PVs will not trip then we can simply get rid of the constraints corresponding to them on when estimating the CSR. This area of using heuristics to reduce constraints can be further explored. For our case, let us go ahead and relax the constraints for preventing the tripping of PVs at buses 2 and 3 which makes the problem as follows,

Table 4.17 Example 4.7 Relaxed Constraints

Fault Int. #	1	2

Constraint	$v_{inv1} \geq LVRT_1$, $\cancel{v_{inv2} \geq LVRT_2, v_{inv3} \geq LVRT_3}$	$None$ $\cancel{v_{inv2} \geq LVRT_2, v_{inv3} \geq LVRT_3}$

The CSR estimates under relaxed constraints are shown below which are evidently bigger.

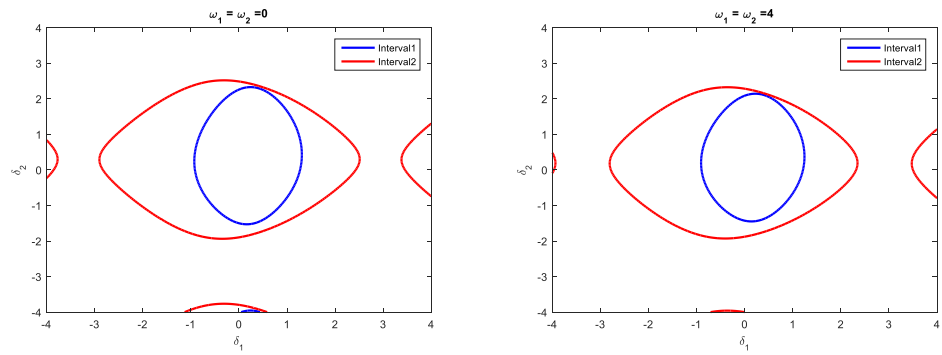

Figure 4.46 Example 4.7 Relaxed CSR Estimates

Table 4.18 Example 4.7 Stability Results Relaxed Constraints

Clearing Time (s)	0.01-0.36	0.37-0.41	0.4-2.01
Proposed Approach	S	U	U
Time Domain Simulation	S	S	U
Reference	?	U	U

The stability assessment for different fault clearing times can be seen to be considerably less conservative. However, this result is reliable as long as the assumption for PV 2 and 3 not tripping holds true.

Chapter 5 Conclusions and Future Work

We start with presenting the well-established energy function theory and the characterization of stability boundary under certain assumptions which led to the popular direct method of BCU. We use this method to do a parametric study on locational inertia reduction resulting from displacement of conventional units by PV with is effectively a zero inertia machine. A method was proposed to visualize approximately the changes in stability boundary with inertia changes using the BCU results for larger systems. It was seen that the displacement among generators having a significant participation in the disturbance under study negatively impacted the transient stability of the system. This was followed by a study in which the conventional generation re-dispatch was varied as a parameter to accommodate a fixed amount of PV in the system. The PEBS which under most conditions gives the intersection of SR with the $\omega = 0$ plane was plotted against the parameter. It was observed that the increasing under-loading of generators to accommodate PV increased the relative distance of the stability boundary from the SEP. This confirms that original hypothesis of increasing stability with decreasing loading. The overall conclusion to be drawn from these two studies was that unit commitment would be a serious problem from the point of view of stability for systems with high penetration of PV. The next part of our work tried to answer the question of how the transient stability problem will be formulated and studied using direct methods for systems having PVs that are allowed to trip during disturbances by the utilities. The conventional direct methods were concerned with only studying the stability of a single system configuration with no further switching changes allowed. However, in the mentioned scenario, the system configuration freely changes thus requiring a need to track the stability of a changing system. This led us to a need for a more flexible technique for estimating the SR of such complex systems. We started by presenting some ideas in SOS programming which is a powerful tool when dealing with polynomial systems. This was followed by its application in estimating the SR systematically for a power systems classical model using Lyapunov theory which had been previously demonstrated. Inspired by the idea of CUEP, a technique to incorporate the disturbance trajectory in the estimation process in order to reduce the conservativeness in CCT estimates was proposed with its

effectiveness demonstrated. Moving back to the problem of stability due to trippable PVs, the first set of approaches treated the tripping as an instability phenomenon due to a risk of initiating a cascading sequence. This imposed operating constraints on the system. These approaches were shown to be inherently conservative through a small example. We proposed ways to model these constraints independent of time and further estimate the CSR using SOS programming. The second proposed approach were more liberal in dealing with PV tripping. The overall system was modeled as a switched system where the tripping of PV meant a switching to a new vector field. Firstly, the estimation of SR under a fixed switching sequence independent of the time between switchings was proposed using Lyapunov's direct method and SOS. We then started by addressing a more general problem of assessing the impact of cascading tripping of PVs on stability. The risk of instability region was defined which coupled the chances of cascading tripping based on historical data with the SR estimates for each cascading sequence. While still in the conceptual phase, this idea has potential applications in helping the system planner identify the cascading scenarios to be stopped by strategizing the blocking of certain PVs from tripping to save the system from potential collapse. This was followed by a methodology for the transient stability assessment of systems with trippable PV which used a different CSR for each range of fault clearing time. While the proposed technique had inherent conservativeness resulting from the Lyapunov approach as well as the LVRT curve approximations, nevertheless it provided a reliable estimate of system stability for such systems.

In totality, the motivation behind this work was to modify and develop direct methods for transient stability assessment of power systems with added complexities resulting from increasing PV penetration. That being said, there are a lot of questions still left unanswered which opens several topics for future research –

- **Analyzing the influence of detailed inverter models:** PV was modelled as a constant real power injection thus ignoring the inverter side dynamics as well as grid support capabilities in our studies. With the increasing penetration of these generators, the inverter dynamics are expected to play a major role in the system behavior thus requiring further assessment. Also, the inverter grid support capabilities in the form of

VAR support, virtual inertia, etc could help boost system stability. As a good start, tracking the system Eigen value changes with changing inverter control strategies can help get a better understanding of the potential of this technology.

- **Impact of uncertainties in PV outputs:** One of the major issues with operating a grid with a large penetration of PV or other renewable generators is the associated uncertainties in the output. This results in a system with multiple possible operating conditions which requires the stability assessment of each. A direction of research could be in exploring the potential of SOS programming in dealing with parameter uncertainties. Also, exploring sampling methods in order to reduce the number of operating conditions analyzed individually using any of the direct methods.
- **Dealing with large scale systems:** One of the biggest drawbacks of the SOS techniques is the high computational requirements. In its current form, this limits the size of the power system that can be dealt with. In this regard, the idea of decomposition using a vector Lyapunov function can be explored. This idea is applicable for large interconnected systems like a power system where the system can be decomposed into independently stable subsystems. The SR for each subsystem is estimated independently and then modified in order to account for the coupling with other systems. These lower dimensional SR estimates together makeup the SR in the overall high dimensional state space. One challenge when dealing with a large system with LVRT constraints would be in how to optimally deal with LVRT constraints that couple various subsystems.
- **Power system detailed models:** Our current work was limited to the power systems classical network reduced model which resulted in a system with dynamics modelled using ODEs. While this approximation has shown to be effective in capturing first swing instabilities, a more detailed system model is important in order to truly capture the problems with renewables. The resulting system will be modelled as a DAE with larger number of states as compared to the reduced version. The most popular approaches when analyzing the stability of DAE systems using direct methods are singular perturbation and regularization of vector fields. A first step in this direction could be in

exploring the variable transformations to convert to a polynomial system with the constraint being the resulting SOS problem's dimensionality.

- **Improving CSR estimate:** When estimating the CSR under the LVRT constraint modelled using an auxiliary system, it was noticed that the feasibility region was narrowest near the SEP of the auxiliary system and grew wider as we moved away from it. A variable center for the expanding interior region failed as well. A good start to the research could be in exploring the applications for rational Lyapunov functions for approximating CSRs through SOS which has shown promising results in estimating more complex regions [102]. Also, the impact of the studied disturbance may not be felt by the PVs all over the network. In those cases, the constraints corresponding to those PVs can be relaxed further increasing the size of the feasible region however at an added risk to reliability of the results.
- **Practicality of risk of instability:** The first limitation of the proposed idea is that while for fairly lower dimensional systems, the stability regions can be visualized, for larger systems, it is difficult to relate to them. Therefore, there is a need for scalar metrics that truly reflect the increase in risk due to PVs tripping. One option could be, using the proposed stability region estimates to evaluate the changes in CCTs for a set of faults which is a more relatable quantity. Thus, the operator would be presented with options for PV blocking that result in the maximum increase in CCTs across critical faults.
- **Reducing conservativeness in nested invariant sets:** We presented a sequential estimation approach to estimating the SR under a fixed cascading sequence. The conservativeness in this strategy is inherently increases for cases with increasing number of nested sets to be found. One option is to use start with the estimate from the sequential algorithm and then expand the innermost set while keeping the outer sets as variable, effectively an expanding interior algorithm with more than two regions.
- **Impact of PV on voltage dynamics:** While one of the focus of this work was to understand the implications of displacing conventional generation by PV on the angular stability, the other equally important problem is to study the impact on voltage security and stability [103][104][105].

References

[1] "Department of Energy." [Online]. Available: https://energy.gov/. [Accessed: 19-Jan-2017].

[2] D. Yang, H. Latchman, D. Tingling, and A. A. Amarsingh, "Design and Return on Investment Analysis of Residential Solar Photovoltaic Systems," *IEEE Potentials*, vol. 34, no. 4, pp. 11–17, Jul. 2015.

[3] P. Kruger, *Alternative Energy Resources : The Quest for Sustainable Energy*, 1 edition. Hoboken, N.J: Wiley, 2006.

[4] O. US EPA, "Clean Power Plan for Existing Power Plants." [Online]. Available: https://www.epa.gov/cleanpowerplan/clean-power-plan-existing-power-plants. [Accessed: 19-Jan-2017].

[5] Ecofys, "Retrofitting of PV systems to solve 50.2 Hz problem," *Ecofys*. [Online]. Available: http://www.ecofys.com/en/publication/retrofitting-of-pv-systems-to-solve-502-hz-problem///. [Accessed: 19-Jan-2017].

[6] "California ISO - Renewables Reporting." [Online]. Available: http://www.caiso.com/market/Pages/ReportsBulletins/DailyRenewablesWatch.aspx. [Accessed: 22-Jan-2017].

[7] J. S. John, "Retired CPUC Commissioner Takes Aim at CAISO's Duck Curve," 24-Mar-2014. [Online]. Available: https://www.greentechmedia.com/articles/read/retired-cpuc-commissioner-takes-aim-at-caisos-duck-curve. [Accessed: 31-Mar-2017].

[8] P. Kundur, *Power System Stability and Control*, 1st edition. New York: McGraw-Hill Education, 1994.

[9] S. Umans, *Fitzgerald & Kingsley's Electric Machinery*, 7 edition. New York: McGraw-Hill Education, 2013.

[10] P. W. Sauer and M. A. Pai, *Power System Dynamics and Stability*, 1 edition. Champaign, IL.: Stipes Publishing Co., 2007.

[11] A. Pai, *Energy Function Analysis for Power System Stability*, Softcover reprint of the original 1st ed. 1989 edition. Springer, 2013.

[12] "Tinney, W.F. and Hart, C.E. (1967) Power Flow Solution by Newton's Method. IEEE Transactions on Power Apparatus and Systems, PAS-86, 1449-1460. - References - Scientific Research Publish." [Online]. Available: http://www.scirp.org/(S(vtj3fa45qm1ean45vvffcz55))/reference/ReferencesPapers.aspx?ReferenceID=1580339. [Accessed: 22-Jan-2017].

[13] A. Ulbig, T. S. Borsche, and G. Andersson, "Impact of Low Rotational Inertia on Power System Stability and Operation," *ArXiv13126435 Math*, Dec. 2013.

[14] T. Athay, R. Podmore, and S. Virmani, "A Practical Method for the Direct Analysis of Transient Stability," *IEEE Trans. Power Appar. Syst.*, vol. PAS-98, no. 2, pp. 573–584, Mar. 1979.

[15] C. L. Barrett *et al.*, "Impact of a Surface Nuclear Blast on the Transient Stability of the Power System," in *Critical Information Infrastructures Security*, 2014, pp. 153–158.

[16] B. Stott, "Power system dynamic response calculations," *Proc. IEEE*, vol. 67, no. 2, pp. 219–241, Feb. 1979.

[17] H.-D. Chiang, F. F. Wu, and P. P. Varaiya, “A BCU method for direct analysis of power system transient stability,” *IEEE Trans. Power Syst.*, vol. 9, no. 3, pp. 1194–1208, Aug. 1994.
[18] H. d Chiang and J. S. Thorp, “The closest unstable equilibrium point method for power system dynamic security assessment,” in *26th IEEE Conference on Decision and Control*, 1987, vol. 26, pp. 72–76.
[19] A. M. Lyapunov, *General Problem of the Stability Of Motion*. London ; Washington, DC: CRC Press, 1992.
[20] H. D. Chiang, J. Tong, and Y. Tada, “On-line transient stability screening of 14,000-bus models using TEPCO-BCU: Evaluations and methods,” in *IEEE PES General Meeting*, 2010, pp. 1–8.
[21] A. Pal, C. Mishra, A. K. S. Vullikanti, and S. S. Ravi, “General optimal substation coverage algorithm for phasor measurement unit placement in practical systems,” *Transm. Distrib. IET Gener.*, vol. 11, no. 2, pp. 347–353, 2017.
[22] C. Mishra, K. D. Jones, A. Pal, and V. A. Centeno, “Binary particle swarm optimisation-based optimal substation coverage algorithm for phasor measurement unit installations in practical systems,” *Transm. Distrib. IET Gener.*, vol. 10, no. 2, pp. 555–562, 2016.
[23] A. Pal, G. A. Sanchez-Ayala, V. A. Centeno, and J. S. Thorp, “A PMU Placement Scheme Ensuring Real-Time Monitoring of Critical Buses of the Network,” *IEEE Trans. Power Deliv.*, vol. 29, no. 2, pp. 510–517, Apr. 2014.
[24] K. D. Jones, A. Pal, and J. S. Thorp, “Methodology for Performing Synchrophasor Data Conditioning and Validation,” *IEEE Trans. Power Syst.*, vol. 30, no. 3, pp. 1121–1130, May 2015.
[25] K. D. Jones, “Synchrophasor-Only Dynamic State Estimation & Data Conditioning,” Aug. 2013.
[26] C. Mishra, V. A. Centeno, and A. Pal, “Kalman-filter based recursive regression for three-phase line parameter estimation using synchrophasor measurements,” in *2015 IEEE Power Energy Society General Meeting*, 2015, pp. 1–5.
[27] M. Li, A. Pal, A. G. Phadke, and J. S. Thorp, “Transient stability prediction based on apparent impedance trajectory recorded by PMUs,” *Int. J. Electr. Power Energy Syst.*, vol. 54, no. Supplement C, pp. 498–504, Jan. 2014.
[28] B. Wang, B. Fang, Y. Wang, H. Liu, and Y. Liu, “Power System Transient Stability Assessment Based on Big Data and the Core Vector Machine,” *IEEE Trans. Smart Grid*, vol. 7, no. 5, pp. 2561–2570, Sep. 2016.
[29] A. Pal, J. S. Thorp, S. S. Veda, and V. A. Centeno, “Applying a robust control technique to damp low frequency oscillations in the WECC,” *Int. J. Electr. Power Energy Syst.*, vol. 44, no. 1, pp. 638–645, Jan. 2013.
[30] D. Yang, “A Data Analytics Framework for Regional Voltage Control,” Aug. 2017.
[31] S. Shukla and L. Mili, “Hierarchical Decentralized Control for Enhanced Rotor Angle and Voltage Stability of Large-Scale Power Systems,” *IEEE Trans. Power Syst.*, vol. 32, no. 6, pp. 4783–4793, Nov. 2017.
[32] R. Sun and V. A. Centeno, “Wide Area System Islanding Contingency Detecting and Warning Scheme,” *IEEE Trans. Power Syst.*, vol. 29, no. 6, pp. 2581–2589, Nov. 2014.
[33] *Topics in Morse Theory*. Stanford University Department of Mathematics, 1991.

[34] H.-D. Chiang and L. F. C. Alberto, *Stability Regions of Nonlinear Dynamical Systems: Theory, Estimation, and Applications*, 1 edition. Cambridge University Press, 2015.
[35] H.-D. Chiang, *Direct Methods for Stability Analysis of Electric Power Systems: Theoretical Foundation, BCU Methodologies, and Applications*, 1 edition. Wiley, 2011.
[36] L. F. C. Alberto and H. D. Chiang, "Towards development of generalized energy functions for electric power systems," in *2012 IEEE Power and Energy Society General Meeting*, 2012, pp. 1–6.
[37] N. Kakimoto, Y. Ohsawa, and M. Hayashi, "Transient Stability Analysis of Multimachine Power System with Field Flux Decays via Lyapunov's Direct Method," *IEEE Trans. Power Appar. Syst.*, vol. PAS-99, no. 5, pp. 1819–1827, Sep. 1980.
[38] G.C.Ejebe and J.Tong, "Discussion of clarifications on the BCU method for transient stability analysis.," *IEEE Trans. Power Syst*, no. 10, pp. 218–219, 1995.
[39] F. Paganini and B. C. Lesieutre, "Generic properties, one-parameter deformations, and the BCU method [power system stability]," *IEEE Trans. Circuits Syst. Fundam. Theory Appl.*, vol. 46, no. 6, pp. 760–763, Jun. 1999.
[40] R. T. Treinen, V. Vittal, and W. Kliemann, "An improved technique to determine the controlling unstable equilibrium point in a power system," *IEEE Trans. Circuits Syst. Fundam. Theory Appl.*, vol. 43, no. 4, pp. 313–323, Apr. 1996.
[41] "Dynamic gradient method for PEBS detection in power system transient stability assessment (PDF Download Available)," *ResearchGate*.
[42] J.-J. Deng and H.-D. Chiang, "Convergence Region of Newton Iterative Power Flow Method: Numerical Studies," *J. Appl. Math.*, vol. 2013, p. e509496, Nov. 2013.
[43] J. S. Thorp and S. A. Naqavi, "Load-flow fractals draw clues to erratic behaviour," *IEEE Comput. Appl. Power*, vol. 10, no. 1, pp. 59–62, Jan. 1997.
[44] H.-D. Chiang, H. Li, Y. Tada, and R. Tanabe, "Stable equilibrium point (sep) calculation apparatus of power system," US20100324872 A1, 23-Dec-2010.
[45] A. Llamas, J. D. L. R. Lopez, L. Mili, A. G. Phadke, and J. S. Thorp, "Clarifications of the BCU method for transient stability analysis," *IEEE Trans. Power Syst.*, vol. 10, no. 1, pp. 210–219, Feb. 1995.
[46] "Some Concrete Aspects Of Hilbert's 17th Problem," *ResearchGate*.
[47] Zachary William Jarvis-Wloszek, "Lyapunov Based Analysis and Controller Synthesis for Polynomial Systems using Sum-of-Squares Optimization," University of California, Berkley, 2013.
[48] "An algorithm for sums of squares of real polynomials," *ResearchGate*.
[49] P. A. Parrilo, "Structured semidefinite programs and semialgebraic geometry methods in robustness and optimization," phd, California Institute of Technology, 2000.
[50] P. Seiler, "SOSOPT: A Toolbox for Polynomial Optimization," *ArXiv13081889 Cs Math*, Aug. 2013.
[51] A. Papachristodoulou and S. Prajna, "A tutorial on sum of squares techniques for systems analysis," in *Proceedings of the 2005, American Control Conference, 2005.*, 2005, pp. 2686–2700 vol. 4.
[52] M. Anghel, F. Milano, and A. Papachristodoulou, "Algorithmic Construction of Lyapunov Functions for Power System Stability Analysis," *IEEE Trans. Circuits Syst. Regul. Pap.*, vol. 60, no. 9, pp. 2533–2546, Sep. 2013.

[53] A. Papachristodoulou and S. Prajna, “Analysis of Non-polynomial Systems Using the Sum of Squares Decomposition,” in *Positive Polynomials in Control*, D. Henrion and A. Garulli, Eds. Springer Berlin Heidelberg, 2005, pp. 23–43.
[54] I. Dobson, F. Alvarado, and C. L. DeMarco, “Sensitivity of Hopf bifurcations to power system parameters,” in *[1992] Proceedings of the 31st IEEE Conference on Decision and Control*, 1992, pp. 2928–2933 vol.3.
[55] D. S. Siqueira, L. F. C. Alberto, and N. G. Bretas, “Generalized energy functions for a class of lossy networking preserving power system models,” in *2015 IEEE International Symposium on Circuits and Systems (ISCAS)*, 2015, pp. 926–929.
[56] L. F. C. Alberto, W. Suampun, and H. D. Chiang, “Towards development of a CUEP method for Network-preserving power system models,” in *2013 IEEE International Symposium on Circuits and Systems (ISCAS2013)*, 2013, pp. 1548–1551.
[57] M. A. Pai, *Power System Stability: Analysis by the Direct Method of Lyapunov*. Amsterdam ; New York : New York, N.Y: Elsevier Science Ltd, 1981.
[58] R. Genesio, M. Tartaglia, and A. Vicino, “On the estimation of asymptotic stability regions: State of the art and new proposals,” *IEEE Trans. Autom. Control*, vol. 30, no. 8, pp. 747–755, Aug. 1985.
[59] V. I. Zubov, *Methods of A.M. Lyapunov and their application*. Izdatel’stvo Leningradskogo Universiteta, 1961.
[60] Y. n Yu and K. Vongsuriya, “Nonlinear Power System Stability Study by Liapunov Function and Zubov’s Method,” *IEEE Trans. Power Appar. Syst.*, vol. PAS-86, no. 12, pp. 1480–1485, Dec. 1967.
[61] F. S. PRABHAKARA, A. H. EL-ABIAD, and A. J. KOIVO, “Application of generalized Zubov’s method to power system stability,” *Int. J. Control*, vol. 20, no. 2, pp. 203–212, Aug. 1974.
[62] J. L. Willems and J. C. Willems, “The Application of Lyapunov Methods to the Computation of Transient Stability Regions for Multimachine Power Systems,” *IEEE Trans. Power Appar. Syst.*, vol. PAS-89, no. 5, pp. 795–801, May 1970.
[63] W. Ma and J. S. Thorp, “An efficient algorithm to locate all the load flow solutions,” *IEEE Trans. Power Syst.*, vol. 8, no. 3, pp. 1077–1083, Aug. 1993.
[64] T. van Cutsem and C. Vournas, *Voltage Stability of Electric Power Systems*, 1 edition. New York: Springer, 2008.
[65] I. Dobson, H. D. Chiang, J. S. Thorp, and L. Fekih-Ahmed, “A model of voltage collapse in electric power systems,” in *Proceedings of the 27th IEEE Conference on Decision and Control*, 1988, pp. 2104–2109 vol.3.
[66] W. Govaerts, *Numerical Methods for Bifurcations of Dynamical Equilibria*. Society for Industrial and Applied Mathematics, 2000.
[67] K. P. F.R.S, “LIII. On lines and planes of closest fit to systems of points in space,” *Philos. Mag.*, vol. 2, no. 11, pp. 559–572, Nov. 1901.
[68] X. Wang, M. Yue, and E. Muljadi, “PV generation enhancement with a virtual inertia emulator to provide inertial response to the grid,” in *2014 IEEE Energy Conversion Congress and Exposition (ECCE)*, 2014, pp. 17–23.
[69] C. Concordia and P. G. Brown, “Effects of Trends in Large Steam Turbine Driven Generator Parameters on Power System Stability,” *IEEE Trans. Power Appar. Syst.*, vol. PAS-90, no. 5, pp. 2211–2218, Sep. 1971.

[70] H. E. Lokay and P. O. Thoits, “Effects of Future Turbine-Generator Characteristics on Transient Stability,” *IEEE Trans. Power Appar. Syst.*, vol. PAS-90, no. 6, pp. 2427–2431, Nov. 1971.
[71] T. K. Basu and J. Nanda, “Effect of Different Parameters on Transient Stability of Power Systems,” *Journal of the Institution of Engineers (India)*, vol. 58, pp. 256–261, Apr. 1978.
[72] “Concepts of power system dynamic stability,” *ResearchGate*. [Online]. Available: https://www.researchgate.net/publication/3458216_Concepts_of_power_system_dynamic_stability. [Accessed: 16-Apr-2017].
[73] S. Na Nakorn, “Effects of reduced inertia on the transient stability of a power system,” *Retrosp. Theses Diss.*, Jan. 1980.
[74] D. Gautam, V. Vittal, and T. Harbour, “Impact of increased penetration of DFIG based wind turbine generators on transient and small signal stability of power systems,” in *IEEE PES General Meeting*, 2010, pp. 1–1.
[75] L. G. W. Roberts, A. R. Champneys, K. R. W. Bell, and M. di Bernardo, “Analytical Approximations of Critical Clearing Time for Parametric Analysis of Power System Transient Stability,” *IEEE J. Emerg. Sel. Top. Circuits Syst.*, vol. 5, no. 3, pp. 465–476, Sep. 2015.
[76] P. K. Naik, N.-K. C. Nair, and A. K. Swain, “Impact of reduced inertia on transient stability of networks with asynchronous generation,” *Int. Trans. Electr. Energy Syst.*, vol. 26, no. 1, pp. 175–191, Jan. 2016.
[77] S. Eftekharnejad, G. Heydt, and V. Vittal, “Optimal generation dispatch with high penetration of photovoltaic generation,” in *2015 IEEE Power Energy Society General Meeting*, 2015, pp. 1–1.
[78] L. Roberts, G. Kafanas, A. Champneys, M. di Bernardo, and K. Bell, “A parametric investigation on the effects of inertia on the stability of power systems,” in *2015 IEEE Eindhoven PowerTech*, 2015, pp. 1–6.
[79] W. Suampun and H. D. Chiang, “Critical evaluation of methods for estimating stability boundary for transient stability analysis in power systems,” in *IEEE PES General Meeting*, 2010, pp. 1–8.
[80] C. Mishra, S. P. Singh, and J. Rokadia, “Optimal power flow in the presence of wind power using modified cuckoo search,” *Transm. Distrib. IET Gener.*, vol. 9, no. 7, pp. 615–626, 2015.
[81] E. Mitchell-Colgan, C. Mishra, and V. A. Centeno, “Optimal wind farm placement considering system constraints and investment and uncertainty costs,” in *2015 IEEE Power Energy Society General Meeting*, 2015, pp. 1–5.
[82] V. Vittal, “Power system transient stability using the critical energy of individual machines,” *Retrosp. Theses Diss.*, Jan. 1982.
[83] H. d Chiang, J. S. Thorp, and M. Varghese, “Potential energy boundary surface method: Simulation study,” in *26th IEEE Conference on Decision and Control*, 1987, vol. 26, pp. 879–884.
[84] “Reliability Standards.” [Online]. Available: http://www.nerc.net/standardsreports/standardssummary.aspx. [Accessed: 19-Jan-2017].
[85] “IEEE Draft Standard for Interconnecting Distributed Resources with Electric Power Systems - Amendment 1,” *IEEE P1547aD3 Dec. 2013*, pp. 1–12, Mar. 2014.

[86] B. R. Williams, W. R. Schmus, and D. C. Dawson, “Transmission voltage recovery delayed by stalled air conditioner compressors,” *IEEE Trans. Power Syst.*, vol. 7, no. 3, pp. 1173–1181, Aug. 1992.
[87] A. P. Sohn, A. L. Abrantes, L. F. C. Alberto, and H. D. Chiang, “Stability region of a wind power system under low-voltage ride-through constraint,” in *2016 IEEE Power and Energy Society General Meeting (PESGM)*, 2016, pp. 1–5.
[88] K. L. Praprost and K. A. Loparo, “A stability theory for constrained dynamic systems with applications to electric power systems,” *IEEE Trans. Autom. Control*, vol. 41, no. 11, pp. 1605–1617, Nov. 1996.
[89] V. Venkatasubramanian, H. Schättler, and J. Zaborszky, “Stability Regions for Differential-Algebraic Systems,” in *Systems, Models and Feedback: Theory and Applications*, Birkhäuser, Boston, MA, 1992, pp. 385–402.
[90] F. M. Amaral and L. F. C. Alberto, “Stability boundary characterization of nonlinear autonomous dynamical systems in the presence of saddle-node equilibrium points,” *TEMA São Carlos*, vol. 13, no. 2, pp. 143–154, 2012.
[91] D. J. Hill and I. M. Y. Mareels, “Stability theory for differential/algebraic systems with application to power systems,” *IEEE Trans. Circuits Syst.*, vol. 37, no. 11, pp. 1416–1423, Nov. 1990.
[92] J. Kennedy and R. Eberhart, “Particle swarm optimization,” in *, IEEE International Conference on Neural Networks, 1995. Proceedings*, 1995, vol. 4, pp. 1942–1948 vol.4.
[93] “Stability Region Analysis Using Polynomial and Composite Polynomial Lyapunov Functions and Sum-of-Squares Programming,” *ResearchGate*.
[94] E. Glassman, A. L. Desbiens, M. Tobenkin, M. Cutkosky, and R. Tedrake, “Region of attraction estimation for a perching aircraft: A Lyapunov method exploiting barrier certificates,” in *2012 IEEE International Conference on Robotics and Automation*, 2012, pp. 2235–2242.
[95] S. Prajna, “Barrier certificates for nonlinear model validation,” in *42nd IEEE International Conference on Decision and Control (IEEE Cat. No.03CH37475)*, 2003, vol. 3, p. 2884–2889 Vol.3.
[96] “Frequency Response Initiative,” NERC, Oct. 2012.
[97] *Transient Stability of Power Systems - A Unified Approach to | Mania Pavella | Springer*. .
[98] X. Xu and G. Zhai, “Practical stability and stabilization of hybrid and switched systems,” *IEEE Trans. Autom. Control*, vol. 50, no. 11, pp. 1897–1903, Nov. 2005.
[99] “A stability result for switched systems with multiple equilibria (PDF Download Available),” *ResearchGate*.
[100] R. Kuiava, R. A. Ramos, H. R. Pota, and L. F. C. Alberto, “Practical stability of continuous-time switched systems without a common equilibria and governed by a time-dependent switching signal,” in *2011 9th IEEE International Conference on Control and Automation (ICCA)*, 2011, pp. 1156–1161.
[101] M. C. Valentino, V. A. Oliveira, L. F. C. Alberto, and D. A. Sant’Anna, “An extension of the invariance principle for switched nonlinear systems,” in *2011 50th IEEE Conference on Decision and Control and European Control Conference*, 2011, pp. 1178–1182.
[102] G. Valmorbida and J. Anderson, “Region of Attraction Estimation Using Invariant Sets and Rational Lyapunov Functions,” *Automatica*, vol. 75, no. C, pp. 37–45, Jan. 2017.

[103] Z. Nie, D. Yang, V. Centeno, and K. D. Jones, “A PMU-based voltage security assessment framework using hoeffding-tree-based learning,” in *2017 19th International Conference on Intelligent System Application to Power Systems (ISAP)*, 2017, pp. 1–6.
[104] A. Tbaileh, C. Mishra, and K. Thomas, “PV impacts on dynamic voltage stability,” in *SoutheastCon 2017*, 2017, pp. 1–5.
[105] S. Shukla and L. Mili, “A hierarchical decentralized coordinated voltage instability detection scheme for SVC,” in *2015 North American Power Symposium (NAPS)*, 2015, pp. 1–6.